中国高等科学技术中心

CCAST—WL WORKSHOP SERIES: VOLUME 149

Baryon, Dibaryon and Exotic Quark-Gluon States

中 国 高 等 科 学 技 术 中 心

CCAST—WL WORKSHOP SERIES: VOLUME 149

Baryon, Dibaryon and Exotic Quark-Gluon States

重子、双重子和奇特夸克 — 胶子态

Organized by

Fan Wang

Nanjing University
Nanjing, P. R. China
and

Zong-Ye Zhang
and

Bing-Song Zou
Institute of High Energy Physics
Chinese Academy of Sciences
Beijing, P. R. China

Proceedings of
CCAST (World Laboratory) Workshop
held in
Beijing, P. R. China
April 22-26, 2002

Printed in February 2003

Preface to the CCAST–World Laboratory Series

The China Center of Advanced Science and technology (CCAST) was established on October 17, 1986 through the strong support of World Laboratory and the Chinese Government. Its purpose is to introduce important frontier areas of science to China, to foster their growth by providing a suitable environment, and to promote free exchange of scientific information between China and other nations.

An important component of CCAST's activities is the organization of domestic and international* symposium/workshops. Each academic year we hold about 20 domestic symposium/workshops which last an average of one to two weeks each. The subjects are carefully chosen to cover advanced areas that are of particular interest to Chinese scientists. About 30–60 participants, from senior scientists to graduate students, are selected on a nationwide basis for each program. During each workshop these scientists hold daily seminars and work closely with each other.

Since 1990, CCAST has also sponsored a vigorous program for young Chinese scientists who have already made world–class contributions and are currently doing research abroad. They return to China to participate the domestic symposium/workshops, to lecture at CCAST and to collaborate with their colleagues at home. In this way, they can bring to China their own expertise, and when they go back to their institutions abroad they will be able to circulate in turn the knowledge they have acquired in China.

China is at a pivotal point in her scientific development. She is gradually emerging as an important and dynamic force in shaping the advanced science and technology of the future. This series is part of the this remarkable evolution. It records the effort, dedication, and sharing of knowledge by the Chinese scientists, at home and abroad.

T.D. Lee

* The CCAST international symposium/workshop series is published separately by Gordon and Breach Scientific Publishers.

Contents*

* 感谢世界实验室、中国科学院、国家自然科学基金委员会、财政部对中国高等科学技术中心的资助

Quark model for baryons

Qiang ZHAO
Department of Physics, University of Surrey, Guildford, GU2 7XH, UK
email: qiang.zhao@surrey.ac.uk

In this lecture, a pedagogic introduction to the nonrelativistic constituent quark model phenomenology for baryons is presented. Concerning the recent interests in the study of baryons in meson photo- and electroproduction, quark model approaches with effective Lagrangians for quark-meson couplings are introduced. A brief review of the experimental status is also provided.

1 Introduction

Understanding the structure of hadrons based on the fundamental interaction of constituent quarks and gluons is one of the challenges in strong interaction physics [1].

The phenomenological nonrelativistic constituent quark model (NRCQM) provides a picture for hadrons in which the constituent quarks are very heavy compared to the QCD scale. One of the basic assumption applied to such a picture is the adiabatic (Born-Oppenhimer) approximation for the low-lying hadronic structures, in which the gluonic fields of QCD generate effective potentials which depend on the positions and spins of the nearly static quarks. Since creation of heavy quark pairs would be suppressed, the simplest and low-lying color-singlet states thus have structure of $q\bar{q}$ and qqq. Meanwhile, since in the adiabatic approximation the low-lying states move along a potential surface generated by the gluonic ground state, the hadronic wavefunction will depend only on quarks.

Take one step further, when two quarks are close together, they would expose the configuration of a meson, where one expects that a linear potential (e.g. $V(r) = br$) is in operation. In terms of an effective two-body potential, in the direction between the "meson"-like configuration and the third quark, each of the two nearby quark would attract the third with a potential $\frac{1}{2}br$. It was demonstrated that a sum of two body potentials with half strength of the mesonic potential provides a good approximation for the descriptions of the low-lying baryons.

We concentrate on the baryons made up of light constituent quarks: u, d and s. These quarks have spin 1/2, in which u and d form a nonstrange isospin doublet, and s is a strange isospin singlet. Therefore, we have the fundamental representation of a SU(6) group symmetry for the spin and isospin wavefunctions:

$$u\uparrow, u\downarrow, d\uparrow, d\downarrow, s\uparrow, s\downarrow, \tag{1}$$

where u, d, and s are Pauli spinors in the isospin space, while $\uparrow$ and $\downarrow$ are spinors in the spin space.

The total wavefunction of such a baryon system consists of four parts: i) spatial wavefunction ψ; ii) flavor wavefunction ϕ; iii) spin wavefunction χ; and iv) color wavefunction ϕ_c. For such a Fermion system, the Pauli principle requires that the total wavefunction is antisymmetric under exchange of any two quarks. Therefore, the total wavefunction must be antisymmetrized. Note that such a normal baryon state should be a color singlet and thus the color wavefunction is antisymmetric under exchange of any two quarks. As a consequence, we need only to *symmetrize* the rest part of the total wavefunction, i.e. spatial, spin and isospin, to obtain an antisymmetric baryon wavefunction. Such a simple picture has provided a basis on which the hadron spectroscopies were first constructed.

The quark model achieved significant successes in the interpretation of a lot of static properties of nucleons and the excited resonances. However, it also raised the famous puzzle of "missing resonances", which were predicted by the quark model in the baryon spectroscopy, but have not been found in the π-N scattering experiments. Historically, most of the nucleon resonances were established in pion-nucleon (πN) scattering experiments. Since it is likely that those "missing resonances" couple to πN channel weakly, while they may have strong couplings to other meson or baryon production channel (we should come back to this later), for instance, $\Delta\pi$, ηN, $K\Lambda$, $K\Sigma$, ωN, ρN, ϕN, etc. both experimental and theoretical efforts were devoted to searching for "missing resonances" in meson photo- and electroproduction, where the photon serves as a clean electromagnetic probe for detecting the nucleon resonance structures. A large number of experiments are undertaking at JLab (CLAS), ESRF (GRAAL), ELSA (SAPHIR), MAMI (Mainz), SPring-8, etc., and a large database in the near future would undoubtedly improve our knowledge of the baryon static properties and the non-perturbative QCD phenomena.

In the following parts, I shall introduce the nonrelativistic quark model. Its success and failure in the description of baryon static properties will be

addressed. Consequently, I shall introduce its application to the study of the photo-excitation of baryon resonances. Closely related to the experimental efforts, I shall introduce a quark model approach to meson photo- and electroproduction at the resonance region. Relevant experimental progresses will be addressed.

2 The spin-independent potential and naive quark model

Isgur and Karl [2] first systematically studied the baryon spectroscopy by solving the Schrödinger equation for the quarks in a baryon system by expressing the Hamiltonian as

$$\hat{H} = \sum_i \left(m_i + \frac{\mathbf{p}_i^2}{2m_i} \right) + \sum_{i<j} (V_{conf}^{ij} + \hat{H}_{hyp}^{ij}) \ , \tag{2}$$

where V_{conf}^{ij} is the potential for confinement, and has the following expression:

$$V_{conf}^{ij} = C_{qqq} + \frac{1}{2} b r_{ij} - \frac{2}{3} \frac{\alpha_s}{r_{ij}} \ . \tag{3}$$

In the harmonic oscillator basis, V_{conf}^{ij} can be expressed as

$$V_{conf}^{ij} \equiv \frac{1}{2} \beta r_{ij}^2 + U_{ij} \ , \tag{4}$$

where U_{ij} is treated as an anharmonic perturbation. Leaving the spin-dependent term $\hat{H}_{hyp}^{ij}$ to be discussed later, one can solve the eigenstates of the harmonic oscillator potential, and minimize the anharmonic part by choosing a proper value for β.

In this case, total angular momentum of the three quark system is a good quantum number. Therefore, the spatial wavefunction has an O(3) orbital angular momentum symmetry. Remember that the spin and flavor wavefunction are combined under SU(6) symmetry, we thus label such a quark system with SU(6)$\otimes$O(3) symmetry.

2.1 SU(6) wavefunction

Recalling that we require the product of spatial, spin and flavor wavefunctions to be symmetric, therefore, the product of the spin and flavor wavefunctions could be any possible combinations. We use the representations

of the permutation group S_3 to construct the SU(6) wavefunctions for spin and flavor space.

Generally, there are four representations of S_3: total symmetric basis e^s, total antisymmetric e^a, and two mixed-symmetry bases e^λ and e^ρ, which are defined under permutation transformations:

$$P_{12}\begin{pmatrix} e^\lambda \\ e^\rho \end{pmatrix} = \begin{pmatrix} 1 & 0 \\ 0 & -1 \end{pmatrix}\begin{pmatrix} e^\lambda \\ e^\rho \end{pmatrix}, \tag{5}$$

and

$$P_{13}\begin{pmatrix} e^\lambda \\ e^\rho \end{pmatrix} = \begin{pmatrix} -\frac{1}{2} & -\frac{\sqrt{3}}{2} \\ -\frac{\sqrt{3}}{2} & \frac{1}{2} \end{pmatrix}\begin{pmatrix} e^\lambda \\ e^\rho \end{pmatrix}, \tag{6}$$

where P_{12} and P_{13} are permutation operators for exchange of $1 \leftrightarrow 2$ and $1 \leftrightarrow 3$, respectively.

Since the representations of SU(N), which can be constructed from three fundamental representations of group S_3, are also representations of S_3, for SU(2), SU(3) and SU(6), we can obtain

$$SU(2) \quad \mathbf{2}\otimes\mathbf{2}\otimes\mathbf{2} = \mathbf{4}_s + \mathbf{2}_\rho + \mathbf{2}_\lambda, \tag{7}$$

$$SU(3) \quad \mathbf{3}\otimes\mathbf{3}\otimes\mathbf{3} = \mathbf{10}_s + \mathbf{8}_\rho + \mathbf{8}_\lambda + \mathbf{1}_a, \tag{8}$$

$$SU(6) \quad \mathbf{6}\otimes\mathbf{6}\otimes\mathbf{6} = \mathbf{56}_s + \mathbf{70}_\rho + \mathbf{70}_\lambda + \mathbf{20}_a, \tag{9}$$

where the subscripts denote the corresponding S_3 basis for each representation, and the bold numbers denote the dimension of the corresponding representation. Note that we cannot construct an antisymmetric spin state with identical spin 1/2 fermions.

The spin-flavor wavefunctions thus can be expressed as $|\mathbf{N}_6, {}^{2S+1}\mathbf{N}_3\rangle$, where $\mathbf{N}_6$ and $\mathbf{N}_3$ denote the SU(6) and SU(3) representation and S stands for the total spin of the wavefunction. More explicitly, we have the SU(6) wavefunctions:

$$\begin{aligned}
|\mathbf{56},{}^2\mathbf{8}\rangle^s &= \frac{1}{\sqrt{2}}(\phi^\rho\chi^\rho + \rho^\lambda\chi^\lambda), \\
|\mathbf{56},{}^4\mathbf{10}\rangle^s &= \phi^s\chi^s, \\
|\mathbf{70},{}^2\mathbf{8}\rangle^\rho &= \frac{1}{\sqrt{2}}(\phi^\rho\chi^\lambda + \phi^\lambda\chi^\rho), \\
|\mathbf{70},{}^4\mathbf{8}\rangle^\rho &= \phi^\rho\chi^s, \\
|\mathbf{70},{}^2\mathbf{10}\rangle^\rho &= \phi^s\chi^\rho, \\
|\mathbf{70},{}^2\mathbf{1}\rangle^\rho &= \phi^a\chi^\lambda,
\end{aligned}$$

$$
\begin{aligned}
|\mathbf{70},^2\mathbf{8}\rangle^\lambda &= \frac{1}{\sqrt{2}}(\phi^\rho\chi^\rho - \phi^\lambda\chi^\lambda) \,, \\
|\mathbf{70},^4\mathbf{8}\rangle^\lambda &= \phi^\lambda\chi^s \,, \\
|\mathbf{70},^2\mathbf{10}\rangle^\lambda &= \phi^s\chi^\lambda \,, \\
|\mathbf{70},^2\mathbf{1}\rangle^\lambda &= \phi^a\chi^\rho \,, \\
|\mathbf{20},^2\mathbf{8}\rangle^a &= \frac{1}{\sqrt{2}}(\phi^\rho\chi^\lambda - \phi^\lambda\chi^\rho) \,, \\
|\mathbf{20},^4\mathbf{1}\rangle^a &= \phi^a\chi^s \,.
\end{aligned} \tag{10}
$$

2.2 Spatial wavefunctions

The spin-independent potential leads to conservation of the total orbital angular momentum $\mathbf{L}$ and the total spin $\mathbf{S}$. The total angular momentum of the baryon is $\mathbf{J} = \mathbf{L} + \mathbf{S}$, and thus the spatial wavefunctions possess O(3) symmetry under a rotation transformation. Meanwhile, the Hamiltonian for such a three-quark system can be invariant under the permutation group S_3. One thus can express the spatial wavefunctions as representations of the S_3 group.

Although the energy level (mass position) and symmetries of the baryon states are dependent on the potential, generally the ground state should be a symmetric basis of S_3 with $L^P = 0^+$, and the next (excited) states are of mixed symmetry with $L^P = 1^-$. As a first order approximation, the eigenstates of harmonic oscillators provide an ideal basis to build up the spatial wavefunctions for those low-lying baryons.

The Hamitonian for the harmonic oscillator can be expressed as,

$$
\hat{H} = \sum_{i=1}^{3} \frac{\mathbf{p}_i^2}{2m_q} + \frac{1}{6} m_q \omega_h^2 \sum_{i<j} (\mathbf{r}_j - \mathbf{r}_i)^2 \,, \tag{11}
$$

where $\mathbf{r}_{i(j)}$ and $\mathbf{p}_i$ are coordinate and momentum of the constituent quark; ω_h is the harmonic oscillator potential strength.

One can also express the three coordinates in a basis of S_3 group symmetry, which is the same as Jacobi coordinate as shown by Fig. 1. The symmetric coordinates $\mathbf{R}$ (or $\mathbf{P}_R$ in momentum space) describe the c.m. motions, which are symmetric under the exchange of any two quarks. The two mixed coordinates $\boldsymbol{\rho}$ and $\boldsymbol{\lambda}$ (or $\mathbf{p}_\rho$ and $\mathbf{p}_\lambda$ in momentum space) describe the internal motions which are antisymmetric and symmetric under the exchange of quark one and two. It should be noted that although the

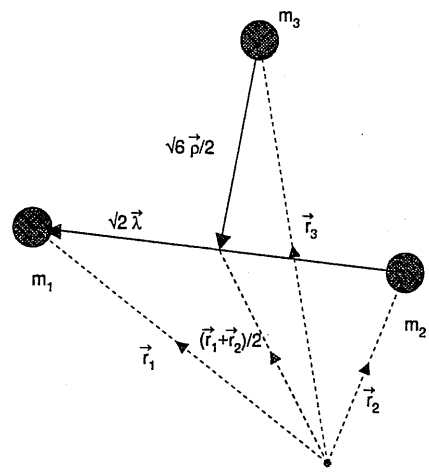

Figure 1: The Jacobi coordinate for a three-quark system.

quarks are labelled by number indices, we will not lose any generality after the symmetrization of the system.

With the new coordinates, the harmonic oscillator Hamitonian can be rewritten as

$$\hat{H} = \frac{\mathbf{P}_R^2}{6m_q} + \frac{\mathbf{p}_\rho^2}{2m_q} + \frac{\mathbf{p}_\lambda^2}{2m_q} + \frac{3}{2}m_q\omega_h^2(\boldsymbol{\rho}^2 + \boldsymbol{\lambda}^2)\ , \tag{12}$$

where the transformations between these two coordinates are

$$\begin{aligned} \mathbf{R} &= \frac{1}{3}(\mathbf{r}_1 + \mathbf{r}_2 + \mathbf{r}_3) \\ \boldsymbol{\rho} &= \frac{1}{\sqrt{2}}(\mathbf{r}_1 - \mathbf{r}_2) \end{aligned}$$

$$\boldsymbol{\lambda} = \frac{1}{\sqrt{6}}(\mathbf{r}_1 + \mathbf{r}_2 - 2\mathbf{r}_3) , \tag{13}$$

or

$$\begin{aligned} \mathbf{P}_R &= \mathbf{p}_1 + \mathbf{p}_2 + \mathbf{p}_3 \\ \mathbf{p}_\rho &= \frac{1}{\sqrt{2}}(\mathbf{p}_1 - \mathbf{p}_2) \\ \mathbf{p}_\lambda &= \frac{1}{\sqrt{6}}(\mathbf{p}_1 + \mathbf{p}_2 - 2\mathbf{p}_3) . \end{aligned} \tag{14}$$

The eigenstates for the above Hamitonian can be expressed as

$$\psi(\mathbf{r}_1, \mathbf{r}_2, \mathbf{r}_3) = \frac{1}{(2\pi)^{3/2}} e^{i\mathbf{P}_R \cdot \mathbf{R}} \psi^\sigma_{NLL_z}(\boldsymbol{\rho}, \boldsymbol{\lambda}) , \tag{15}$$

where $\psi^\sigma_{NLL_z}(\boldsymbol{\rho}, \boldsymbol{\lambda})$ is the harmonic oscillator wavefunction; $\sigma = s, \rho, \lambda, a$ denotes the representation of the S_3 group; N, L, and L_z denote the main quantum number, total orbital angular momentum, and total orbital angular momentum projection along z-axis. Taking the notation of Karl and Obryk [3], the harmonic oscillator wavefunction can be written as

$$\psi^\sigma_{NLL_z}(\boldsymbol{\rho}, \boldsymbol{\lambda}) = P^\sigma_{NLL_z} \frac{\alpha_h^3}{\pi^{3/2}} e^{-\alpha_h^2(\boldsymbol{\rho}^2 + \boldsymbol{\lambda}^2)/2} , \tag{16}$$

where $\alpha_h \equiv m\omega_h$, and $P^\sigma_{NLL_z}$ is a polynomial of $\boldsymbol{\rho}$ and $\boldsymbol{\lambda}$. In this way, the symmetry charactor of the wavefunctions is highlighted.

Explicitly, the states with $N \leq 2$ can be obtained:

$$\begin{aligned} N = 0, \quad L = 0, \quad & P^s_{000} = 1, \\ N = 1, \quad L = 1, \quad & P^\rho_{111} = \alpha_h \rho_+, \\ & P^\lambda_{111} = \alpha_h \lambda_+, \\ N = 2, \quad L = 0, \quad & P^s_{200} = \frac{\alpha_h^2}{\sqrt{3}}(\boldsymbol{\rho}^2 + \boldsymbol{\lambda}^2 - 3\alpha_h^{-2}), \\ & P^\rho_{200} = \frac{\alpha_h^2}{\sqrt{3}} 2\boldsymbol{\rho} \cdot \boldsymbol{\lambda}, \\ & P^\lambda_{200} = \frac{\alpha_h^2}{\sqrt{3}}(\boldsymbol{\rho}^2 - \boldsymbol{\lambda}^2), \\ L = 2, \quad & P^s_{222} = \frac{1}{2}\alpha_h^2(\rho_+^2 + \lambda_+^2), \\ & P^\rho_{222} = \alpha_h^2 \rho_+ \lambda_+, \end{aligned}$$

$$P^{\lambda}_{222} = \frac{1}{2}\alpha_h^2(\rho_+^2 - \lambda_+^2),$$
$$L=1, \quad P^{a}_{211} = \alpha_h^2(\rho_+\lambda_z - \lambda_+\rho_z). \tag{17}$$

2.3 Total wavefunctions

Now it is quite direct to construct the total wavefunction of baryons in the SU(6)⊗O(3) symmetry limit:

$$\phi_c|\mathrm{SU}(6)\otimes \mathrm{O}(3)\rangle = \phi_c|\mathbf{N}_6,\ {}^{2S+1}\mathbf{N}_3,\ N, L, J\rangle\ , \tag{18}$$

where again we stress that the O(3) symmetry leads to the total orbital angular momentum to be a good quantum number with $\mathbf{J} = \mathbf{L} + \mathbf{S}$.

As discussed before, apart from the anti-symmetric color wavefunction ϕ_c, we need to construct $|\mathrm{SU}(6)\otimes \mathrm{O}(3)\rangle$ to be symmetric. The assignments of these states to resonances are denoted by $L_{(2I)(2J)}(M)$, where I, J, and M represent the isospin, spin, and mass (in MeV) of the resonance, and L is the relative orbital angular momentum between π and N in the resonance decay into πN channel. In the following, we also give the resonance experimental status rated by "*" (See convention of PDG [4]).

i) Ground state baryons with $N = 0$, $L = 0$, $L^P = 0^+$.

Nucleon (p and n) (****):

$$|\mathbf{56},\ {}^2\mathbf{8},\ 0, 0, \frac{1}{2}\rangle = \frac{1}{\sqrt{2}}(\phi^\rho\chi^\rho + \phi^\lambda\chi^\lambda)\psi^s_{000}(\boldsymbol{\rho}, \boldsymbol{\lambda})\ . \tag{19}$$

$P_{33}(1232)$ $(\Delta^{++}, \Delta^+, \Delta^0, \Delta^-)$ (****):

$$|\mathbf{56},\ {}^4\mathbf{10},\ 0, 0, \frac{3}{2}\rangle = \phi^s\chi^s\psi^s_{000}(\boldsymbol{\rho}, \boldsymbol{\lambda})\ . \tag{20}$$

ii) The first excited states with $N = 1$, $L = 1$, $L^P = 1^-$. Since the spatial wavefunction with $L = 1$ cannot be symmetrized, it implies that only the spatial wavefunction with mixed symmetries can contribute, i.e. $\mathbf{N}_6 = \mathbf{70}$.

- $S_{11}(1535)$ (****), $D_{13}(1520)$ (****):

$$\begin{aligned}|\mathbf{70},\ {}^2\mathbf{8},\ 1, 1, J\rangle \ = \ & \sum_{L_z+S_z=J_z} \langle 1L_z, \frac{1}{2}S_z|JJ_z\rangle \\ & \times\frac{1}{2}[(\phi^\rho\chi^\lambda_{S_z} + \phi^\lambda\chi^\rho_{S_z})\psi^\rho_{11L_z}(\boldsymbol{\rho}, \boldsymbol{\lambda}) \\ & +(\phi^\rho\chi^\rho_{S_z} - \phi^\lambda\chi^\lambda_{S_z})\psi^\lambda_{11L_z}(\boldsymbol{\rho}, \boldsymbol{\lambda})]\ .\end{aligned} \tag{21}$$

- $S_{11}(1650)$ (****), $D_{13}(1700)$ (***), $D_{15}(1675)$ (****):

$$
\begin{aligned}
&|\mathbf{70},\ {}^4\mathbf{8},\ 1,1,J\rangle \\
&= \sum_{L_z+S_z=J_z} \langle 1L_z, \frac{3}{2}S_z|JJ_z\rangle \\
&\times \frac{1}{\sqrt{2}}[\phi^\rho \chi^s_{S_z}\psi^\rho_{11L_z}(\boldsymbol{\rho},\boldsymbol{\lambda}) + \phi^\lambda \chi^s_{S_z}\psi^\lambda_{11L_z}(\boldsymbol{\rho},\boldsymbol{\lambda})] \ . \qquad (22)
\end{aligned}
$$

- $S_{31}(1620)$ (****), $D_{33}(1670)$ (****):

$$
\begin{aligned}
&|\mathbf{70},\ {}^2\mathbf{10},\ 1,1,J\rangle \\
&= \sum_{L_z+S_z=J_z} \langle 1L_z, \frac{1}{2}S_z|JJ_z\rangle \\
&\times \frac{1}{\sqrt{2}}[\phi^s \chi^\rho_{S_z}\psi^\rho_{11L_z}(\boldsymbol{\rho},\boldsymbol{\lambda}) + \phi^s \chi^\lambda_{S_z}\psi^\lambda_{11L_z}(\boldsymbol{\rho},\boldsymbol{\lambda})]_J \ . \qquad (23)
\end{aligned}
$$

- States with anti-symmetric flavor wavefunction (only for Λ baryons):

$$
\begin{aligned}
&|\mathbf{70},\ {}^2\mathbf{1},\ 1,1,J\rangle \\
&= \sum_{L_z+S_z=J_z} \langle 1L_z, \frac{1}{2}S_z|JJ_z\rangle \\
&\times \frac{1}{\sqrt{2}}[\phi^a \chi^\lambda_{S_z}\psi^\rho_{11L_z}(\boldsymbol{\rho},\boldsymbol{\lambda}) - \phi^a \chi^\rho_{S_z}\psi^\lambda_{11L_z}(\boldsymbol{\rho},\boldsymbol{\lambda})]_J \ . \qquad (24)
\end{aligned}
$$

iii) Higher excited states with $N = 2$.

Since the spatial wavefunction can be symmetric, anti-symmetric or mixed symmetric, the SU(6)⊗O(3) representation can be **56**, **70**, and **20**.

A) For $\mathbf{N}_6 = \mathbf{56}$:

- Radial excitation with $L = 0$:

  $P_{11}(1440)$ (Roper resonance) (****)

$$
|\mathbf{56},\ {}^2\mathbf{8},\ 2,0,\frac{1}{2}\rangle = \frac{1}{\sqrt{2}}(\phi^\rho\chi^\rho + \phi^\lambda\chi^\lambda)\psi^s_{200}(\boldsymbol{\rho},\boldsymbol{\lambda}) \ . \qquad (25)
$$

  $P_{33}(1600)(****)$

$$
|\mathbf{56},\ {}^4\mathbf{10},\ 2,0,\frac{3}{2}\rangle = \phi^s\chi^s\psi^s_{200}(\boldsymbol{\rho},\boldsymbol{\lambda}) \ . \qquad (26)
$$

- $L = 2$:

$P_{13}(1720)$ (****), $F_{15}(1680)$ (****)

$$|\mathbf{56},\ {}^2\mathbf{8},\ 2,2,J\rangle = \sum_{L_z+S_z=J_z} \langle 2L_z, \frac{1}{2} S_z | J J_z\rangle \times \frac{1}{\sqrt{2}}(\phi^\rho \chi^\rho_{S_z} + \phi^\lambda \chi^\lambda_{S_z}) \psi^s_{22L_z}(\boldsymbol{\rho}, \boldsymbol{\lambda}) \ . \quad (27)$$

$P_{31}(1910)$ (****), $P_{33}(1920)$ (***), $F_{35}(1905)$ (****), $F_{37}(1950)$ (****)

$$|\mathbf{56},\ {}^4\mathbf{10},\ 2,2,J\rangle = \sum_{L_z+S_z=J_z} \langle 2L_z, \frac{3}{2} S_z | J J_z\rangle \phi^s \chi^s_{S_z} \psi^s_{22L_z}(\boldsymbol{\rho}, \boldsymbol{\lambda}) \ . \quad (28)$$

B) For $\mathbf{N_6 = 70}$:

- Radial excitation with $L = 0$:

$P_{11}(1710)$ (***)

$$|\mathbf{70},\ {}^2\mathbf{8},\ 2,0,\frac{1}{2}\rangle = \frac{1}{2}[(\phi^\rho \chi^\lambda_{S_z} + \phi^\lambda \chi^\rho_{S_z}) \psi^\rho_{200}(\boldsymbol{\rho}, \boldsymbol{\lambda}) + (\phi^\rho \chi^\rho_{S_z} - \phi^\lambda \chi^\lambda_{S_z}) \psi^\lambda_{200}(\boldsymbol{\rho}, \boldsymbol{\lambda})] \ . \quad (29)$$

$P_{13}(1900)$ (**)

$$|\mathbf{70},\ {}^4\mathbf{8},\ 2,0,\frac{3}{2}\rangle = \frac{1}{\sqrt{2}}[\phi^\rho \chi^s_{S_z} \psi^\rho_{200}(\boldsymbol{\rho}, \boldsymbol{\lambda}) + \phi^\lambda \chi^s_{S_z} \psi^\lambda_{200}(\boldsymbol{\rho}, \boldsymbol{\lambda})] \ . \quad (30)$$

$P_{31}(1750)$ (*)

$$|\mathbf{70},\ {}^2\mathbf{10},\ 2,0,\frac{1}{2}\rangle = \frac{1}{\sqrt{2}}[\phi^s \chi^\rho_{S_z} \psi^\rho_{200}(\boldsymbol{\rho}, \boldsymbol{\lambda}) + \phi^s \chi^\lambda_{S_z} \psi^\lambda_{200}(\boldsymbol{\rho}, \boldsymbol{\lambda})]_J \ . \quad (31)$$

P_{01} with anti-symmetric flavor wavefunction (only for Λ baryons):

$$|\mathbf{70},\ {}^2\mathbf{1},\ 2,0,\frac{1}{2}\rangle = \frac{1}{\sqrt{2}}[\phi^a \chi^\lambda_{S_z} \psi^\rho_{200}(\boldsymbol{\rho}, \boldsymbol{\lambda}) - \phi^a \chi^\rho_{S_z} \psi^\lambda_{200}(\boldsymbol{\rho}, \boldsymbol{\lambda})]_J \ . \quad (32)$$

- $L = 2$

  $P_{13}(1900)$ (**), $F_{15}(2000)$ (**)

$$|\mathbf{70},\ {}^2\mathbf{8},\ 2,2,J\rangle = \sum_{L_z+S_z=J_z} \langle 2L_z, \frac{1}{2} S_z | J J_z \rangle \times \frac{1}{2}[(\phi^\rho \chi^\lambda_{S_z} + \phi^\lambda \chi^\rho_{S_z}) \psi^\rho_{22L_z}(\boldsymbol{\rho}, \boldsymbol{\lambda}) + (\phi^\rho \chi^\rho_{S_z} - \phi^\lambda \chi^\lambda_{S_z}) \psi^\lambda_{22L_z}(\boldsymbol{\rho}, \boldsymbol{\lambda})] \ . \quad (33)$$

  $P_{11}(2100)$ (*), $P_{13}(1900)$ (**), $F_{15}(2000)$ (**), $F_{17}(1990)$ (**)

$$|\mathbf{70},\ {}^4\mathbf{8},\ 2,2,J\rangle = \sum_{L_z+S_z=J_z} \langle 2L_z, \frac{3}{2} S_z | J J_z \rangle \times \frac{1}{\sqrt{2}}[\phi^\rho \chi^s_{S_z} \psi^\rho_{22L_z}(\boldsymbol{\rho}, \boldsymbol{\lambda}) + \phi^\lambda \chi^s_{S_z} \psi^\lambda_{22L_z}(\boldsymbol{\rho}, \boldsymbol{\lambda})] \ . \quad (34)$$

  $P_{33}(1985)$ (missing), $F_{35}(2000)$ (**)

$$|\mathbf{70},\ {}^2\mathbf{10},\ 2,2,J\rangle = \sum_{L_z+S_z=J_z} \langle 2L_z, \frac{1}{2} S_z | J J_z \rangle \times \frac{1}{\sqrt{2}}[\phi^s \chi^\rho_{S_z} \psi^\rho_{22L_z}(\boldsymbol{\rho}, \boldsymbol{\lambda}) + \phi^s \chi^\lambda_{S_z} \psi^\lambda_{22L_z}(\boldsymbol{\rho}, \boldsymbol{\lambda})]_J \ . \quad (35)$$

C) For $\mathbf{N_6} = \mathbf{20}$, it must require $L = 1$. So far no experimental evidence for the existence of such resonances was found. For non-strange resonance, we have

$$|\mathbf{20},\ {}^2\mathbf{8},\ 2,1,J\rangle = \sum_{L_z+S_z=J_z} \langle 1L_z, \frac{1}{2} S_z | J J_z \rangle \times \frac{1}{\sqrt{2}}(\phi^\rho \chi^\lambda_{S_z} - \phi^\lambda \chi^\rho_{S_z}) \psi^a_{21L_z}(\boldsymbol{\rho}, \boldsymbol{\lambda}) \ , \quad (36)$$

and for Λ baryon with anti-symmetric flavor wavefunction, we have

$$|\mathbf{20},\ {}^4\mathbf{1},\ 2,1,J\rangle = \sum_{L_z+S_z=J_z} \langle 1L_z, \frac{3}{2} S_z | J J_z \rangle \chi^s_{S_z} \phi^a \psi^a_{21L_z}(\boldsymbol{\rho}, \boldsymbol{\lambda}) \ . \quad (37)$$

2.4 The anharmonic and spin-dependent potential

Based on the SU(6)⊗O(3) symmetry, the quark model succeeded in the classification of the baryon spectrum. But quantitative results could not be expected since more elaborate details about the dynamics were needed. A famous example was that the Roper resonance $P_{11}(1440)$ was assigned to the radial excitation state with $N = 2$, and $L = 0$, which was found to have lower mass than the first excited multiplets with $N = 1$ and $L = 1$. The inclusion of the anharmonic and spin-dependent quark potential turned to be necessary.

The perturbative anharmonic interaction U_{ij} brought the first order energy shift to different SU(6)⊗O(3) representations. It led to the largest energy shift for the SU(6)⊗O(3) state $[\mathbf{56}, 0^+]_{N=2}$ (Roper), while it vanished for the state $[\mathbf{20}, 1^+]_{N=2}$. This gave a reasonable explanation to the lower mass of the Roper resonance, and presumably explained why states of $[\mathbf{20}, 1^+]_{N=2}$ were not observed in experiment since they were predicted to have higher mass scale.

The spin-dependent effects are introduced through the hyperfine interaction for the light quark system:

$$\hat{H}_{hyp} = \sum_{i<j} \frac{2\alpha_s(r_{ij})}{3m_i m_j} \left[\frac{8\pi}{3} \mathbf{S}_i \cdot \mathbf{S}_j \delta^3(\mathbf{r}_{ij}) + \frac{1}{r_{ij}^3} \left(\frac{3\mathbf{S}_i \cdot \mathbf{r}_{ij} \mathbf{S}_j \cdot \mathbf{r}_{ij}}{r_{ij}^2} - \mathbf{S}_i \cdot \mathbf{S}_j \right) \right] , \tag{38}$$

where $\mathbf{S}_i$ is the spin operator for the i-th quark.

For the ground state baryons, the hyperfine interaction could be completely isolated since both the ρ and λ type orbital angular momentum operators would annihilate the ground states. The hyperfine interaction can only contribute via the contact term of $\mathbf{S}_i \cdot \mathbf{S}_j$. Notice that

$$\langle \psi^s_{000} | \delta^3(\mathbf{r}_{ij}) | \psi^s_{000} \rangle = \frac{\alpha_h^3}{(2\pi)^{3/2}} , \tag{39}$$

and

$$\langle \mathbf{S}_i \cdot \mathbf{S}_j \rangle = \begin{cases} +1/4 & \text{if } i \text{ and } j \text{ have spin 1} \\ -3/4 & \text{if } i \text{ and } j \text{ have spin 0} \end{cases} , \tag{40}$$

the ground state diagonal splittings can be then obtained:

$$\delta \equiv \frac{4\alpha_s \alpha_h^3}{3\sqrt{2}\pi m_q^2} r_{hyp} , \tag{41}$$

where r_{hyp} is a factor introduced as a relativistic correction for the naive hyperfine interaction. Taking the approximation, $m_u = m_d$ and $x \equiv m_u/m_s \approx 2/3$, one obtains the following relation for the ground state baryons:

$$\begin{aligned}
\delta M_N &= -\frac{1}{2}\delta \,, \\
\delta M_\Delta &= +\frac{1}{2}\delta \,, \\
\delta M_\Sigma &= (\frac{1}{6} - \frac{2x}{3})\delta \,, \\
\delta M_{\Sigma^*} &= (\frac{x}{3} + \frac{1}{6})\delta \,, \\
\delta M_\Lambda &= -\frac{1}{2}\delta \,, \\
\delta M_\Xi &= (\frac{x^2}{6} - \frac{2x}{3})\delta \,, \\
\delta M_{\Xi^*} &= (\frac{x}{3} + \frac{x^2}{6})\delta \,, \\
\delta M_\Omega &= +\frac{x^2}{2}\delta \,. \qquad (42)
\end{aligned}$$

An interesting feature can be immediately seen is that the hyperfine interaction leads to a heavier Δ mass than the nucleon. Nevertheless, the mass of Λ (uds, 1.115 GeV) is lowered by as much as the nucleon.

On the other hand, the total spin and total orbital angular momentum were no longer conserved due to the tensor interaction, which led to the configuration mixings among SU(6)⊗O(3) states. One thus had to diagonise a matrix for each of the spin-parity (physical) states, which were superposition of the SU(6)⊗O(3) states. Namely

$$|\Psi_B\rangle = \sum_i C_i |\Psi^i_{SU(6)\otimes O(3)}\rangle \,. \qquad (43)$$

As an example, Isgur *et al* [5] showed that the ground state nucleon $P_{11}(938)$ ($J^P = \frac{1}{2}^+$) could be expressed as

$$\begin{aligned}
|\Psi_N\rangle &= +0.91|\mathbf{56},^2\mathbf{8},0,0,\frac{1}{2}\rangle - 0.34|\mathbf{56},^2\mathbf{8},2,0,\frac{1}{2}\rangle \\
&\quad -0.27|\mathbf{70},^2\mathbf{8},2,0,\frac{1}{2}\rangle - 0.06|\mathbf{70},^2\mathbf{8},2,2,\frac{1}{2}\rangle \,. \qquad (44)
\end{aligned}$$

2.5 Electromagnetic moments of ground state baryons

One of the most impressive successes of the non-relativistic quark model could be its description of the static property, the electromagnetic moments of ground state baryons. Based on the simple assumption that all constituent quarks are in S-wave orbitals. That is to say, except for the spin of the constituents, no orbital angular momentum would contribute to the electromagnetic moment.

The magnetic moment for the quarks can be expressed as:

$$\mu_u = e_u/2m_u, \ \mu_d = e_d/2m_d, \ \mu_s = e_s/2m_s \ , \tag{45}$$

where $e_u = +(2/3)e$, $e_d = e_s = -(1/3)e$, are the quark charges.

The assumption above implies that the operator for the ground state baryon electromagnetic moment can be written as:

$$\mu_N \sigma_z = \langle N | \sum_i \mu_i \sigma_z^i | N \rangle \ , \tag{46}$$

where σ_z is the z projection of the baryon spin, while σ_z^i is the z projection of the i-th quark.

For the proton some simple algebra gives

$$\begin{aligned}
\mu_p &= \langle P\uparrow | \sum_i \mu_i \sigma_z^i | P\uparrow \rangle \\
&= \sum_i \frac{1}{\sqrt{2}}(\phi^\rho \chi^\rho(\uparrow) + \phi^\lambda \chi^\lambda(\uparrow)) \mu_i \sigma_z^i \frac{1}{\sqrt{2}}(\phi^\rho \chi^\rho(\uparrow) + \phi^\lambda \chi^\lambda(\uparrow)) \\
&= 2\mu_u \frac{2}{3} + \mu_d(-\frac{1}{3}) \\
&= \frac{4\mu_u - \mu_d}{3} \ .
\end{aligned} \tag{47}$$

Similarly, the neutron magnetic moment can be derived:

$$\mu_n = \frac{4\mu_d - \mu_u}{3} \ . \tag{48}$$

Given that $m_u = m_d$ is a good approximation, the ratio of magnetic moment between proton and neutron is

$$\frac{\mu_p}{\mu_n} = \frac{4\mu_u - \mu_d}{4\mu_d - \mu_u} = -\frac{3}{2} \ , \tag{49}$$

which is in good agreement with the experimental results -1.46. Nevertheless, if we assume that the nucleon mass $m_N \approx 3m_q$, the absolute values for μ_p and μ_n are also in good agreement with the experiment, although more sophisticated approaches are needed to better describe the nucleon magnetic moment (see e.g. Ref. [6]).

Similarly, the magnetic moment for Σ and Ξ can be derived,

$$\begin{aligned}
\mu_{\Sigma^+} &= \frac{4\mu_u - \mu_s}{3}, \\
\mu_{\Sigma^-} &= \frac{4\mu_d - \mu_s}{3}, \\
\mu_{\Xi^0} &= \frac{4\mu_s - \mu_u}{3}, \\
\mu_{\Xi^-} &= \frac{4\mu_s - \mu_d}{3}, \\
\mu_\Lambda &= \mu_{\Sigma^0} = \mu_s . \qquad (50)
\end{aligned}$$

Meanwhile, the magnetic transition between Λ and Σ^0 can be also evaluated:

$$\langle \Sigma^0(\uparrow) | \sum_i \mu_i \sigma_z^i | \Lambda(\uparrow) \rangle = \frac{\mu_u - \mu_d}{\sqrt{3}} . \qquad (51)$$

Although not all of these evaluations hold a good accuracy, the relations provide a possible way to fit the experimental data for these magnetic moments by treating μ_u $(= -2\mu_s)$ and μ_s as parameters. As shown by Ref. [7], an overall fit can be achieved with high accuracies.

One essential point is that one cannot negect the "color" degrees of freedom at all. As a simple test, if we antisymmetrize the total wavefunction without the color part taken into account, we then have, $\mu_p/\mu_n = \mu_d/\mu_u = -1/2$, which obviously deviates far away from the reality.

Back to the fact that the CQM is indeed tackling something essential, we are however confronted with big difficulties to disentangle it based on this model itself. As shown by recent development [6], the meson cloud effects and chiral phenomenology in baryon magnetic moments turned to be important, which however is not our subject here.

2.6 "missing resonances" in baryon spectroscopy

It should be useful for us to come back to the question about "missing resonances". As we have known that the quark model predicted a much richer baryon spectrum than observed in πN scatterings, a logic consequence

therefore could be, "The quark model may have overestimated the internal degrees of freedom of baryons". Following such a direction, a quark-diquark model was proposed in the literature, which could efficiently reduce the baryon internal degrees of freedom. According to this model, the short-range forces would tightly bind two quarks to form a scalar-isoscalar di-quark. Therefore, few baryon states were predicted. Unfortunately, such a treatment did not bring much significance to solving the puzzle. Even apart from the question whether such a model could account for the existing states (several "missing" positive parity states around 2 GeV would be ruled out), a sensible question arising is that it was too drastic to imagine that two of these three quarks had larger probabilities to be close to each other.

In a quite dramatical way, Koniuk and Isgur [8] suggested an alternative solution for this problem. They claimed that the missing states may be caused by experimental limit rather than a theoretical failure. It was suggested that some of those predicted states would have much weaker couplings to the πN channels, which were the only inelastic channels measured. Therefore, experiments on other meson decay channels, to which those missing states might have strong couplings, could be useful for pinning down missing resonance signals, e.g. ηN, $\eta' N$, $\Delta\pi$, ωN, ρN, etc. An immediate support for this idea came from pair-creation models [9, 10, 11] and partial wave analyses (PWA), of which calculations indicated that a few "missing resonances" indeed had stronger couplings to the $\Delta\pi$ and ρN channels.

This idea has effectively initiated a great number of experiments at JLab, ESRF, ELSA, MAMI, SPring-8, etc., namely, to search for "missing resonances" in meson photo- and electroproduction. Experimental evidence will also provide insights into baryon structure, which has been the subject in various theoretical efforts (see Ref. [12] for a recent review).

3 Electromagnetic coupling of baryons

The high intensity electron and photon beams serve as a clean electromagnetic probe in the study of nucleon internal structures. The baryon resonances can be can be excited by high energy photons and then investigated via their decays into various channels, e.g. γN, πN, $\pi\pi N$, ηN, $K\Lambda$, $K\Sigma$, ρN, ωN, $K^*\Lambda$, $K^*\Sigma$, etc. We shall concentrate here the baryon excitations and leave their decays to be discussed in meson photo- and electroproduction.

The electromagnetic excitation of baryon resonances in effect provides informations about the baryon electromagnetic form factors. In general, one useful observable is the helicity amplitude, i.e., $A_{1/2}(Q^2)$, $A_{3/2}(Q^2)$ and $S_{1/2}(Q^2)$ for $\gamma^* N \to N^*$, where $A_{1/2}$ and $A_{3/2}$ are transverse amplitudes for the nucleon spin anti-parallel or parallel to the incoming photon, and $S_{1/2}$ is the amplitude for the longitudinal (virtual) photon excitation. These quantities denote the $\gamma N N^*$ EM couplings and can be measured as a function of photon four-momentum Q^2, thus provide information about the baryon structures.

3.1 Photoproduction of baryon resonances in the nonrelativistic quark model

The NRCQM proposed a simple picture for the baryon resonances as we have seen in the previous Section. Meanwhile, taking the assumption that a single quark absorbs a photon and then is excited to be a resonance, one obtains again the simple picture for resonance photoexcitations. Supposing the constituent quark has a mass m_i ($\approx$ 330 MeV for the u and d), the magnetic moment of the constituent quark thus can be expressed as

$$\mu_i = g\frac{e_i}{2m_i} = \mu_0 \frac{e_i}{e} \ , \tag{52}$$

where $\mu_0 = e/2m_q = \sqrt{4\pi\alpha_e}/2m_q = \sqrt{4\pi} \times 0.13$ GeV^{-1} is the proton magnetic moment, and e_i is the fractional charge of the quark.

The electromagnetic field of a photon in form of the second quantization is

$$\mathbf{A}_k(\mathbf{r}_i) = \frac{1}{\sqrt{2\omega_\gamma}} \boldsymbol{\epsilon}_\gamma (a_k^\dagger e^{i\mathbf{k}\cdot\mathbf{r}_i} + a_k e^{-i\mathbf{k}\cdot\mathbf{r}_i}) \ , \tag{53}$$

where the photon couples to the i-th constituent quark. Taking the direction of the photon momentum $\mathbf{k}$ as the z-axis, and taking the advantage of the

permutation symmetry of the baryon wavefunctions, we can express the EM interaction Hamiltonian as

$$\begin{aligned} & \langle \Psi_f | H_1 + H_2 + H_3 | \Psi_i \rangle \\ = \; & \langle \Psi_f | P_{13} H_3 P_{13}^{-1} + P_{23} H_3 P_{23}^{-1} + H_3 \Psi_i \rangle \\ = \; & 3 \langle \Psi_f | H_3 | \Psi_i \rangle \ , \end{aligned} \tag{54}$$

where H_i is the single quark-photon interaction. The factor 3 implies that the photon couples to the three constituent the same way when the baryon total wavefunctions are antisymmetrized. One thus can "define" that in the EM excitation, the photon "only" couples to the third quark. Explicitly, the EM interaction can be expressed as:

$$\begin{aligned} H_{em} &= \sum_{i=1}^{3} H_i = 3H_3 \\ &= \frac{3}{\sqrt{2\omega_\gamma}} \mu_0 \sqrt{2} q_3 e^{ikz_3} \left(k S_{3+} + \frac{1}{g} P_{3+} \right) \ , \end{aligned} \tag{55}$$

where $S_{3+} \equiv S_x + iS_y$ and $P_{3+} \equiv P_x + iP_y$. The first term is the magnetic interaction which would raise the 3rd quark's spin projection by one unit, while the second term, the electric multipole interaction, would raise orbital angular momentum by one unit. In the end, the total angular momentum projection of the three quark system will be raised by one unit. We thus can express the above equation into a more compact form:

$$H_{em} = q_3 (A L_+ + B S_+) \ , \tag{56}$$

where quantity A and B are determined by the transitions in the spatial space:

$$A = \frac{3}{\sqrt{2\omega_\gamma}} \mu_0 \sqrt{2} \frac{1}{g} \langle \Psi_f | e^{ikz_3} P_{3+} | \Psi_i \rangle \ , \tag{57}$$

and

$$B = \frac{3}{\sqrt{2\omega_\gamma}} \mu_0 \sqrt{2} k \langle \Psi_f | e^{ikz_3} | \Psi_i \rangle \ . \tag{58}$$

Now given the initial and final state baryon wavefunctions, we can compute the EM transition amplitudes between these two states. The amplitudes can be expressed as two independent helicity amplitudes. Namely,

$$A_{1/2} = \langle \Psi_f (J^f, J_z^f = +\frac{1}{2}) | H_{em} | \Psi_i (J^i, J_z^i = -\frac{1}{2}) \rangle \ , \tag{59}$$

and

$$A_{3/2} = \langle \Psi_f(J^f, J^f_z = +\frac{3}{2}) | H_{em} | \Psi_i(J^i, J^i_z = +\frac{1}{2}) \rangle \ , \tag{60}$$

where the subscripts 1/2 and 3/2 denote the photon and nucleon helicity anti-parallel and parallel to each other.

We show below an example for the transition $\gamma p \to S_{11}(1535)$. Including the spin and isospin wavefunctions explicitly, we have

$$\begin{aligned}
A_{\frac{1}{2}} &= \sum_{L_z+S_z=1/2} \langle 1 L_z, \frac{1}{2} S_z | J \frac{1}{2} \rangle \frac{1}{2} [(\phi^\rho_p \chi^\lambda_{\frac{1}{2}} + \phi^\lambda_p \chi^\rho_{\frac{1}{2}}) \psi^\rho_{11 L_z}(\mathbf{R}, \boldsymbol{\rho}, \boldsymbol{\lambda}) \\
&\quad + (\phi^\rho_p \chi^\rho_{\frac{1}{2}} - \phi^\lambda_p \chi^\lambda_{\frac{1}{2}}) \psi^\lambda_{11 L_z}(\mathbf{R}, \boldsymbol{\rho}, \boldsymbol{\lambda})] \ q_3 (A L_+ + B S_+) \\
&\quad \times \frac{1}{2} (\phi^\rho_p \chi^\rho_{-\frac{1}{2}} + \phi^\lambda_p \chi^\lambda_{-\frac{1}{2}}) \psi^s_{000}(\mathbf{R}, \boldsymbol{\rho}, \boldsymbol{\lambda}) \\
&= \frac{1}{2\sqrt{2}} \Big[\langle 11, \frac{1}{2} \ -\frac{1}{2} | J \frac{1}{2} \rangle A (\langle \phi^\rho_p | q_3 | \phi^\rho_p \rangle - \langle \phi^\lambda_p | q_3 | \phi^\lambda_p \rangle) \\
&\quad + \langle 10, \frac{1}{2} \frac{1}{2} | J \frac{1}{2} \rangle B (\langle \phi^\rho_p | q_3 | \phi^\rho_p \rangle \langle \chi^\rho_{\frac{1}{2}} | S_{3+} | \chi^\rho_{-\frac{1}{2}} \rangle \\
&\quad - \langle \phi^\lambda_p | q_3 | \phi^\lambda_p \rangle \langle \chi^\lambda_{\frac{1}{2}} | S_{3+} | \chi^\lambda_{-\frac{1}{2}} \rangle) \Big] \ ,
\end{aligned} \tag{61}$$

where we have adopted the factor:

$$\langle \phi^\rho | \hat{O}_3 | \psi^\lambda \rangle \equiv \langle \phi^\lambda | \hat{O}_3 | \psi^\rho \rangle \equiv 0 \ , \tag{62}$$

since the operator $\hat{O}_3$ does not change the symmetry properties of quark 1 and 2.

Given the spin and flavor wavefunctions (Section 2), one can easily compute the following elements in spin and flavor space:

$$\begin{aligned}
\langle \chi^\rho_{\frac{1}{2}} | S_{3+} | \chi^\rho_{-\frac{1}{2}} \rangle &= 1 \\
\langle \chi^\lambda_{\frac{1}{2}} | S_{3+} | \chi^\lambda_{-\frac{1}{2}} \rangle &= -\frac{1}{3} \ ,
\end{aligned} \tag{63}$$

and

$$\begin{aligned}
\langle \phi^\rho_p | q_3 | \phi^\rho_p \rangle &= \frac{2}{3} \\
\langle \phi^\lambda_p | q_3 | \phi^\lambda_p \rangle &= 0 \ .
\end{aligned} \tag{64}$$

It is useful to give the corresponding elements for the neutron transition,

$$\begin{aligned}\langle\phi_n^\rho|q_3|\phi_n^\rho\rangle &= -\frac{1}{3}\\ \langle\phi_n^\lambda|q_3|\phi_n^\lambda\rangle &= \frac{1}{3}\,.\end{aligned} \tag{65}$$

Consequently, we have the helicity amplitude for $\gamma p \to S_{11}$:

$$\begin{aligned}A_{\frac{1}{2}} &= \frac{1}{3\sqrt{2}}\left[A\langle 11,\frac{1}{2}\,-\frac{1}{2}|J\frac{1}{2}\rangle + B\langle 10,\frac{1}{2}\frac{1}{2}|J\frac{1}{2}\rangle\right]\\ &= \frac{1}{3\sqrt{3}}A - \frac{1}{3\sqrt{6}}B\,,\end{aligned} \tag{66}$$

where for the S_{11}, $J = 1/2$. A and B can be worked out by explicitly introducing the spatial wavefunctions (See Appendix II for details). We thus have:

$$A_{\frac{1}{2}} = \mu_0\frac{1}{\sqrt{2\omega_\gamma}}\frac{2}{3}\left(\frac{\alpha_h}{g} + \frac{\mathbf{k}^2}{2\alpha_h}\right)e^{-\mathbf{k}^2/6\alpha_h^2}\,. \tag{67}$$

In the $S_{11}(1535)$ mass system, substituting $\alpha_h = 0.41$ GeV, $\mu_0 = \sqrt{4\pi}\times 0.13\ \mathrm{GeV}^{-1}$, and the kinematical variables $\omega_\gamma = |\mathbf{k}| = (M_{S_{11}}^2 - M_p^2)/2M_{S_{11}} = 0.48$ GeV, into Eq. (67) gives $A_{\frac{1}{2}} \approx 0.172\ \mathrm{GeV}^{-\frac{1}{2}}$. Compare to the experimental value $A_{\frac{1}{2}}^{exp.} = 0.090 \pm 0.030\ \mathrm{GeV}^{-\frac{1}{2}}$ (See PDG [4]), the naive quark model has overestimated the experimental values significantly.

Taking into account the Lorentz contracting effects, more realistic number can be obtained by introducing a Lorentz boost factor for the spatial part, i.e., $\frac{1}{\gamma_k} \equiv \frac{M_p}{E_p} = \frac{M_p}{\sqrt{M_p^2+\mathbf{k}^2}}$. The spatial part changes as, $f(|\mathbf{k}|) \to \frac{1}{\gamma_k^2}f\left(\frac{|\mathbf{k}|}{\gamma_k}\right)$. In this way, we have

$$A_{\frac{1}{2}} = \mu_0\frac{1}{\sqrt{2\omega_\gamma}}\frac{2}{3\gamma_k^2}\left(\frac{\alpha_h}{g} + \frac{\mathbf{k}^2}{2\alpha_h\gamma_k}\right)e^{-\mathbf{k}^2/6\alpha_h^2\gamma_k^2}\,, \tag{68}$$

which gives $A_{\frac{1}{2}} = 0.125\ \mathrm{GeV}^{-\frac{1}{2}}$, which is significantly reduced.

The property of the $S_{11}(1535)$ attracts a lot of attentions from experiment and theory at this moment. We shall come back to this with a brief discussion about the η production.

Here, we give a brief summary of the NRCQM prescription for baryon resonance excitations.

- The Delta resonance $P_{33}(1232)$ is classified as the ground state of isospin 3/2 baryons. Since it has the same spatial wavefunction as the nucleons, its excitation from the nucleons can only occur via the magnetic interaction, i.e., its helicity amplitudes $A_{\frac{1}{2}}$ and $A_{\frac{3}{2}}$ are both proportional to B. The quark model predicts:

$$\frac{A_{\frac{3}{2}}}{A_{\frac{1}{2}}} = \sqrt{3}\,, \tag{69}$$

while the PDG gives 1.67 [4].

- The Roper resonance $P_{11}(1440)$ is classified as the nucleon radial excitations with $N = 2$ and $L = 0$. Since compared to the proton and neutron, the $P_{11}(1470)$ has only the spatial wavefunction different from the nucleons, the quark model predicts

$$\frac{A^p_{\frac{1}{2}}(P_{11})}{A^n_{\frac{1}{2}}(P_{11})} = \frac{\mu_p}{\mu_n} = -\frac{3}{2}\,, \tag{70}$$

which is the ratio of the magnetic moments between the proton and neutron.

- The resonance $P_{13}(1720)$ and $F_{15}(1680)$ are assigned to representation $|\mathbf{56},^2\mathbf{8}, 2, 2, J\rangle$, which has the same spin and flavor wavefunctions as the ground state nucleons. Since the total spin for this representation is 1/2, in order to have spin 3/2 for the P_{13} and spin 5/2 for the F_{15}, the total orbital angular momentum projection $L_z \neq 0$. The transition can thus occur only via the A mode which is proportional to the charge operator. For the neutron transition, the transition element in the flavor space vanishes which results in $A^n_{\frac{3}{2}} \equiv 0$. This selection rule based on only quark model symmetry is consistent with the experimental observation.

- Moorhouse selection rule [13]: excitations of states of representation $[\mathbf{70},^4\mathbf{8}]$ from the proton vanish. Since the excitation changes the total spin from 1/2 to 3/2, it can only occur via the magnetic transition. Explicitly, the amplitude has the following expression:

$$A_{S_z} = \frac{1}{2}B\langle 10, \frac{3}{2}S_z|JS_z\rangle\langle\phi^\lambda_p|q_3|\phi^\lambda_p\rangle\langle\chi^s_{S_z}|S_{3+}|\chi^\lambda_{S_z-1}\rangle\,, \tag{71}$$

where we only keep the term of $B \sim \langle \psi_f^\lambda | e^{ikz_3} | \psi_i^s \rangle$ since the other one $\langle \psi_f^\rho | e^{ikz_3} | \psi_i^s \rangle \equiv 0$. Notice that $\langle \phi_p^\lambda | q_3 | \phi_p^\lambda \rangle \equiv 0$, it leads to $A_{S_z} = 0$.

3.2 Brief summary

The nonrelativistic quark model unavoidably suffers the problem that the excitation energies of the resonances are comparable to the constituent masses, which certainly makes the nonrelativistic treatment questionable. Although it is still unclear why such a nonrelativistic model works so well for the light flavor quark system consisting of u, d and s, there is no doubt of its extensive empirical successes. Various investigations are making progress on providing a firm basis for the quark model phenomenology, and it is believed to be a good approximation for non-perturbative QCD. For instance, the progress on lattice QCD is providing evidence for the effective degrees of freedom known as constituent quarks inside the nucleon. Readers are refered to Ref. [14] for a systematic and still-intriguing view of baryon structures and quark degrees of freedom in hadrons.

On the other hand, attempts to the development of a relativistic version have been made since early 70's [15]. During recent decades, progresses in the development of a relativistic-version quark model for baryon spectroscopy have been made by taking into account different ingredients in the quark interactions. These subjects deserve a full-time lecture by themselves, and we refer the readers to a recent review and references therein [12]. It is worth noting that Close and Li [16, 17, 18] showed that the inclusion of the spin-orbital angular momentum coupling in the EM interaction for the three quark system required a simultaneous consideration of recoil effects, which arose at the same order as their analogues in quark potential. Consequently, it suggested that a separation of the internal excitation from the motion of the center mass would lead to a "nonadditive" term, which was related to the Wigner transformation of the quark spins from the frame of the recoiling quark to the frame of the recoiling baryon. Interestingly, it was found that in most cases, the inclusion of the relativistic effects survived the nonrelativistic quark model [19].

4 Study baryon properties via meson photo- and electroproduction

As presented in the previous Section, the high intensity electron and photon beams provide clean probes for the study of internal structure of baryon resonances. In this Section, we will concentrate on meson photo- and electroproduction reaction. The production of pseudoscalar and vector meson will be discussed.

4.1 Pseudoscalar meson production

We discuss pseudoscalar meson photoproduction in the quark model.

4.1.1 The kinematics

We select the center of motion (c.m.) system for meson photoproduction. As shown by Fig. 2, the production plane is determined by x_i (x_f) and z_i (z_f) -axis. The energies and momenta of the initial photon and nucleon are denoted by $(\omega_\gamma, \mathbf{k})$ and $(E_i, \mathbf{P}_i)$, while those of the final state meson and nucleon are denoted by $(\omega_m,\ \mathbf{q})$ and $(E_f,\ \mathbf{P}_f)$. Note that $\mathbf{P}_i = -\mathbf{k}$ and $\mathbf{P}_f = -\mathbf{q}$.

Count over the polarization of the two-body reaction system, in pseudoscalar meson photoproduction, the degrees of freedom is $2\times2\times2$. Given that the two transverse polarizations of the real photon are not independent, at each energy W and each angle $\theta_{c.m.}$, we need 4 amplitudes (8 complex numbers) to determine the dynamics. Taking into account the cross section which provides a normalization constraint, we still need 7 complex numbers.

A standard way to express the four independent transition amplitudes is to define them in the helicity space:

$$\begin{aligned}
H_1 &= \langle \lambda_f = -1/2 | \mathcal{T} | \lambda_\gamma = +1, \lambda_i = +1/2 \rangle \\
&= \langle m_f = +1/2 | \mathcal{T} | m_\gamma = +1, m_i = -1/2 \rangle \\
H_2 &= \langle \lambda_f = -1/2 | \mathcal{T} | \lambda_\gamma = +1, \lambda_i = -1/2 \rangle \\
&= \langle m_f = +1/2 | \mathcal{T} | m_\gamma = +1, m_i = +1/2 \rangle \\
H_3 &= \langle \lambda_f = +1/2 | \mathcal{T} | \lambda_\gamma = +1, \lambda_i = +1/2 \rangle \\
&= \langle m_f = -1/2 | \mathcal{T} | m_\gamma = +1, m_i = -1/2 \rangle \\
H_4 &= \langle \lambda_f = +1/2 | \mathcal{T} | \lambda_\gamma = +1, \lambda_i = -1/2 \rangle \\
&= \langle m_f = -1/2 | \mathcal{T} | m_\gamma = +1, m_i = +1/2 \rangle, \qquad (72)
\end{aligned}$$

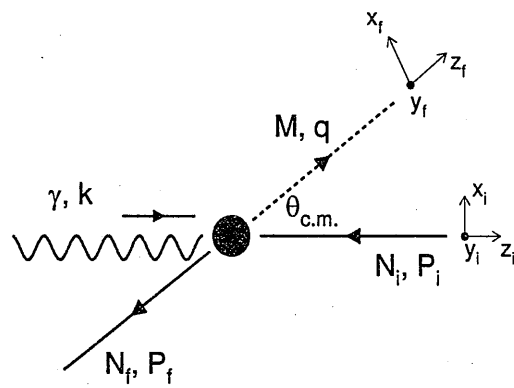

Figure 2: The kinematics for meson photoproduction.

where λ_i (m_i) and λ_f (m_f) are helicities (spin projections) of the initial and final nucleons and λ_γ (m_γ) is the helicity (spin projection) of the photon. Amplitudes with $\lambda_\gamma = -1$ are not independent of those with $\lambda_\gamma = +1$ due to parity conservation. We understand that H_a (a = 1,2,3,4) is also function of energies and momenta of the particles which are not explicitly shown. Our consequent job thus is to work out these amplitudes using a dynamical model.

Before we proceed to the next Section to derive the transition amplitudes using a dynamical model, it is useful to have an idea about the experimental observables, of which a complete set of measurements contains all the dynamical information. It was discussed in the literatures, an unambiguous determination of the pseudoscalar meson photoproduction (in a fixed isospin channel) needs a complete set of three single polarization asymmetries, four independent double polarization asymmetries and the cross section measurement.

As an example, one can do the experiment to study the polarized photon asymmetry Σ, which is defined as

$$\Sigma(\theta) = \frac{\sigma_\perp - \sigma_\parallel}{\sigma_\perp + \sigma_\parallel} , \tag{73}$$

where $\sigma_\perp$ is the cross section for polarizing the photon along the y-axis (perpendicular to the production plane), while $\sigma_\parallel$ is that for polarizing the photon along the x-axis (parallel to the production plane). Such a linearly polarized photon can be expressed in terms of the helicity states of the incoming photon ($\epsilon_{\gamma\pm} = \mp(1, \pm i, 0)/\sqrt{2}$), i.e.,

$$\begin{aligned} \epsilon_\perp &= \hat{y} = i(\epsilon_{\gamma+} + \epsilon_{\gamma-})/\sqrt{2} \\ \epsilon_\parallel &= \hat{x} = -(\epsilon_{\gamma+} - \epsilon_{\gamma-})/\sqrt{2} . \end{aligned} \tag{74}$$

One can thus have

$$\begin{aligned} \sigma_\perp(\theta) &\sim (|H_1 + H_4|^2 + |H_2 - H_3|^2) \\ \sigma_\parallel(\theta) &\sim (|H_1 - H_4|^2 + |H_2 + H_3|^2) . \end{aligned} \tag{75}$$

More explicitly, we have

$$\Sigma(\theta) = \frac{1}{\mathcal{I}} \mathrm{Re}(H_1 H_4^* - H_2 H_3^*) \tag{76}$$

where $\mathcal{I} \equiv \frac{1}{2}\sum_i H_i^2$ denotes the unpolarized cross section which normalizes the asymmetry to the range $-1 \leq \Sigma \leq +1$.

Similarly, the polarized target asymmetry T and the recoil polarization asymmetry P can be defined:

$$\begin{aligned} T(\theta) &= \frac{\sigma_+ - \sigma_-}{\sigma_+ + \sigma_-} \\ &= \frac{1}{\mathcal{I}} \mathrm{Im}(H_1 H_2^* + H_3 H_4^*) , \end{aligned} \tag{77}$$

where σ_+ and σ_- are cross sections for the target nucleon polarized "up" and "down" in the $\hat{y}$ direction. Similar to the target polarization, but polarize the final state nucleon along the $\hat{y}' \parallel \hat{y}$, and measure the cross sections "up" and "down", we have

$$\begin{aligned} P(\theta) &= \frac{\sigma'_+ - \sigma'_-}{\sigma'_+ + \sigma'_-} \\ &= -\frac{1}{\mathcal{I}} \mathrm{Im}(H_1 H_3^* + H_2 H_4^*) . \end{aligned} \tag{78}$$

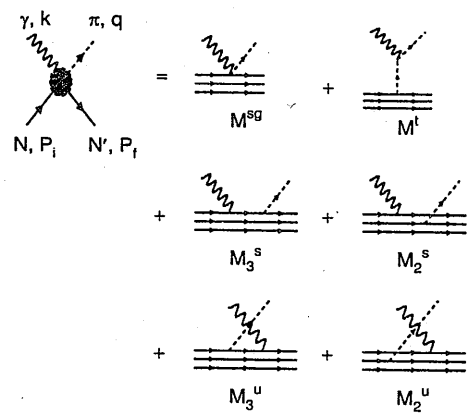

Figure 3: The schematic diagram for tree level transition processes in pseudoscalar meson photoproduction.

The differential cross section is

$$\frac{d\sigma}{d\Omega_{c.m.}} = \alpha_e \alpha_s \frac{|\mathbf{q}|}{8s|\mathbf{k}|} \frac{(E_f + M_f)(E_i + M_i)}{M_f M_i} \frac{1}{2} \sum_{i=1}^{4} H_i^2 \ . \tag{79}$$

The transition amplitudes of pseudoscalar meson photoproduction can be expressed in terms of standard CGLN amplitudes [20], or multipoles by a standard transformation [21, 22].

4.1.2 The theory

For pion photoproduction, the low energy theorem (LET) provides a crucial test near threshold. As shown in previous investigation by Li [23], to recover the LET, one has to rely on the low energy QCD Lagrangian which keeps the

meson-baryon interaction invariant under the chiral transformation. Combining the low energy QCD Lagrangian with the quark model, we introduce the quark-meson interaction through the effective Lagrangian [24, 25]:

$$\mathcal{L} = \overline{\psi}[\gamma_\mu(i\partial^\mu + V^\mu + \gamma_5 A^\mu) - m]\psi + \cdots, \tag{80}$$

where the vector and axial currents are

$$\begin{aligned} V_\mu &= \frac{1}{2}(\xi^\dagger\partial_\mu\xi + \xi\partial_\mu\xi^\dagger), \\ A_\mu &= i\frac{1}{2}(\xi^\dagger\partial_\mu\xi - \xi\partial_\mu\xi^\dagger), \end{aligned} \tag{81}$$

and the chiral transformation is,

$$\xi = e^{i\phi_m/f_m}, \tag{82}$$

where f_m is the decay constant of the meson. The quark field ψ in the SU(3) symmetry is

$$\psi = \begin{pmatrix} \psi(u) \\ \psi(d) \\ \psi(s) \end{pmatrix}, \tag{83}$$

and the meson field ϕ_m is a 3⊗3 matrix:

$$\phi_m = \begin{pmatrix} \frac{1}{\sqrt{2}}\pi^0 + \frac{1}{\sqrt{6}}\eta & \pi^+ & K^+ \\ \pi^- & -\frac{1}{\sqrt{2}}\pi^0 + \frac{1}{\sqrt{6}}\eta & K^0 \\ K^- & \overline{K}^0 & -\sqrt{\frac{2}{3}}\eta \end{pmatrix}, \tag{84}$$

where the pseudoscalar mesons π, η and K are treated as Goldstone bosons. Thus, the Lagrangian in Eq. (80) is invariant under the chiral transformation. Expanding the nonlinear field ξ in Eq. (82) in terms of the Goldstone boson field ϕ_m, i.e. $\xi = 1 + i\phi_m/f_m + \cdots$, we obtain the standard quark-meson pseudovector coupling at tree level:

$$H_m = \sum_j \frac{1}{f_m}\overline{\psi}_j\gamma_\mu^j\gamma_5^j\psi_j\partial^\mu\phi_m \ , \tag{85}$$

where ψ_j ($\overline{\psi}_j$) represents the jth quark (anti-quark) field in the nucleon.

It is still not clear whether the Goldstone bosons couple to the nucleon through a pseudoscalar or pseudovector coupling, or even both. To our

present knowledge, at low energies, the pseudovector coupling satisfies partial conservation of axial current (PCAC) and is consistent with the LET and chiral perturbation theory to leading order, while the high energy study prefers a pseudoscalar coupling. As pointed out in Ref. [26], the operators for the pseudoscalar and pseudovector coupling have the same leading order expression at quark tree level. Therefore, Eq. (85) can be regarded as a reasonable starting point for investigations of pion photoproduction in the resonance region.

The quark-photon electromagnetic coupling is

$$H_e = -\sum_j e_j \gamma_\mu^j A^\mu(\mathbf{k}, \mathbf{r}), \tag{86}$$

where the photon has three-momentum $\mathbf{k}$, and the constituent quark carries a charge e_j.

The photoproduction amplitudes can be expressed in terms of the Mandelstam variables,

$$M_{fi} = M_{fi}^{sg} + M_{fi}^{s} + M_{fi}^{u} + M_{fi}^{t}, \tag{87}$$

where M_{fi}^{sg} is the seagull term and M_{fi}^{s}, M_{fi}^{u} and M_{fi}^{t} represent the s-, u-, and t-channel processes as illustrated in Fig. 3. As shown in Ref. [25], the seagull term is composed of two parts,

$$M_{fi}^{sg} = \langle N_f | H_{m,e} | N_i \rangle + i \langle N_f | [g_e, H_m] | N_i \rangle, \tag{88}$$

where $|N_i\rangle$ and $|N_f\rangle$ are the initial and final state nucleon, respectively, and

$$H_{m,e} = \sum_j \frac{e_m}{f_m} \phi_m(\mathbf{q}, \mathbf{r}_j) \overline{\psi}_j \gamma_\mu^j \gamma_5^j \psi_j A^\mu(\mathbf{k}, \mathbf{r}_j) \tag{89}$$

is the contact term from the pseudovector coupling, and

$$g_e = \sum_j e_j \mathbf{r}_j \cdot \boldsymbol{\epsilon}_\gamma e^{i\mathbf{k}\cdot\mathbf{r}_j} \tag{90}$$

comes from the transformation of the electromagnetic interaction in the s- and u-channel [27, 25].

The s- and u-channel amplitudes have the following expression:

$$\begin{aligned} & M_{fi}^{s} + M_{fi}^{u} \\ = \; & i\omega_\gamma \sum_j \langle N_f | H_m | N_j \rangle \langle N_j | \frac{1}{E_i + \omega_\gamma - E_j} h_e | N_i \rangle \\ + \; & i\omega_\gamma \sum_j \langle N_f | h_e \frac{1}{E_i - \omega_m - E_j} | N_j \rangle \langle N_j | H_m | N_i \rangle, \end{aligned} \tag{91}$$

where

$$h_e = \sum_j e_j \mathbf{r}_j \cdot \boldsymbol{\epsilon}_\gamma (1 - \boldsymbol{\alpha}_j \cdot \hat{\mathbf{k}}) e^{i\mathbf{k}\cdot\mathbf{r}_j}, \tag{92}$$

and $\hat{\mathbf{k}} \equiv \mathbf{k}/\omega_\gamma$ is the unit vector in the direction of the photon momentum.

The nonrelativistic expansions of Eqs. (92) and (85) become [25]:

$$h_e = \sum_j \left[e_j \mathbf{r}_j \cdot \boldsymbol{\epsilon}_\gamma - \frac{e_j}{2m_j} \boldsymbol{\sigma}_j \cdot (\boldsymbol{\epsilon}_\gamma \times \hat{\mathbf{k}}) \right] e^{i\mathbf{k}\cdot\mathbf{r}_j}, \tag{93}$$

and

$$\begin{aligned} H_m^{nr} \;=\; & \sum_j \left[\frac{\omega_m}{E_f + M_f} \boldsymbol{\sigma}_j \cdot \mathbf{P}_f + \frac{\omega_m}{E_i + M_i} \boldsymbol{\sigma}_j \cdot \mathbf{P}_i \right. \\ & \left. - \boldsymbol{\sigma}_j \cdot \mathbf{q} + \frac{\omega_m}{2\mu_q} \boldsymbol{\sigma}_j \cdot \mathbf{p}_j \right] \frac{\hat{I}_j}{g_A} e^{-i\mathbf{q}\cdot\mathbf{r}_j}, \end{aligned} \tag{94}$$

where M_i (M_f), E_i (E_f) and $\mathbf{P}_i$ ($\mathbf{P}_f$) are mass, energy and three-vector momentum for the initial (final) nucleon; $\mathbf{r}_j$ and $\mathbf{p}_j$ are the internal coordinate and momentum for the jth quark in the nucleon rest system. Note that, g_A, the axial vector coupling, relates the hadronic operator $\boldsymbol{\sigma}$ to the quark operator $\boldsymbol{\sigma}_j$ for the jth quark, and is defined by,

$$\langle N_f | \sum_j \hat{I}_j \boldsymbol{\sigma}_j | N_i \rangle \equiv g_A \langle N_f | \boldsymbol{\sigma} | N_i \rangle. \tag{95}$$

4.1.3 Transition amplitudes in the harmonic oscillator basis

The seagull term in this model differs from the traditional definition due to the appearance of a transformed electromagnetic interaction coupling to the meson at the same vertex. This term can be worked out explicitly in the SU(6)⊗O(3) symmetry limit:

$$M_{fi}^{sg} = -e^{-(\mathbf{k}-\mathbf{q})^2/6\alpha^2} e_m \left[1 + \frac{\omega_m}{2} \left(\frac{1}{E_i + M_i} + \frac{1}{E_f + M_f} \right) \right] \boldsymbol{\sigma} \cdot \boldsymbol{\epsilon}_\gamma, \tag{96}$$

where the exponential factor is the corresponding quark model form factor in the harmonic oscillator basis.

The t-channel charged pion exchange amplitude can be derived by treating the exchanged pion as an elementary particle:

$$M_{fi}^{t} = e^{-(\mathbf{k}-\mathbf{q})^2/6\alpha^2} \frac{e_m (M_f + M_i)}{q \cdot k} \left(\frac{\boldsymbol{\sigma} \cdot \mathbf{q}}{E_f + M_f} - \frac{\boldsymbol{\sigma} \cdot \mathbf{k}}{E_i + M_i} \right) \mathbf{q} \cdot \boldsymbol{\epsilon}_\gamma, \tag{97}$$

where q and k are four-vector-momenta of the pion and photon, respectively.

As illustrated in Eqs. (96) and (97), the leading order amplitudes from chiral perturbation theory are reproduced. The quark model modifications to these two terms come from three-body effects, which add an additional term (the second term in Eq. (96)) to the amplitudes. Note also the appearance of a form factor, which is essential to sustain the forward "spike" in π^+ production.

Generalized expressions for the s- and u-channel amplitudes are:

$$M^s_{fi} = \sum_n (M^s_2 + M^s_3) e^{-(\mathbf{k}^2+\mathbf{q}^2)/6\alpha^2}, \tag{98}$$

and

$$M^u_{fi} = \sum_n (M^u_2 + M^u_3) e^{-(\mathbf{k}^2+\mathbf{q}^2)/6\alpha^2}, \tag{99}$$

where the M_3 and M_2 represent transitions in which the photon and meson couple to the same quark or different quarks, respectively. The general framework was presented in Ref. [25]. Here, we present the transition amplitudes in terms of the harmonic oscillator shell n as follows:

$$\begin{aligned}
\frac{M^s_3}{g^s_3} &= -\frac{1}{2m_q}\left[ig_v \mathbf{A}_s\cdot(\boldsymbol{\epsilon}_\gamma\times\mathbf{k}) - \boldsymbol{\sigma}\cdot(\mathbf{A}_s\times(\boldsymbol{\epsilon}_\gamma\times\mathbf{k}))\right] \\
&\quad \times \frac{M_n}{n!(P_i\cdot k - nM\omega_h)}\left(\frac{\mathbf{k}\cdot\mathbf{q}}{3\alpha^2}\right)^n \\
&+ \frac{1}{6}\left[\frac{\omega_\gamma\omega_m}{\mu_q}(1+\frac{\omega_\gamma}{2m_q})\boldsymbol{\sigma}\cdot\boldsymbol{\epsilon}_\gamma + \frac{2\omega_\gamma}{\alpha^2}\boldsymbol{\sigma}\cdot\mathbf{A}_s\boldsymbol{\epsilon}_\gamma\cdot\mathbf{q}\right] \\
&\quad \times \frac{M_n}{(n-1)!(P_i\cdot k - nM\omega_h)}\left(\frac{\mathbf{k}\cdot\mathbf{q}}{3\alpha^2}\right)^{n-1} \\
&+ \frac{\omega_\gamma\omega_m}{18\mu_q\alpha^2}\boldsymbol{\sigma}\cdot\mathbf{k}\boldsymbol{\epsilon}_\gamma\cdot\mathbf{q}\frac{M_n}{(n-2)!(P_i\cdot k - nM\omega_h)}\left(\frac{\mathbf{k}\cdot\mathbf{q}}{3\alpha^2}\right)^{n-2},
\end{aligned} \tag{100}$$

and

$$\begin{aligned}
\frac{M^s_2(-2)^n}{g^s_2} &= -\frac{1}{2m_q}\left[ig'_v \mathbf{A}_s\cdot(\boldsymbol{\epsilon}_\gamma\times\mathbf{k}) - g'_a\boldsymbol{\sigma}\cdot(\mathbf{A}_s\times(\boldsymbol{\epsilon}_\gamma\times\mathbf{k}))\right] \\
&\quad \times \frac{M_n}{n!(P_i\cdot k - nM\omega_h)}\left(\frac{\mathbf{k}\cdot\mathbf{q}}{3\alpha^2}\right)^n \\
&+ \frac{1}{6}\left[\frac{\omega_\gamma\omega_m}{\mu_q}(1+g'_a\frac{\omega_\gamma}{2m_q})\boldsymbol{\sigma}\cdot\boldsymbol{\epsilon}_\gamma + \frac{2\omega_\gamma}{\alpha^2}\boldsymbol{\sigma}\cdot\mathbf{A}_s\boldsymbol{\epsilon}_\gamma\cdot\mathbf{q}\right]
\end{aligned}$$

$$\times \frac{M_n}{(n-1)!(P_i\cdot k - nM\omega_h)}\left(\frac{\mathbf{k}\cdot\mathbf{q}}{3\alpha^2}\right)^{n-1}$$
$$+ \quad \frac{\omega_\gamma\omega_m}{18\mu_q\alpha^2}\boldsymbol{\sigma}\cdot\mathbf{k}\boldsymbol{\epsilon}_\gamma\cdot\mathbf{q}\frac{M_n}{(n-2)!(P_i\cdot k - nM\omega_h)}\left(\frac{\mathbf{k}\cdot\mathbf{q}}{3\alpha^2}\right)^{n-2} \quad (101)$$

result for the s-channel, while

$$\begin{aligned}\frac{M_3^u}{g_3^u} &= \frac{1}{2m_q}\left[ig_v\mathbf{A}_u\cdot(\boldsymbol{\epsilon}_\gamma\times\mathbf{k}) + \boldsymbol{\sigma}\cdot(\mathbf{A}_u\times(\boldsymbol{\epsilon}_\gamma\times\mathbf{k}))\right]\\ &\times\frac{M_n}{n!(P_f\cdot k + nM\omega_h)}\left(\frac{\mathbf{k}\cdot\mathbf{q}}{3\alpha^2}\right)^{n}\\ &- \frac{1}{6}\left[\frac{\omega_\gamma\omega_m}{\mu_q}(1+\frac{\omega_\gamma}{2m_q})\boldsymbol{\sigma}\cdot\boldsymbol{\epsilon}_\gamma + \frac{2\omega_\gamma}{\alpha^2}\boldsymbol{\sigma}\cdot\mathbf{A}_u\boldsymbol{\epsilon}_\gamma\cdot\mathbf{q}\right]\\ &\times\frac{M_n}{(n-1)!(P_f\cdot k + nM\omega_h)}\left(\frac{\mathbf{k}\cdot\mathbf{q}}{3\alpha^2}\right)^{n-1}\\ &- \frac{\omega_\gamma\omega_m}{18\mu_q\alpha^2}\boldsymbol{\sigma}\cdot\mathbf{k}\boldsymbol{\epsilon}_\gamma\cdot\mathbf{q}\frac{M_n}{(n-2)!(P_f\cdot k + nM\omega_h)}\left(\frac{\mathbf{k}\cdot\mathbf{q}}{3\alpha^2}\right)^{n-2}, \quad (102)\end{aligned}$$

and

$$\begin{aligned}\frac{M_2^u(-2)^n}{g_2^u} &= \frac{1}{2m_q}\left[ig_v'\mathbf{A}_u\cdot(\boldsymbol{\epsilon}_\gamma\times\mathbf{k}) - g_a'\boldsymbol{\sigma}\cdot(\mathbf{A}_u\times(\boldsymbol{\epsilon}_\gamma\times\mathbf{k}))\right]\\ &\times\frac{M_n}{n!(P_f\cdot k + nM\omega_h)}\left(\frac{\mathbf{k}\cdot\mathbf{q}}{3\alpha^2}\right)^{n}\\ &- \frac{1}{6}\left[\frac{\omega_\gamma\omega_m}{\mu_q}(1+g_a'\frac{\omega_\gamma}{2m_q})\boldsymbol{\sigma}\cdot\boldsymbol{\epsilon}_\gamma + \frac{2\omega_\gamma}{\alpha^2}\boldsymbol{\sigma}\cdot\mathbf{A}_u\boldsymbol{\epsilon}_\gamma\cdot\mathbf{q}\right]\\ &\times\frac{M_n}{(n-1)!(P_f\cdot k + nM\omega_h)}\left(\frac{\mathbf{k}\cdot\mathbf{q}}{3\alpha^2}\right)^{n-1}\\ &- \frac{\omega_\gamma\omega_m}{18\mu_q\alpha^2}\boldsymbol{\sigma}\cdot\mathbf{k}\boldsymbol{\epsilon}_\gamma\cdot\mathbf{q}\frac{M_n}{(n-2)!(P_f\cdot k + nM\omega_h)}\left(\frac{\mathbf{k}\cdot\mathbf{q}}{3\alpha^2}\right)^{n-2} \quad (103)\end{aligned}$$

are corresponding terms for the u-channel. Vectors $\mathbf{A}_s$ and $\mathbf{A}_u$ are determined by the meson transitions in the s- and u-channels:

$$\mathbf{A}_s = -\left(\frac{\omega_m}{E_f+M_f}+1\right)\mathbf{q}, \quad (104)$$

and

$$\mathbf{A}_u = -\left(\frac{\omega_m}{E_i+M_i}+\frac{\omega_m}{E_f+M_f}\right)\mathbf{k} - \left(\frac{\omega_m}{E_f+M_f}+1\right)\mathbf{q}. \quad (105)$$

In Eqs. (100)-(103), P_i and P_f are four-vector momenta of the initial and final state nucleons in the total c.m. system; M_n is the mass of excited state in the nth shell, while ω_h $(= \alpha^2/m_q)$ is the typical energy of the harmonic oscillator potential. The factor $M_n/(P_i \cdot k - nM\omega_h)$ and $M_n/(P_f \cdot k + nM\omega_h)$ have clear physical meanings in the s- and u-channels that can be related to the propagators.

The quark level operators have been related to the hadronic level ones through g-factors defined as below:

$$g_3^u = \langle N_f | \sum_j e_j \hat{I}_j \sigma_j^z | N_i \rangle / g_A, \tag{106}$$

$$g_2^u = \langle N_f | \sum_{i \neq j} e_j \hat{I}_i \sigma_i^z | N_i \rangle / g_A, \tag{107}$$

$$g_v = \frac{1}{g_3^u g_A} \langle N_f | \sum_j e_j \hat{I}_j | N_i \rangle, \tag{108}$$

$$g_v' = \frac{1}{3 g_2^u g_A} \langle N_f | \sum_{i \neq j} e_j \hat{I}_i \boldsymbol{\sigma}_i \cdot \boldsymbol{\sigma}_j | N_i \rangle, \tag{109}$$

and

$$g_a' = \frac{1}{2 g_2^u g_A} \langle N_f | \sum_{i \neq j} e_j \hat{I}_i (\boldsymbol{\sigma}_i \times \boldsymbol{\sigma}_j)_z | N_i \rangle. \tag{110}$$

Numerical values for these g-factors can be explicitly calculated in the SU(6)⊗O(3) symmetry limit [25].

So far, the resonance contributions have not been explicitly separated out. The intermediate states are still degenerate in the quantum number of the harmonic oscillator shell. Notice that the factor $M_n/(P_i \cdot k - nM\omega_h)$ can be written as $2M_n/(s - M_n^2)$, where $s = W^2 = (P_i + k)^2$ is the square of the total c.m. energy, we thus substitute a Breit-Wigner distribution for the resonances, $2M_R/(s - M_R^2 + iM_R\Gamma_R(\mathbf{q}))$, where the resonance mass and width effects are taken into account. Explicitly, all the contributing resonances with $n \leq 2$ in the quark model symmetry limit can be included. In pion production, this is the place where the imaginary part of the transition amplitude comes out. The role of the imaginary part can be investigated more directly in the polarization observables, e.g. polarized target asymmetry T and recoil polarization asymmetry P, where direct interferences between the real and imaginary part are highlighted.

Consequently, we must separate out the resonance excitation amplitudes for each n. For $n = 0$, the contributing terms are the Delta resonance

excitation and the nucleon pole terms. One can see that only the first terms in Eqs. (100)-(103) can contribute. For the s-channel, we have

$$\begin{aligned} M^s(n=0) &= -\frac{1}{2m_q}[i(g_3^s g_v + g_2^u g_v')\mathbf{A}_s \cdot (\boldsymbol{\epsilon}_\gamma \times \mathbf{k}) \\ &\quad -(g_3^s + g_2^u g_a')\boldsymbol{\sigma} \cdot (\mathbf{A}_s \times (\boldsymbol{\epsilon}_\gamma \times \mathbf{k}))] \\ &\quad \times \frac{M_0}{P_i \cdot k - \delta M^2/2} e^{-(\mathbf{k}^2+\mathbf{q}^2)/6\alpha^2}, \end{aligned} \tag{111}$$

where $\delta M^2/2$ denotes the mass square difference between the intermediate state and initial state nucleon. The amplitude for the spin 1/2 nucleon pole term is,

$$\begin{aligned} M^s(nucleon) &= \langle N_f|H_m|N(J=1/2)\rangle\langle N(J=1/2)|h_e|N_i\rangle \\ &= -\frac{i\mu_i}{2m_q}\boldsymbol{\sigma} \cdot \mathbf{A}_s\boldsymbol{\sigma} \cdot (\boldsymbol{\epsilon}_\gamma \times \mathbf{k}) \\ &\quad \times \frac{2M_N}{s - M_N^2} e^{-(\mathbf{k}^2+\mathbf{q}^2)/6\alpha^2}, \end{aligned} \tag{112}$$

where we have used $\delta M^2/2 = 0$ and $P_i \cdot k = (s - M_N^2)/2$ for the nucleon pole; μ_i is the magnetic moment of the initial nucleon in terms of the nuclear magnetic moment $e/2M_N$. In this way, the Delta resonance excitation amplitude is derived,

$$\begin{aligned} M^s(\Delta) &= M^s(n=0) - M^s(nucleon) \\ &= -\frac{1}{2m_q}[i(g_3^s g_v + g_2^u g_v' - \mu_i)\mathbf{A}_s \cdot (\boldsymbol{\epsilon}_\gamma \times \mathbf{k}) \\ &\quad -(g_3^s + g_2^u g_a' - \mu_i)\boldsymbol{\sigma} \cdot (\mathbf{A}_s \times (\boldsymbol{\epsilon}_\gamma \times \mathbf{k}))] \\ &\quad \times \frac{2M_\Delta}{s - M_\Delta^2 + iM_\Delta\Gamma_\Delta} e^{-(\mathbf{k}^2+\mathbf{q}^2)/6\alpha^2}, \end{aligned} \tag{113}$$

where $M_0/(P_i \cdot k - \delta M^2/2) \equiv 2M_\Delta/(s - M_N^2 - (M_\Delta^2 - M_N^2))$ is used and the Breit-Wigner distribution is introduced after the separation of the spin operators.

Similarly, the Delta resonance and nucleon pole terms in the u-channel with $n = 0$ can be separated:

$$\begin{aligned} M^u(nucleon) &= \langle N_f|h_e|N(J=1/2)\rangle\langle N(J=1/2)|H_m|N_i\rangle \\ &= -\frac{i\mu_f}{2m_q}\boldsymbol{\sigma} \cdot (\boldsymbol{\epsilon}_\gamma \times \mathbf{k})\boldsymbol{\sigma} \cdot \mathbf{A}_u \\ &\quad \times \frac{2M_N}{u - M_N^2} e^{-(\mathbf{k}^2+\mathbf{q}^2)/6\alpha^2}, \end{aligned} \tag{114}$$

and

$$M^u(\Delta) = -\frac{1}{2m_q}[i(g_3^u g_v + g_2^u g_v' - \mu_f)\mathbf{A}_u \cdot (\epsilon_\gamma \times \mathbf{k}) + (g_3^u - g_2^u g_a' - \mu_f)\boldsymbol{\sigma} \cdot (\mathbf{A}_u \times (\epsilon_\gamma \times \mathbf{k}))] \times \frac{2M_\Delta}{u - M_\Delta^2} e^{-(\mathbf{k}^2+\mathbf{q}^2)/6\alpha^2}, \quad (115)$$

where μ_f is the magnetic moment of the final state nucleon in terms of the proton magnetic moment $e/2m_q$.

Several points can be learned from Eqs. (100)-(103). First, the nucleon pole terms and Delta resonance transition only involve the c.m. part of their spatial wavefunctions. Therefore, only the first terms in these equations contribute to the amplitudes. For resonances with $n > 0$, the internal motion of constituents will be involved. Specifically, terms relating to $(n-1)$ are due to correlations between c.m. motion and internal ones, while $(n-2)$ terms are due to correlations between internal motions at two vertices.

Secondly, amplitudes for processes having the photon and meson coupled to different quarks are relatively suppressed. This can be seen clearly through the factors $(-2)^n$. In Ref. [28], this qualitative feature was discussed, but not shown explicitly. Here, we show how the indirect diagram can be exactly calculated, and show that the direct diagram will become dominant with increasing energy and the excitation of higher states.

From Eq. (113), the analytical expression for the Delta multipole can be derived,

$$M_{1+}^{3/2} = -g_{\pi NN} g_R \frac{1}{2m_q}\left[\frac{\omega_m}{E_f + M_f} + 1\right] \frac{2M_\Delta}{s - M_\Delta^2 + iM_\Delta\Gamma_\Delta} e^{-(\mathbf{k}^2+\mathbf{q}^2)/6\alpha^2}, \quad (116)$$

where $g_R \equiv g_3^s g_v + g_2^u g_v' - \mu_i$, and $g_{\pi NN}$ has been taken into account. The real and imaginary parts of the Delta multipole $M_{1+}^{3/2}$ are calculated and shown in Fig. 4. We shall discuss the quark model form factor effects in the following Section. Therefore, it would be useful to present the calculation of $M_{1+}^{3/2}$ *without* the exponent, which comes from the spatial integral and serves as a form factor for the multipole. As illustrated by the dotted and dot-dashed curve in Fig. 4, apparent deviations from the experimental data occur with the increasing energies. In another word, the quark model turns to be indispensible to account for the correct energy dependence.

Multipole $E_{1+}^{3/2}$ vanishes in this approach for the s-channel Delta resonance. Experimentally, $E_{1+}^{3/2}$ is found to be much smaller than $M_{1+}^{3/2}$ [29, 30].

4.1.4 Pion photoproduction

The study of pion photoproduction provided a direct test of this model approach. We shall not go to details about the numerical results, but only outline some features which would be sensible for a fundamental framework [31].

- We showed that an overall fit of the data up to 500 MeV was obtained by introducing the effective Lagrangian for the quark-meson coupling and treating the $\pi N\Delta$ coupling strength as a free parameter. This result had non-trivial implications. It suggested that the quark model within an effective Lagrangian provided correct signs and even reasonable form factors for the Delta excitation and nucleon pole terms.

- The role of the it u-channel resonance excitations was highlighted, which was not included in isobaric models.

- In π^+ photoproduction, the most prominent features seen in the cross section are forward peaking and the dip at $-t = m_\pi^2$, which is attributed to the Born terms. Our results also reproduced this feature. Some new ingredients appearing in this approach concerned the roles played by the Born terms and the Delta resonance, and the influence of their associated form factors.

  As found in previous studies, the Born terms deviated significantly from the experimental data at intermediate and backward angles as photon energies increased to the GeV level. The cross section due to Born terms alone was much larger than the data suggest. One possible explanation was that the Born terms were cancelled by resonance contributions away from the forward peak. As discussed by Barbour, Malone and Moorhouse in a fixed-t dispersion relation [28], the real parts of the resonance amplitudes tended to cancel the Born terms at $-t > m_\pi^2$, while the region $-t < m_\pi^2$ was slightly enhanced by low-lying resonance contributions.

  In Fig. 5, we illustrate the results for the Born terms and Born terms plus Delta excitation, with and without the quark model form factors, respectively. Clearly, form factors are vital in the quark-model description, though no free parameters have been introduced. Comparing the full result to one in which the form factors are switched off, we see potential problems for those who compare quark-model results

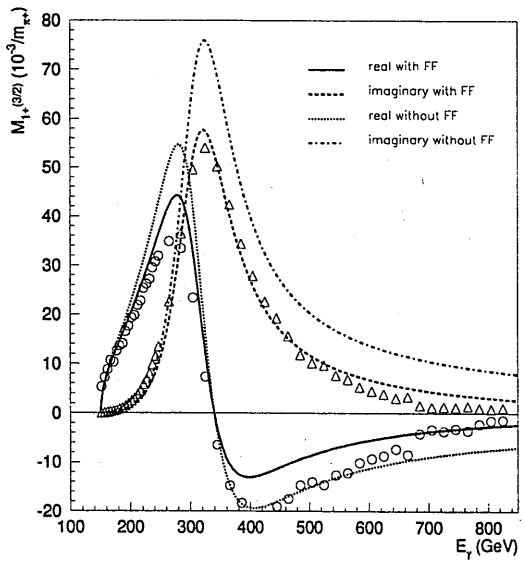

Figure 4: Real and imaginary parts of the multipole $M_{1+}^{3/2}$ derived from the Delta amplitude in π^0 channel. Model results *with* and *without* the quark model form factor (FF) are compared. Data are from SAID analysis [32].

directly to fits (such as SAID and MAID) which do not introduce form factors.

4.1.5 Eta photo- and electroproduction

Large discrepancies existed in the study of the $S_{11}(1535)$ helicity amplitude $A_{\frac{1}{2}}$. In the photoproduction, it was shown that the uncertainties of the total width, and partial branching ratio $S_{11}(1535) \rightarrow \eta N$ could go to the same direction without change too much the fitting results [33].

The recently published data from JLab [34] covered the kinematics $1.490 \leq W \leq 1.615$ GeV at Q^2 =2.4 and 3.6 $(\mathrm{GeV/c})^2$. Accompanied with data for photoproduction from GRAAL [35] and Mainz [36], and focussing on the $S_{11}(1535)$ mass region, we showed that an explicit constraint on the $S_{11}(1535)$ could be obtained [37]. It suggests that the $\eta N S_{11}$ coupling has

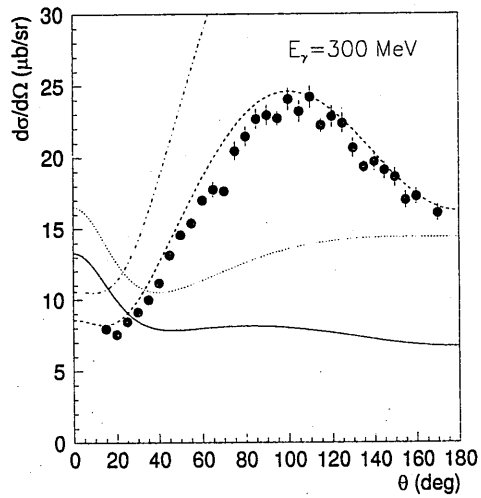

Figure 5: Cross sections for $\gamma p \to \pi^+ n$ at 300 MeV. Plotted are the Born terms with (solid curve) and without (dotted) form factor, and for the Born terms plus the Delta transition with (dashed) and without (dot-dashed) form factors, respectively.

been restricted within an uncertainty of about 15%.

4.2 Vector meson photoproduction

4.2.1 The kinematics

In vector meson photo-production, the final state vector meson decays ($\omega \to \pi^+\pi^-\pi^0$) provide access to the measurements of the vector meson decay density matrix elements, which can be related to the vector or tensor polarizations of the vector meson, or angular distributions of the cross sections [38, 39]:

$$\begin{aligned} W(\cos\theta, \phi, \Phi) &= W^0(\cos\theta, \phi, \rho^0_{\alpha\beta}) - P_\gamma \cos 2\Phi W^1(\cos\theta, \phi, \rho^1_{\alpha\beta}) \\ &\quad -P_\gamma \sin 2\Phi W^2(\cos\theta, \phi, \rho^2_{\alpha\beta}) \end{aligned}$$

$$+\lambda_\gamma P_\gamma W^3(\cos\theta,\phi,\rho^3_{\alpha\beta})\ . \tag{117}$$

where

$$\begin{aligned}
W^0(\cos\theta,\phi,\rho^0_{\alpha\beta}) &= \frac{3}{4\pi}[\frac{1}{2}\sin^2\theta+\frac{1}{2}(3\cos^2\theta-1)\rho^0_{00} \\
&\quad -\sqrt{2}\mathrm{Re}\rho^0_{10}\sin 2\theta\cos\phi-\rho^0_{1-1}\sin^2\theta\cos 2\phi]\ , \\
W^1(\cos\theta,\phi,\rho^1_{\alpha\beta}) &= \frac{3}{4\pi}[\rho^1_{11}\sin^2\theta+\rho^1_{00}\cos^2\theta \\
&\quad -\sqrt{2}\mathrm{Re}\rho^1_{10}\sin 2\theta\cos\phi-\rho^1_{1-1}\sin^2\theta\cos 2\phi]\ , \\
W^2(\cos\theta,\phi,\rho^2_{\alpha\beta}) &= \frac{3}{4\pi}[\sqrt{2}\mathrm{Im}\rho^2_{10}\sin 2\theta\sin\phi+\mathrm{Im}\rho^2_{1-1}\sin^2\theta\sin 2\phi]\ , \\
W^3(\cos\theta,\phi,\rho^3_{\alpha\beta}) &= \frac{3}{4\pi}[\sqrt{2}\mathrm{Re}\rho^3_{10}\sin 2\theta\sin\phi+\mathrm{Im}\rho^3_{1-1}\sin^2\theta\sin 2\phi]
\end{aligned} \tag{118}$$

In the above equations, θ and ϕ are the polar and azimuthal angles of the normal direction of the ω decay plane with respect to the z-axis in the production plane, which in the helicity frame is defined as the direction of the ω meson momentum. Φ is the angle of the photon polarization vector with respect to the production plane, and P_γ is the photon polarization degree.

In the helicity space, the density matrix elements can be explicitly expressed in terms of the 12 independent helicity amplitudes:

$$\begin{aligned}
\rho^0_{ik} &= \frac{1}{A}\sum_{\lambda\lambda_2\lambda_1} H_{\lambda_{v_i}\lambda_2,\lambda\lambda_1}H^*_{\lambda_{v_k}\lambda_2,\lambda\lambda_1}, \\
\rho^1_{ik} &= \frac{1}{A}\sum_{\lambda\lambda_2\lambda_1} H_{\lambda_{v_i}\lambda_2,-\lambda\lambda_1}H^*_{\lambda_{v_k}\lambda_2,\lambda\lambda_1}, \\
\rho^2_{ik} &= \frac{i}{A}\sum_{\lambda\lambda_2\lambda_1} \lambda H_{\lambda_{v_i}\lambda_2,-\lambda\lambda_1}H^*_{\lambda_{v_k}\lambda_2,\lambda\lambda_1}, \\
\rho^3_{ik} &= \frac{i}{A}\sum_{\lambda\lambda_2\lambda_1} \lambda H_{\lambda_{v_i}\lambda_2,\lambda\lambda_1}H^*_{\lambda_{v_k}\lambda_2,\lambda\lambda_1},
\end{aligned} \tag{119}$$

and

$$A=\sum_{\lambda_{v_i}\lambda\lambda_2\lambda_1} H_{\lambda_{v_i}\lambda_2,\lambda\lambda_1}H^*_{\lambda_{v_i}\lambda_2,\lambda\lambda_1}, \tag{120}$$

where ρ_{ik} stands for $\rho_{\lambda_{v_i}\lambda_{v_k}}$, and λ_{v_i}, λ_{v_k} denote the helicity of the produced vector mesons. A is the cross section function.

With the linearly polarized photon beam, ρ^0_{ik}, ρ^1_{ik} and ρ^2_{ik} can be measured while with the circularly polarized photon beam, ρ^0_{ik} and ρ^3_{ik} can be measured. It also gives access to some other spin observables [42, 43], e.g. the polarized photon asymmetry $\hat{\Sigma}$. With the linearly polarized photon beam, the distribution of the vector meson decay will be described by the first three terms in Eq. (117). Then, the integratal over θ and ϕ gives

$$W(\Phi) = 1 + P_\gamma \hat{\Sigma} \cos 2\Phi \ , \tag{121}$$

where

$$\hat{\Sigma} \equiv \frac{2\rho^1_{11} + \rho^1_{00}}{2\rho^0_{11} + \rho^0_{00}} \tag{122}$$

is the polarized photon-beam asymmetry. The additional relations, $2\rho^0_{11} + \rho^0_{00} \equiv 1$, which represents the normalized cross section, was implied in the above equation. Therefore, only 11 density matrix elements are linearly independent. Explicit relations between the helicity amplitudes and polarization observables (and multipoles) were available in the literatures [40, 41].

4.2.2 The theory

In the $SU(6) \otimes O(3)$ symmetry limit, the quark-vector-meson coupling is described by the effective Lagrangian [44, 45]:

$$L_{eff} = -\overline{\psi}\gamma_\mu p^\mu \psi + \overline{\psi}\gamma_\mu e_q A^\mu \psi + \overline{\psi}(a\gamma_\mu + \frac{ib\sigma_{\mu\nu}q^\nu}{2m_q})\phi^\mu_V \psi, \tag{123}$$

where ψ and $\overline{\psi}$ represent the quark and antiquark field, respectively, and ϕ^μ_V denotes the vector meson field. The two parameters, a and b represent the vector and tensor couplings of the quark to the vector meson, respectively. m_q and e_q are the mass and charge of the constituent quark, respectively. For the quark model parameters, m_q and α (harmonic oscillator potential strength), the commonly used values 330 and 385 MeV are adopted, respectively.

With such an effective coupling, the transition amplitudes for the s- and u-channel can be explicitly derived [45]. The intermediate resonances will be introduced in the harmonic oscillator basis. Resonances with masses less than 2 GeV are assigned to the states of $n \leq 2$ in the harmonic oscillator basis, therefore, can be taken into account explicitly in the NRCQM. Then, in the helicity space the amplitude for each resonance with spin J can be

expressed as:

$$H^J_{a\lambda_v} = \frac{2M_R}{s - M_R^2 + iM_R\Gamma(\mathbf{q})} \sum_{\Lambda_f} d^J_{\Lambda_f,\Lambda_i}(\theta) A^v_{\Lambda_f} A^\gamma_{\Lambda_i}, \tag{124}$$

where s is the c.m. energy square and M_R is the resonance mass. $\Gamma(\mathbf{q})$ is the momentum dependence of the resonance width, which has been given in Ref. [45]. Λ_f and Λ_i are defined as, $\Lambda_f \equiv \lambda_v - \lambda_2$, and $\Lambda_i \equiv \lambda - \lambda_1$. Here $\lambda_\gamma = \pm 1$, $\lambda_v = 0, \pm 1$, $\lambda_1 = \pm 1/2$ and $\lambda_2 = \pm 1/2$ denote the helicities of the photon, ω meson, initial and final state nucleon, respectively. $A^\gamma_{\Lambda_i}$ and $A^v_{\Lambda_f}$ are the helicity amplitudes for the photon excitation and vector meson decay of an intermediate resonance, respectively. $d^J_{\Lambda_f,\Lambda_i}(\theta)$ is the Wigner-d function which rotate the vector $A^\gamma_{\Lambda_i}$ from the initial state coordinate system to the final state coordinate system.

For a resonance of the SU(6)⊗O(3)quark model with spin J, its 12 independent transition amplitudes can be written as

$$\begin{aligned}
H^J_{11} &= d^J_{1/2,3/2}(\theta) A^v_{1/2} A^\gamma_{3/2}, \\
H^J_{10} &= d^J_{-1/2,3/2}(\theta) S^v_{-1/2} A^\gamma_{3/2} = (-1)^{J_v} d^J_{1/2,3/2}(\pi+\theta) S^v_{1/2} A^\gamma_{3/2}, \\
H^J_{1-1} &= d^J_{-3/2,3/2}(\theta) A^v_{-3/2} A^\gamma_{3/2} = (-1)^{J_v+1} d^J_{3/2,3/2}(\pi+\theta) A^v_{3/2} A^\gamma_{3/2}, \\
H^J_{21} &= d^J_{1/2,1/2}(\theta) A^v_{1/2} A^\gamma_{1/2}, \\
H^J_{20} &= d^J_{-1/2,1/2}(\theta) S^v_{-1/2} A^\gamma_{1/2} = (-1)^{J_v} d^J_{1/2,1/2}(\pi+\theta) S^v_{1/2} A^\gamma_{1/2}, \\
H^J_{2-1} &= d^J_{-3/2,1/2}(\theta) A^v_{-3/2} A^\gamma_{1/2} = (-1)^{J_v} d^J_{3/2,1/2}(\pi+\theta) A^v_{3/2} A^\gamma_{1/2}, \\
H^J_{31} &= d^J_{3/2,3/2}(\theta) A^v_{3/2} A^\gamma_{3/2}, \\
H^J_{30} &= d^J_{1/2,3/2}(\theta) S^v_{1/2} A^\gamma_{3/2}, \\
H^J_{3-1} &= d^J_{-1/2,3/2}(\theta) A^v_{-1/2} A^\gamma_{3/2} = (-1)^{J_v} d^J_{1/2,3/2}(\pi+\theta) A^v_{1/2} A^\gamma_{3/2}, \\
H^J_{41} &= d^J_{3/2,1/2}(\theta) A^v_{3/2} A^\gamma_{1/2} = -d^J_{1/2,3/2}(\theta) A^v_{3/2} A^\gamma_{1/2}, \\
H^J_{40} &= d^J_{1/2,1/2}(\theta) S^v_{1/2} A^\gamma_{1/2}, \\
H^J_{4-1} &= d^J_{-1/2,1/2}(\theta) A^v_{-1/2} A^\gamma_{1/2} = (-1)^{J_v} d^J_{1/2,1/2}(\pi+\theta) A^v_{-1/2} A^\gamma_{1/2},
\end{aligned} \tag{125}$$

where $S^v_{\Lambda_f}$ denotes the longitudinal helicity amplitude of vector meson decay of the intermediate resonances. In some of the above equations, parity conservation allows us to relate $A^v_{-\Lambda_f}$ with $A^v_{\Lambda_f}$ for each SU(6)⊗O(3) state with spin J which then decays into a vector meson and a nucleon with

relative angular momentum J_v,

$$A^v_{-\Lambda_f}(J) = (-1)^{1/2-J-J_v} A^v_{\Lambda_f}(J), \tag{126}$$

where the factor 1/2 denotes the spin of the final state nucleon. The parity of such a state is $(-1)^N$, where N is the main quantum number of the harmonic oscillator shell. Meanwhile, the final state system has a parity $(+1)(-1)(-1)^{J_v}$ which is determined by the parity of the nucleon, vector meson, and their relative angular momentum. Equivalence of these two parities gives $(-1)^N = (-1)^{J_v+1}$, and thus

$$A^v_{-\Lambda_f}(J) = (-1)^{(1/2-J)-(N-1)} A^v_{\Lambda_f}(J). \tag{127}$$

So far, the dynamical feature has not been explicitly involved. Note that the change of the rotation functions has been taken into account as well in Eq. (125). Symmetric feature for each state of SU(6)⊗O(3) quark model can be seen clearly. The nodal structure is determined by the interfering amplitudes, therefore can be studied in an explicit model. We explicitly include resonances (states) with $n \leq 2$ in the SU(6)⊗O(3) quark model, while states with $n > 2$ are treated as degenerate due to our lacking knowledge of their properties.

In the case of the neutral vector meson (ω, ρ^0 and ϕ) photoproduction, the t-channel and the seagull term from Eq. (123) vanish since they are proportional to the charge of the outgoing vector meson. The nucleon pole terms have been explicitly included [45]. Meanwhile, the diffractive process will be accounted for through a pomeron exchange model [46], in which the pomeron mediates the long range interaction between two confined quarks, and behaves rather like a $C = +1$ isoscalar photon. Qualitatively, Pomeron exchange can be understood as background contributions from exchange of vaccuum quantum number in the t-channel with no quark lines connected, i.e. non-Regge-pole contributions [47].

We summarize the vertices as follows [48, 49]:

(i) pomeron-nucleon coupling:

$$F_\mu(t) = 3\beta_0 \gamma_\mu f(t), \;\; f(t) = \frac{(4M_N^2 - 2.8t)}{(4M_N^2 - t)(1 - t/0.7)^2}, \tag{128}$$

where $\beta_0 = 1.27$ GeV^{-1} is the coupling of the pomeron to one light constituent quark; $f(t)$ is the isoscalar nucleon electromagnetic form factor with four-momentum transfer t; the factor 3 comes from the "quark-counting rule".

(ii) Quark-ϕ-meson coupling:

$$V_\nu(p-\frac{1}{2}q,p+\frac{1}{2}q)=f_V M_\phi \gamma_\nu \ , \tag{129}$$

where f_V is the radiative decay constant of the vector meson, and determined by $\Gamma_{V\to e^+e^-}=8\pi\alpha_e^2 e_Q^2 f_V^2/3M_V$. A form factor $\mu_0^2/(\mu_0^2+p^2)$ is adopted for the pomeron-off-shell-quark vertex, where $\mu_0=1.2$ GeV is the cut-off energy, and p is the four-momentum of the quark. The pomeron trajectory is $\alpha(t)=1+\epsilon+\alpha' t$, with $\alpha'=0.25$ GeV^{-2}.

The π^0 exchange is also included in the model, which is introduced with the following Lagrangians for the πNN and $\phi\pi\gamma$ coupling:

$$L_{\pi NN}=-ig_{\pi NN}\overline{\psi}\gamma_5(\boldsymbol{\tau}\cdot\boldsymbol{\pi})\psi \ . \tag{130}$$

and

$$L_{V\pi^0\gamma}=e_N\frac{g_{V\pi\gamma}}{M_V}\epsilon_{\alpha\beta\gamma\delta}\partial^\alpha A^\beta \partial^\gamma V^\delta \pi^0 \ . \tag{131}$$

where the commonly used couplings, $g_{\pi NN}^2/4\pi=14$, $g_{\omega\pi\gamma}^2=3.315$ and $g_{\phi\pi\gamma}^2=0.143$, are adopted.

An exponential factor $e^{-(\mathbf{q}-\mathbf{k})^2/6\alpha_\pi^2}$ from the nucleon wavefunctions plays a role as a form factor for the πNN and $\phi\pi\gamma$ vertices, where $\alpha_\pi=270$ MeV is adopted. This factor comes out naturally in the harmonic oscillator basis where the nucleon is treated as a 3-quark system.

For ρ^0 production, the σ meson exchange is included to account for the $J^{PC}=0^{++}$ pole exchange in the t-channel [45]. Although this process is part of natural-parity exchanges, it behaves differently from the Pomeron exchange. Due to the suppression of the propagator, the pole exchange generally will drop down at high energies, while the Pomeron exchange will sustain a stable cross section to a wide energy region.

A detailed calculation of this approach was recently carried out intending to interpret the new experimental data from GRAAL Collaboration [50].

5 Experimental projects on baryon physics and some open questions

5.1 CLAS at JLab

The N^* program at JLab has a wide scope of interest to cover the study of baryon properties from the ground state to the complete set of excited baryon resonances. In principle, CLAS has access to all the photo- and electroproduction (charged) channels covering the whole resonance region.

Program:

i) The first resonance region

Electroproduction of π meson in the Δ resonance region: $\gamma^* p \to \Delta(1232) \to p\pi^0$ [51].

The experiment was devoted to the study of the $\gamma N\Delta$ quadrupole transition. The magnetic dipole M_{1+} is dominant in $\gamma N\Delta$ transitions. The nonrelativisitic quark model predicted the electric quadrupole E_{1+} to be small (vanishing) at the real photon limit. The ratio of the electric quadrupole E_{1+} and scalar quadrupole S_{1+} to the magnetic dipole were measured and the results suggested sizable contributions from the E_{1+} and S_{1+} transition. Models including pion cloud effects showed promising in the explanation of the sizable ratios at the real photon limit and their Q^2 dependence.

ii) The second resonance region

Photo- and electroproduction of the $P_{11}(1440)$ (Roper resonance), *Is it a hybrid, a normal three-quark state, or a $N\sigma$ bound state?*

$S_{11}(1535)$ (see Ref. [34, 52] for $\gamma^* p \to S_{11}(1535) \to p\eta$), and $D_{13}(1520)$. Simple quark model and a relativistic quark model predicted a larger $A_{\frac{1}{2}}$ at the real photon limit. At small Q^2, what's the role played by the pion cloud? Also note that, the potential effects turn to be important in the reaction study. For the D_{13}, precise measurements (hep-ex/0203006, GDH and A2-Collaboration) and explicit calculations are both needed.

iii) The third resonance region

Looking for "missing resonances" in meson photo- and electroproduction, e.g. $\gamma^{(*)} N \to \omega N, \rho N, \phi p, \eta' p, K\Lambda, K^*\Sigma$, ... Progresses have been reported on conferences (see e.g. Refs. [53, 54]). Above the traditional resonance regions, experimental results for three channels, $\gamma p \to \phi p$, $\gamma p \to \rho^0 p$, and $\gamma p \to \omega p$, have been published recently [55, 56, 57].

5.2 GRAAL at ESRF

The GRAAL facility provides a polarized and tagged photon beam through the backward Compton scattering of laser light on the 6.04 GeV electrons circulating in the ESRF storage ring. The detectors cover full angles, and have great an advantage of measuring neutral channels, e.g., $\omega \to \pi^0\gamma$ in addition to $\omega \to \pi^0\pi^+\pi^-$. Meanwhile, experiment on γn is possible.

Program:

i) 1996-1997, $E_\gamma = 500 \sim 1100$ MeV,

$$\begin{aligned} \gamma p &\to p\eta\ (\eta \to 3\pi,\ \pi^0\gamma\gamma)\ \text{(published)} \\ &\to p\pi^0,\ n\pi^+\ \text{(published)} \\ &\to p\pi^0\pi^0\ (\Delta^+\pi^0),\ n\pi^+\pi^0\ (\Delta^+\pi^0,\ \Delta^0\pi^+),\ \text{(to be published)} \\ &\to \gamma p\ \text{(to be published)} \end{aligned}$$

ii) 1998-1999, $E_\gamma = 900 \sim 1470$ MeV,

$$\begin{aligned} \gamma p &\to p\eta\ (\eta \to 3\pi,\ \pi^0\gamma\gamma)\ \text{(published)} \\ \gamma p &\to \Lambda K^+,\ \Sigma^0 K^+\ \text{(in analysis and to be published)} \\ &\to p\omega\ \text{(in analysis and to be published)} \\ &\to p\eta'\ \text{(in analysis and to be published)} \end{aligned}$$

iii) 2000, $E_\gamma = 900 \sim 1470$ MeV, statistics improved.

iv) 2001, polarized HD target installed for measurement of double polarization (beam-target) [58].

v) Compton scattering has been measured as well. Preliminary data are available.

vi) Recent future, increasing the photon energy up to 1.8 GeV; experiments on meson photoproduction on light nuclei.

5.3 SAPHIR/Crystal Barrel at ELSA

The ELectron Stretcher Accelerator (ELSA) with a tunable electron energy up to 3.5 GeV provides access to a bremsstrahlungs photon beam up to $E_\gamma = 2.6$ GeV.

Program:

i) Kaon-Hyperon production

$$\begin{aligned} \gamma p &\to K^+\Lambda, \\ &\to K^+\Sigma^0, \\ &\to K^0\Sigma^+. \end{aligned}$$

ii) Vector meson photoproduction [59]

$$\begin{aligned} \gamma p &\rightarrow p\omega \\ &\rightarrow p\rho^0 \\ &\rightarrow p\phi \end{aligned}$$

iii) Recent program using Crystal Barrel

- Direct measurement of the Gerasimov-Drell-Hearn (GDH) sum rule at 600 MeV$\leq E_\gamma \leq$ 3 GeV.
- Double pion production: $\gamma p \rightarrow p\pi^0\pi^0$ via $\Delta^+\pi^0$.
- Study of reaction $\gamma p \rightarrow p\pi^0\eta$ via the following processes:

$$\gamma p \rightarrow \left\{ \begin{array}{c} \Delta^+\eta \\ S_{11}(1535)\pi^0 \\ p\rho(1380) \\ pa_0(980) \end{array} \right\} \rightarrow p\pi^0\eta \ . \qquad (132)$$

- Inelastic photon scattering in $\gamma p \rightarrow p\pi^0\gamma$ and $\gamma p \rightarrow p\eta\gamma$.
- Photoproduction of η and η' up to $E_\gamma = 3$ GeV.

5.4 LEPS at SPring-8

Adopting the technique of backward Compton scattering of laser photons similar to GRAAL, linearly polarized photon beams up to $E_\gamma = 2.4$ GeV are produced from the 8 GeV electron facility SPring-8. This project extended the kinematics of GRAAL to higher energy regions.

Program:

i) Photoproduction of ϕ near threshold.

The strangeness component in nucleons and its knock-out can be detected; Non-diffractive process such as resonance excitations can be also investigated.

ii) Beam polarization asymmetries for $\gamma p \rightarrow K^+\Lambda$ at 1.5 - 2.4 GeV.

In addition to the cross section measurement of SAPHIR, the data for the polarized beam asymmetry would provide more information about the "missing resonance" $D_{13}(1960)$, and be more selective to models.

iii) Study property of $\Lambda(1405)$ (See Particle Data Group [4] for a recent summary).

iv) Photoproduction of ω meson at backward angles.

Higher resonances from the third resonance region can be investigated.

5.5 GDH- and A2 Collaboration at MAMI

MAMI provides an access to double polarization, circularly polarized photon ($E_\gamma < 790$ MeV) and polarized proton. By measuring the exclusive pion production channels, one of the important aims at MAMI is to test the GDH sum rule at low energies. It is promising to precisely derive resonance signals (e.g., $D_{13}(1520)$).

5.6 BEPC N^* program

A unique channel for N^* physics: $J/\Psi \rightarrow N^*\overline{N}$ [60].

6 Perspectives of baryon physics in experiment and theory

Since large degrees of freedom are involved at the resonance region, in principle we need as many as possible measurements of various spin observables to understand the reaction mechanisms. This feature highlights the importance of polarization experiment where small amplitudes could be amplified by interferences.

The new generation of the electron accelerators with the high intensity electron and photon beams have started to provide new data with unprecedented precision for various observables. Theoretical efforts on the interpretation of a wealth of data are needed. Such efforts would significantly improve our quantitative understanding of the nucleon resonance structures, which are essentially non-perturbative QCD phenomena.

On the other hand, modern research on baryon physics, more or less, has to be based on some phenomenologies. This situation might suggest that a better understanding of baryon resonances should be built up on a basis containing as less as possible parameters. Such an approach, even though interprets the experimental data only qualitatively, could however provide more physical insights rather than a perfect fit with a large number of parameters. In this sense, quark model seems likely to be able to provide us with a reasonable starting point for the reaction study. Although, such a phenomenology has many unanswered questions which prevent it from being a fundamental theory, one would expect that the regime where the failure of this phenomenology is exposed should be the point from which one could step further.

acknowledgement

Q.Z. thanks the warm invitation from Prof. B.S. Zou and Prof. W.Q. Chao, and hospitality of CCAST. Many useful discussions with Profs. B.S. Zou, Z.Y. Zhang, F. Wang, and H.C. Chiang are appreciated.

Appendix I

The SU(2) spin wavefunction for a three-quark system:

$$\chi^s(S_z = \frac{3}{2}) \;=\; \uparrow\uparrow\uparrow$$

$$\chi^{\rho}(S_z=\frac{1}{2}) = \frac{1}{\sqrt{2}}(\uparrow\downarrow\uparrow-\downarrow\uparrow\uparrow)$$
$$\chi^{\lambda}(S_z=\frac{1}{2}) = \frac{1}{\sqrt{6}}(2\uparrow\uparrow\downarrow-\downarrow\uparrow\uparrow-\uparrow\downarrow\uparrow)\ , \qquad (133)$$

where χ^s has a total spin 3/2, and the other two have a total spin 1/2.

The SU(3) flavor wavefunction for the light quark system on the basis of the S_3 permutation group could have the four different symmetries labelled by s, λ, ρ and a.

The symmetric wavefunction is

$$\phi^s(\mathbf{10}) = \sum_{permu.} a(1)b(2)c(3)\ , \qquad (134)$$

where a, b and c represent flavor u, d or s.

The mixed octet wavefunctions are

$$\phi^{\lambda}(\mathbf{8}) = \begin{cases} \frac{1}{\sqrt{6}}(2uud-duu-udu) & \text{for } p \\ \frac{1}{\sqrt{6}}(dud+udd-2ddu) & \text{for } n \\ \frac{1}{\sqrt{6}}(2uus-suu-usu) & \text{for } \Sigma^+ \\ \frac{1}{2\sqrt{3}}(sdu+sud+usd+dsu-2uds-2dus) & \text{for } \Sigma^0 \\ \frac{1}{\sqrt{6}}(sdd+dsd-2dds) & \text{for } \Sigma^- \\ \frac{1}{2}(sud+usd-sdu-dsu) & \text{for } \Lambda \\ \frac{1}{\sqrt{6}}(2ssu-sus-uss) & \text{for } \Xi^0 \\ \frac{1}{\sqrt{6}}(2ssd-sds-dss) & \text{for } \Xi^- \end{cases} , \qquad (135)$$

and

$$\phi^{\rho}(\mathbf{8}) = \begin{cases} \frac{1}{\sqrt{2}}(udu-duu) & \text{for } p \\ \frac{1}{\sqrt{2}}(udd-dud) & \text{for } n \\ \frac{1}{\sqrt{2}}(suu-usu) & \text{for } \Sigma^+ \\ \frac{1}{2}(sud+sdu-usd-dsu) & \text{for } \Sigma^0 \\ \frac{1}{\sqrt{2}}(sdd-dsd) & \text{for } \Sigma^- \\ \frac{1}{2\sqrt{3}}(usd+sdu-sud-dsu-2dus+2uds) & \text{for } \Lambda \\ \frac{1}{\sqrt{2}}(sus-uss) & \text{for } \Xi^0 \\ \frac{1}{\sqrt{2}}(sds-dss) & \text{for } \Xi^- \end{cases} . \qquad (136)$$

The anti-symmetric singlet is:

$$\phi^a(\mathbf{1}) = \frac{1}{\sqrt{6}}(uds+dsu+sud-dus-usd-sdu)\ . \qquad (137)$$

Appendix II

Spatial integrals for $[\mathbf{56}, 0^+]_{N=0} \to [\mathbf{70}, 1^-]_{N=1}$:

$$
\begin{aligned}
& \langle \Psi_f | e^{ikz_3} | \Psi_i \rangle \\
= & \frac{\alpha_h^7}{\pi^3} \int d\boldsymbol{\rho} d\boldsymbol{\lambda} e^{-\alpha_h^2(\boldsymbol{\rho}^2+\boldsymbol{\lambda}^2)} e^{-i\sqrt{\frac{2}{3}}k\lambda_z} \sqrt{2}\lambda_z \\
= & \frac{\alpha_h^7}{\pi^3} \left(\frac{\sqrt{\pi}}{\alpha_h}\right)^3 \int_0^{+\infty} d\lambda \lambda^3 e^{-\alpha_h^2\lambda^2} 4\sqrt{\frac{\pi}{3}} Y_{10}(\theta,\phi) \\
& \times \sum_{l=0}^{\infty} (-i)^l (2l+1) P_l(\cos\theta) j_l(\sqrt{\frac{2}{3}}k\lambda) \sin\theta d\theta d\phi \\
= & i\frac{\alpha_h^7}{\pi^3} \left(\frac{\sqrt{\pi}}{\alpha_h}\right)^3 4\sqrt{2}\pi \int_0^{+\infty} d\lambda \lambda^3 e^{-\alpha_h^2\lambda^2} j_l(\sqrt{\frac{2}{3}}k\lambda) \\
= & i4\sqrt{2}\frac{\alpha^4}{\sqrt{\pi}} \frac{k}{2\alpha_h^2} \sqrt{\frac{2}{3}} \frac{\sqrt{\pi}}{4\alpha_h^3} e^{-\mathbf{k}^2/6\alpha^2} \\
= & i\frac{k}{\sqrt{3}\alpha_h} e^{-\mathbf{k}^2/6\alpha^2} \,, \qquad (138)
\end{aligned}
$$

where $P_l(\cos\theta) = \sqrt{\frac{4\pi}{2l+1}} Y_{l0}(\theta,\phi)$, and the orthogonal relation for the spherical harmonics is used,

$$
\int_{\theta=0}^{\pi} \int_{\phi=0}^{2\pi} Y^*_{l_1 m_1}(\theta,\phi) Y_{l_2 m_2}(\theta,\phi) d\Omega = \delta_{l_1 l_1 2} \delta_{m_1 m_2} \,. \qquad (139)
$$

Similarly, the spatial integrals for other transitions can be calculated.

References

[1] White paper on "key issues in hadronic physics", Jeffeson Lab, Dec., 2000, hep-ph/0012238.

[2] N. Isgur and G. Karl, Phys. Rew. D **18**, 4187(1978); Phys. Rev. D **19**, 2194 (1979).

[3] G. Karl and E. Obryk, Nucl. Phys. **B 8**, 609 (1968).

[4] D. E. Groom *et al.* [Particle Data Group], Eur. Phys. J. C **15**, 1 (2000).

[5] N. Isgur, G. Karl, and R. Koniuk, Phys. Rev. Lett. **41**, 1629 (1978).

[6] I.C. Cloet, D.B. Leinweber, and A.W. Thomas, hep-ph/0203023.

[7] G. Karl, Phys. Rev. D **45**, 247 (1992).

[8] R. Koniuk and N. Isgur, Phys. Rev. D **21**, 1868 (1980).

[9] S. Capstick and W. Roberts, Phys. Rev. D **49**, 5470 (1994).

[10] R. Kokoski and N. Isgur, Phys. Rev. D **35**, 907 (1987).

[11] A. Le Yaouanc, L. Oliver, O. Péne, and J.C. Raynal, Phys. Rev. D **11**, 1272 (1975), and references therein.

[12] S. Capstick and W. Roberts, Prog. Part. Nucl. Phys. **45**, 5241 (2000).

[13] R.G. Moorhouse, Phys. Rev. Lett. **16**, 772 (1966).

[14] F.E. Close, "An Introduction to Quarks and Partons", Academic Press Inc. (London) Ltd (1979).

[15] R.P. Feynman, M. Kislinger, and F. Ravndal, Phys. Rev. D **3**, 2706 (1971); F. Ravndal, Phys. Rev. D **4**, 1466 (1971); L.A. Copley, G. Karl, and E. Obryk, Phys. Rev. D **4**, 2844 (1971); R.G. Lipes, Phys. Rev. D **5**, 2849 (1972); S. Godfrey and N. Isgur, Phys. Rev. D **32**, 189 (1985); S. Capstick and N. Isgur, Phys. Rev. D **34**, 2809 (1986).

[16] F.E. Close and Z.-P. Li, Phys. Rev. D **42**, 2194 (1990).

[17] Z.-P. Li and F.E. Close, Phys. Rev. D **42**, 2207 (1990).

[18] Z.-P. Li, Ph.D. thesis, University of Tennessee, 1991.

[19] S. Capstick and B.D. Keister, Phys. Rev. D **51**, 3598 (1995).

[20] G.F. Chew, M.L. Goldberger, F.E. Low, and Y. Nambu, Phys. Rev. **106**, 1345 (1957).

[21] R.L. Walker, Phys. Rev. **182**, 1729 (1969).

[22] C.G. Fasano, F. Tabakin, and B. Saghai, Phys. Rev. C **46**, 2430 (1992).

[23] Z.-P. Li, Phys. Rev. D **50**, 5639 (1994).

[24] A. Manohar and H. Georgi, Nucl. Phys. **B234**, 189 (1984).

[25] Z.-P. Li, H.-X. Ye, and M.-H. Lu, Phys. Rev. C **56**, 1099 (1997).

[26] Le Yaouance *et al*, *Hadron Transitions in the Quark Model*, (New York: Gordon and Breach), 1988.

[27] Z.-P. Li, Phys. Rev. D **48**, 3070 (1993).

[28] I. Barbour, W. Malone and R.G. Moorhouse, Phys. Rev. D **4**, 1521 (1971).

[29] R.A. Arndt, I.I. Strakovsky and R.L. Workman, Phys. Rev. C **53**, 430 (1996).

[30] O. Hanstein, D. Drechsel and L. Tiator, Nucl. Phys. **A 632**, 561 (1998).

[31] Q. Zhao, J.S. Al-Khalili, Z.-P. Li, and R.L. Workman, Phys. Rev. C **65**, 065204 (2002).

[32] SAID on-line database, http://gwdac.phys.gwu.edu.

[33] N.C. Mukhopadhyay and N. Mathur, Phys. Lett. B **444**, 7 (1998).

[34] C.S. Armstrong *et al.*, Phys. Rev. D **60**, 052004 (1999).

[35] F. Renard *et al.*, [The GRAAL Collaboration], Phys. Lett. **B 528**, 215 (2002).

[36] B. Krusche *et al.*, Phys. Rev. Lett. 74, 3736 (1995).

[37] Q. Zhao, B. Saghai, and Z.-P. Li, J. Phys. G **28**, 1293 (2002).

[38] R.L. Thews, Phys. Rev. **175**, 1749 (1968).

[39] K. Schilling, P. Seyboth, and G. Wolf, Nucl. Phys. **B 15**, 397 (1970).

[40] M. Pichowsky, Ç. Şavklı and F. Tabakin, Phys. Rev. C **53**, 593 (1996).

[41] C. Savkli, F. Tabakin and S. N. Yang, Phys. Rev. C **53**, 1132 (1996).

[42] Q. Zhao, Phys. Rev. C **63**, 025203 (2001).

[43] Q. Zhao, Proceeding of EMI2001, Osaka, Japan, p.632 (2001); nucl-th/0202023.

[44] Q. Zhao, Z.P. Li and C. Bennhold, Phys. Lett. B **436**, 42 (1998).

[45] Q. Zhao, Z.P. Li and C. Bennhold, Phys. Rev. C **58**, 2393 (1998).

[46] A. Donnachie and P.V. Landshoff, Phys. Lett. **B 185**, 403 (1987); Nucl. Phys. **B 311**, 509 (1989).

[47] P.D.B. Collins, "An Introduction to Regge Theory and High Energy Physics", Cambridge University Press (1977).

[48] Q. Zhao, J.-P. Didelez, M. Guidal, and B. Saghai, Nucl. Phys. **A 660**, 323 (1999).

[49] Q. Zhao, B. Saghai, and J.S. Al-Khalili, Phys. Lett. **B 509**, 231 (2001).

[50] E. Hourany, Proceeding of N* 2002, Pittsburgh, USA (2002); Y. Assafiri *et al.* [GRAAL Collaboration], to be submitted for publication.

[51] K. Joo *et al.* [The CLAS Collaboration], Phys. Rev. Lett. **88**, 122001 (2002).

[52] R. Thompson *et al.* [The CLAS Collaboration], Phys. Rev. Lett. **86**, 1720 (2001).

[53] P.L. Cole, Proceeding of EMI2001, Osaka, Japan, (2001); JLab proposal E99-013, E94-109.

[54] D.J. Tedeschi, Proceeding of EMI2001, Osaka, Japan, (2001); JLab proposal E98-109.

[55] E. Anciant *et al.* [CLAS Collaboration], Phys. Rev. Lett. **85**, 4682 (2000).

[56] M. Battaglieri *et al.* [CLAS Collaboration], Phys. Rev. Lett. **87**, 172002 (2001).

[57] M. Battaglieri *et al.* [CLAS Collaboration], Phys. Rev. Lett. **90**, 022002 (2003).

[58] S. Bouchygny *et al.* [The GRAAL Collaboration], Proceeding of EMI2001, Osaka, Japan, p.652 (2001).

[59] F.J. Klein, Ph.D. thesis, University of Bonn, Bonn-IR-96-008 (1996); $\pi - N$ Newslett. 14, 141 (1998).

[60] J. Z. Bai *et al.* [BES Collaboration], Phys. Lett. B **510**, 75 (2001).

Dibaryon Systems in Chiral $SU(3)$ Quark Model[1]

Q.B.Li[a], P.N.Shen[b,a,c,d], Z.Y.Zhang[a], Y.W.Yu[a]

a. **Institute of High Energy Physics, Academia Sinica, P.O.Box 918(4), Beijing 100039, China**

b. **China Center of Advanced Science and Technology (World Laboratory), P.O.Box 8730, Beijing 100080, China**

c. **Institute of Theoretical Physics, Academia Sinica, P.O.Box 2735, Beijing 100080, China**

d. **Center of Theoretical Nuclear Physics, National Lab of Heavy Ion Accelerator, Lanzhou 730000, China**

Abstract

The possible candidates of $S-$wave dibaryons with various strange numbers are studied under the chiral $SU(3)$ quark model. It is shown that there are three types of baryon-baryon bound states. The states of the first type are called deuteron-like states. If chiral fields can provide enough attraction between interacting baryons, these systems, such as $[\Xi\Omega - \Xi^*\Omega]_{(1,1/2)}$, $[\Xi\Xi]_{(0,1)}$, $[N\Omega]_{(2,1/2)}$ would be weakly bound. The states of the second type such as $[\Sigma^*\Delta]_{(0,5/2)}$, $[\Sigma^*\Delta]_{(3,1/2)}$, $[\Delta\Delta]_{(0,3)}$ and $[\Delta\Delta]_{(3,0)}$ are named as $\Delta\Delta$-like states. Due to the highly symmetric character in orbital space, these systems could be relatively deeply bound, but the strong decay modes of composed baryons cause the widths of the states much broader. The states of the third type are entitled as $\Omega\Omega$-like states. Due to the same symmetry character shown in the systems of the second type and the only weak decay mode of composed baryons, for instance in $[\Omega\Omega]_{(0,0)}$, or at most one strong decay mode of composed baryons, for example in $[\Xi^*\Omega]_{(0,1/2)}$, these states are deeply bound states with narrow widths. The states of latter two types are most interesting new dibaryon states and should be carefully investigated both theoretically and experimentally.

[1]This work was partly supported by the National Natural Science Foundation of China (NSFC) and the Chinese Academy of Sciences

1. Introduction.

Dibaryon as a six-quark system has shown its special place in the investigation of medium-energy physics since Jaffe published his prediction of H particle in 1977 [1]. As is commonly believed, to study a quark system, the Quantum Chromodynamics (QCD), which governs the strong interaction among quarks and gluons, should be employed as an underline theory although its non-perturbative behavior is still not quite clear and cannot exactly be solved up to now. Jaffe studied the color-magnetic interaction (CMI) of the one-gluon-exchange (OGE) potential in the multi-quark system and found that CMI shows attractive character in the H particle case. This character compels six quarks staying in a smaller volume, say less than $0.85fm$ in radius. Thus dibaryon study could provide more information about the short-range behavior of QCD, and the existence of dibaryon can directly supply the evidence of the quark-gluon degrees of freedom in hadrons and hadronic systems. However, the reason for forming the baryon-baryon bound state presents great complexity. The nonperturbative QCD ($NPQCD$) effect may seriously affect the properties of the dibaryon due to its finite size. The CMI and the interaction describing the action from physical vacuum should be co-responsible for the binding energy of the system. The symmetry structure of the system may also play an important role there. In a word, the character of CMI is no longer dominant. Sometimes, meson clouds may provide predominant effects. Exploring dibaryon may enable us to investigate the short- and medium-range $NPQCD$ effects and to find out a practical way to properly treat them.

In order to reliably study dibaryon, a model that can describe most of short- and medium-range $NPQCD$ effects should be employed. In other word, the model should have predictive power. It should at least contain two-fold requirements: By using this model the ground state properties of baryons should well be fitted, and the experimental data of the nucleon-nucleon ($N-N$) scattering and, especially, the empirical data of the nucleon-hyperon ($N-Y$) scattering and reaction can reasonably be reproduced in the dynamical calculation. When extending this model to dibaryon investigation, no additional parameters are required. There are lots of models such as MIT bag model [2], the constituent quark models of various kinds [3, 7, 8], Skyrme model [9], etc. Among them, the chiral $SU(3)$ quark model [7, 8] is one of the models which

satisfy requested conditions. In terms of this model, investigating and further systematically analyzing possible bound six-quark systems become significant and essential.

Since 70's, dibaryon has been intensively studied. The most interesting dibaryons have been studied are the following: H particle has been theoretically and experimentally investigated for years. The theoretically predicted mass is in a large range [1, 3, 4, 5, 6, 15, 26], say from $2GeV$ to $2.4GeV$. The most believed theoretical prediction is around the $\Lambda\Lambda$ threshold, namely around $2.232GeV$ [4, 5]. However, this particle still has not been found in the experiment yet. The most recent data showed that the lower limit of the H particle mass is about $2.22GeV$ [13]. Except the H particle, possible bound baryon-baryon systems in the non-strangeness sector were also investigated. d^* is one of them. There were number of theoretical predictions by using various models, such as the non-relativistic boson-exchange model [17], the quark cluster model [4], the quark-delocation model [19], the chiral $SU(3)$ quark model [20] and etc.. The predicted masses also spread in a wide range. All the predictions are below the threshold of the $\Delta\Delta$ channel of $2.464GeV$, and most of them are above the threshold of the strong decay channel, $NN\pi\pi$, of $2.154GeV$. $d'(J^P = 0^-, T = 0)$ is another interesting particle. In the experiments of double-charge-exchange reactions, it was found that when the energy of the incident pion is $50MeV$, there exists a resonance with the mass of $2.065GeV$ and the width of $0.5MeV$ in the processes with a variety of targets [22]. To explain that phenomenon, one proposed d'. Although there were many theoretical attempts [23], the theoretical result is still away from the expected value. Whether this phenomenon indicates d' is still under discussion. Up to now, these three interesting candidates of dibaryons are still not found or confirmed by experiments. It seems that one should go beyond these candidates and should search the possible candidates in a wider region, especially the systems with multi-strangeness, in terms of a more reliable model such as chiral $SU(3)$ quark model. According to this idea, Yu et al. analyzed the six-quark system with a simple six-quark cluster configuration [16]. Later, by employing the chiral $SU(3)$ quark model, Zhang, Yu et al. studied $\Omega\Omega(S = 0, T = 0)$ and $\Xi\Omega(S = 1, T = 1/2)$ [16, 14], and Li and Shen explored $\Xi^*\Omega(S = 0, T = 1/2)$ and $\Xi\Omega - \Xi^*\Omega(S = 1, T = 1/2)$ [24]. In this paper, we would present a sys-

tematic study of possible candidates of $S-$wave baryon-baryon bound states in this model.

The paper is arranged in the following way: The chiral $SU(3)$ quark model is briefly introduced in Sect.2. In Sect.3, the results calculated by this model are given, and the symmetry characters of the system concerned are discussed. The effects of chiral-quark field induced interactions on the binding behaviors of systems are detailed analyzed in Sect.4. In Sect.5, the model parameter dependence of the predicted binding energy is further studied. Finally, in Sect.6, the concluding remark is drawn.

2. Brief introduction of chiral $SU(3)$ quark model.

Following Georgi's idea [10], the quark-chiral $SU(3)$ field interaction can be written as

$$\mathcal{L}_I = -g_{ch}(\bar{\psi}_L \Sigma \psi_R - \bar{\psi}_R \Sigma^+ \psi_L) \ , \tag{1}$$

with g_{ch} being the quark-chiral field coupling constant, ψ_L and ψ_R being the quark-left and right spinors, respectively, and

$$\Sigma = exp[i\pi_a \lambda_a / f], \quad a = 1, 2, ...8 \ . \tag{2}$$

where π_a is the Goldstone boson field and λ_a the Gell Mann matrix of the flavor SU(3) group. Generalizing the linear realization of Σ in the $SU(2)$ case to the $SU(3)$ case, one obtains

$$\Sigma = \sum_{a=0}^{8} \sigma_a \lambda_a - i \sum_{a=0}^{8} \pi_a \lambda_a \ , \tag{3}$$

and the interaction Lagrangian

$$\mathcal{L}_I = -g_{ch} \bar{\psi} \left(\sum_{a=0}^{8} \sigma_a \lambda_a + i \sum_{a=0}^{8} \pi_a \lambda_a \gamma_5 \right) \psi \ , \tag{4}$$

where λ_0 is a unitary matrix, $\sigma_0, .., \sigma_8$ the scalar nonet fields and $\pi_0, .., \pi_8$ the pseudo-scalar nonet fields. Clearly, $\mathcal{L}_I$ is invariant under the infinitesimal chiral $SU(3)_L \times SU(3)_R$ transformation. Consequently, one can write the interactive Hamiltonian as

$$H_{ch} = g_{ch} F(q^2) \bar{\psi} \left(\sum_{a=0}^{8} \sigma_a \lambda_a + i \sum_{a=0}^{8} \pi_a \lambda_a \gamma_5 \right) \psi \ . \tag{5}$$

Here we have inserted a form factor $F(q^2)$ to describe the chiral field structure [11]. As usual, $F(q^2)$ is taken as

$$F(q^2) = \left(\frac{\Lambda_{CSB}^2}{\Lambda_{CSB}^2 + q^2}\right)^{1/2} \quad , \tag{6}$$

and the cut-off mass Λ_{CSB} indicates the chiral symmetry breaking scale [11].

Then, the $SU(3)$ chiral-field-induced quark-quark potentials can be derived in the following :

$$\begin{aligned} V_{\sigma_a}(\vec{r}_{ij}) &= -C(g_{ch}, m_{\sigma_a}, \Lambda_{CSB}) X_1(m_{\sigma_a}, \Lambda_{CSB}, r_{ij})(\lambda_a(i)\lambda_a(j)) \\ &+ V_{\sigma_a}^{\vec{l}\cdot\vec{s}}(\vec{r}_{ij}), \end{aligned} \tag{7}$$

$$\begin{aligned} V_{\pi_a}(\vec{r}_{ij}) &= C(g_{ch}, m_{\pi_a}, \Lambda_{CSB}) \frac{m_{\pi_a}^2}{12 m_{qi} m_{qj}} [X_2(m_{\pi_a}, \Lambda_{CSB}, r_{ij})(\vec{\sigma}_i \cdot \vec{\sigma}_j) \\ &+ \left(H(m_{\pi_a} r_{ij}) - (\frac{\Lambda_{CSB}}{m_{\pi_a}})^3 H(\Lambda_{CSB} r_{ij})\right) S_{ij}](\lambda_a(i)\lambda_a(j)) \quad , \end{aligned} \tag{8}$$

with

$$\begin{aligned} V_{\sigma_a}^{\vec{l}\cdot\vec{s}}(\vec{r}_{ij}) &= -C(g_{ch}, m_{\sigma_a}, \Lambda_{CSB}) \frac{m_{\sigma_a}^2}{4 m_{qi} m_{qj}} [G(m_{\sigma_a} r_{ij}) \\ &- (\frac{\Lambda_{CSB}}{m_{\sigma_a}})^3 G(\Lambda_{CSB} r_{ij})](\vec{L} \cdot (\vec{\sigma}_i + \vec{\sigma}_j))(\lambda_a(i)\lambda_a(j)) \quad , \end{aligned} \tag{9}$$

$$C(g_{ch}, m, \Lambda) = \frac{g_{ch}^2}{4\pi} \frac{\Lambda^2}{\Lambda^2 - m^2} m \quad , \tag{10}$$

$$S_{ij} = 3(\vec{\sigma}_i \cdot \hat{r})(\vec{\sigma}_j \cdot \hat{r}) - (\vec{\sigma}_i \cdot \vec{\sigma}_j) \quad , \tag{11}$$

and m_{σ_a} being the mass of the scalar meson and m_{π_a} the mass of the pseudoscalar meson. The explicit forms of functions X_1, X_2, H and G can be found in [7].

As mentioned in [7], the interactions induced by chiral fields describe the NPQCD effect in the low-momentum medium-distance range, which is very important in explaining the short- and medium-range forces between two baryons. To study the baryon structure and baryon-baryon dynamics, one still needs an effective one-gluon-exchange interaction V_{ij}^{OGE} which dominates the short-range perturbative QCD behavior and a confinement potential V_{ij}^{conf} which provides the NPQCD effect in the long distance and confines three quarks to a baryon. Then, the total Hamiltonian of the six-quark system can be written

as

$$H = \sum_i T_i - T_G + \sum_{i<j} V_{ij} \quad , \tag{12}$$

with

$$V_{ij} = V_{ij}^{OGE} + V_{ij}^{conf} + V_{ij}^{ch} \quad , \tag{13}$$

where

$$\begin{aligned} V_{ij}^{OGE} &= \frac{1}{4} g_i g_j (\lambda_i^c \cdot \lambda_j^c) \{ \frac{1}{r_{ij}} - \frac{\pi}{2} \delta(\vec{r}_{ij}) (\frac{1}{m_{qi}^2} + \frac{1}{m_{qj}^2} \\ &+ \frac{4}{3} \frac{1}{m_{qi} m_{qj}} (\vec{\sigma}_i \cdot \vec{\sigma}_j)) - \frac{1}{4 m_{qi} m_{qj} r_{ij}^3} S_{ij} \} + V_{OGE}^{\vec{\ell} \cdot \vec{s}} \quad , \end{aligned} \tag{14}$$

$$V_{OGE}^{\vec{\ell} \cdot \vec{s}} = -\frac{1}{16} g_i g_j (\lambda_i^c \cdot \lambda_j^c) \frac{3}{m_{q_i} m_{q_j}} \frac{1}{r_{ij}^3} \vec{L} \cdot (\vec{\sigma}_i + \vec{\sigma}_j) \quad , \tag{15}$$

$$V_{ij}^{conf} = -a_{ij}^c (\lambda_i^c \cdot \lambda_j^c) r_{ij}^2 - a_{ij}^{c0} (\lambda_i^c \cdot \lambda_j^c) \quad , \tag{16}$$

and

$$V_{ij}^{ch} = \sum_{a=0}^{8} V_{\sigma_a}(\vec{r}_{ij}) + \sum_{a=0}^{8} V_{\pi_a}(\vec{r}_{ij}) \quad . \tag{17}$$

The model parameter should be fixed before calculation. The coupling constant g_{ch} is fixed by

$$\frac{g_{ch}^2}{4\pi} = (\frac{3}{5})^2 \frac{g_{NN\pi}^2}{4\pi} \frac{m_q^2}{M_N^2} \quad , \tag{18}$$

and $g_{NN\pi}^2/4\pi$ is taken to be the empirical value of about 14. The masses of the pseudo-scalar meson $m_\pi, m_\eta, m_{\eta'}$ and m_K can be chosen as the masses of the real π, η, η' and K, and the mass of the scalar meson σ_0 can be taken as $m_{\sigma_0} \simeq 625\ MeV$, according to the relation [12]

$$m_{\sigma_0}^2 = (2m_q)^2 + m_\pi^2 \quad . \tag{19}$$

In our previous investigation [7], it was found the $N-N$ and $N-Y$ scatterings are not sensitive to the masses of strange chiral fields. In order to reduce the numbers of adjustable parameters, $m_{\sigma_a} (a = 1, .., 8)$ are also taken to be the mass of η'. The cut-off mass Λ_{CSB} for various chiral fields is taken to be

$$\Lambda_{CSB} = \begin{cases} 4.2 fm^{-1}, & \text{for } \pi, K \text{ and } \sigma_0 \\ 5.0 fm^{-1}, & \text{for } \eta, \eta', \sigma', \kappa \text{ and } \epsilon. \end{cases} \tag{20}$$

This set of model parameters is called Model I (Set I) which was frequently used in our pervious investigations [7, 8, 5]. Because the systems studied in this paper mostly comprise strange quarks, the strange chiral clouds surrounding the baryons become influential. In order to see this effect, we increase the masses and corresponding cut-masses of κ and ϵ to the values of $1.4GeV$ and $1.5GeV$, respectively, which are close to the masses of real mesons with the same quantum numbers [25]. This set of parameters is called Model I (Set II). When the values of $m_u, m_s, b_u, g_{ch}, m_{\pi_a}, m_{\sigma_a}$ and Λ_{CSB} are fixed, the one gluon exchange coupling constants g_u and g_s can be determined by mass splittings between Δ and N, and Σ and Λ, respectively, the confinement strengths a^c_{uu}, a^c_{us} and a^c_{ss} are fixed by the stability conditions of N, Λ and Ξ, respectively, and the zero point energies a^{c0}_{uu}, a^{c0}_{us} and a^{c0}_{ss} are fixed by the masses of N, Λ and $\overline{\Sigma + \Omega}$, respectively.

As is mentioned above, to predict the dibaryon structure, the model should be able to reproduce the data of the N-N and Y-N scatterings reasonably. The detailed comparison of the theoretical scattering results and the empirical data can be found in [7]. Here, we only show a typical plot, the cross section of the $\Lambda - p$ process in Fig.1. In this figure, the solid and dashed curves represent the results with Sets I and II, respectively. It is shown that both curves are consistent with the experimental data. After confirming the model, we use the same set of parameters to study the dibaryon system.

All the model parameters in Sets I and II are tabulated in Table 1, respectively.

Table 1. Model parameters

	Set I	Set II
$m_u(MeV)$	313	313
$m_s(MeV)$	470	470
$b_u(fm)$	0.505	0.505
g_u	0.936	0.936
g_s	0.924	0.781
$a^c_{uu}(Mev/fm^2)/a^{c0}_{uu}(Mev)$	54.3/-47.7	55.0/-48.9
$a^c_{us}(Mev/fm^2)/a^{c0}_{us}(Mev)$	65.8/-41.7	66.5/-50.6
$a^c_{ss}(Mev/fm^2)/a^{c0}_{ss}(Mev)$	103.0/-50.6	115.4/ -73.7
$m_\pi(fm^{-1})/\Lambda_\pi(fm^{-1})$	0.7/4.2	0.7/4.2
$m_K(fm^{-1})/\Lambda_K(fm^{-1})$	2.51/4.2	2.51/4.2
$m_\eta(fm^{-1})/\Lambda_\eta(fm^{-1})$	2.78/5.0	2.78/5.0
$m_{\eta'}(fm^{-1})/\Lambda_{\eta'}(fm^{-1})$	4.85/5.0	4.85/5.0
$m_{\sigma_0}(fm^{-1})/\Lambda_{\sigma_0}(fm^{-1})$	3.17/4.2	3.17/4.2
$m_{\sigma'}(fm^{-1})/\Lambda_{\sigma'}(fm^{-1})$	4.85/5.0	4.85/5.0
$m_\kappa(fm^{-1})/\Lambda_\kappa(fm^{-1})$	4.85/5.0	7.09/7.6
$m_\epsilon(fm^{-1})/\Lambda_\epsilon(fm^{-1})$	4.85/5.0	7.09/7.6

The binding energy of the baryon-baryon system is dynamically solved by using the Resonating Group Method (RGM). In this method, the trial wave function of the six-quark system can be written as

$$\Psi = \mathcal{A}[\hat{\phi_A}(\xi_1,\xi_2)\hat{\phi_B}(\xi_4,\xi_5)\chi_{rel}(\vec{R})\chi_{CM}(\vec{R}_{CM})]_{ST}, \tag{21}$$

where $\phi_{A(B)}$ denotes the antisymmetrized wave function of the baryon cluster A(B), $\chi_{rel}(\vec{R})$ the trial wave function of the relative motion between interacting clusters A and B, $\chi_{CM}(\vec{R}_{CM})$ the wave function of the motion of the total center of mass, and ξ_i the Jacobi coordinate with $i = 1$ and 2 for cluster A and $i = 4$ and 5 for cluster B, respectively. The symbol $\mathcal{A}$ describes the operation of the antisymmetrization between quarks in two interacting clusters. This operator can be read as

$$\mathcal{A} = N\sum_P \epsilon_P P,$$

where P is an operator which permutes quarks of cluster A and quarks of cluster B, $\epsilon_P = 1(-1)$ when P is an even(odd) permutation and N is the normalization factor. Considering the permutation symmetry, $\mathcal{A}$ can also be written as

$$\mathcal{A} = N'(1 - \sum_{\substack{i\in A\\ j\in B}} P^{osfc}_{ij}), \tag{22}$$

where P_{ij}^{osfc} denotes the permutation operation carried out between the $i-th$ and $j-th$ quarks in the *orbit*, *spin*, $flavor$ and *color* spaces, simultaneously, and again N' represents the normalization constant. Calculating the expectation value of the Hamiltonian operator on the trial wave function in which the unknown $\chi_{rel}(\vec{R})$ is expanded in terms of well-known bases, one deduces a secular equation

$$\sum_{j=1}^{n}(H_{ij}-EN_{ij})c_j=0, \quad (i=1,2,\cdots,n), \tag{23}$$

with H_{ij} and N_{ij} being the Hamiltonian and normalization matrix elements, respectively, E the eigenvalue and c_i the corresponding eigenfunction, namely the expansion coefficients of $\chi_{rel}(\vec{R})$. Solving this equation for c_j, one obtains the binding energy and the corresponding wave function of the six-quark system. The detailed method can be found in our previous paper [24, 5].

3. Symmetry character discussion.

As a comprehensive survey, there are two crucial physical factors which resolve whether a two-baryon system is bound. One is the symmetry property of the system, namely the characteristics of quark exchanges between baryons, and the other is the interaction including both the direct and exchange components between quarks, and eventually between baryons. In this section, we analyze the symmetry property of the system according to the character of the matrix element P_{36}^{sfc}, where the superscript sfc denotes the P operator acts within the $spin-flavor-color$ space only and the subscript 36 represents the exchange operation is between the 3-rd and 6-th quarks. Then, in section 4, we discuss the effects of various chiral-quark field interactions by employing several models.

As is pointed out in Ref.[21], the matrix element $\langle\mathcal{A}^{sfc}\rangle$ is an important measure of the action of the Pauli principle in the two-baryon state. This measure specifies the symmetry character of the state of the system. According to the symmetry characters of systems, namely the mentioned matrix elements, the two-baryon systems concerned can generally be divided into three classes. In the first class, $9\langle P_{36}^{sfc}\rangle\sim 1$, namely, $\langle\mathcal{A}^{sfc}\rangle\sim 0$. The Pauli blocking effect between interacting baryons are incrediblely serious so that the two-baryon $S-$wave state with $[6]_r$, the [6] symmetry in the orbital space, is almost a for-

bidden state. Namely, it is very hard to form a bound state. The state in the second class has the property of $9\langle P_{36}^{sfc}\rangle \sim 0$, or $\langle \mathcal{A}^{sfc}\rangle \sim 1$. In this class, the Pauli blocking effect between interacting baryons are very small so that the exchange effect between quarks which are located in different baryons, respectively, becomes negligible and these two baryons are relatively independent with each other. As a result, the meson-exchange effect may play a dominant role in binding. If the inter-baryon interaction shows an attractive feature with a large enough strength, the system would be bound. This kind of system may also be deduced in terms of a model in the baryon-meson degrees of freedom. The state in the third class possesses a feature of $9\langle P_{36}^{sfc}\rangle \sim -1$, or $\langle \mathcal{A}^{sfc}\rangle \sim 2$. The inter-baryon quark-exchange feature of this kind would be enormously beneficial to form a state with the $[6]_r$ symmetry [21]. If the inter-baryon interaction demonstrates the attractive character with certain strength, it is possible to form not only a bound state, but also a dibaryon with a relative smaller size in radius. We present the resultant binding energies and the corresponding root-mean-square radii (RMS) of the $S-$states which have various strange number $\mathcal{S}$ and belong to the second and third classes in the following subsections.

3.1. The systems in which the expectation values of P_{36}^{sfc} operator are close to zero.

In the deuteron case, $\langle P_{36}^{sfc}\rangle = -1/81$, it is a typical case of the second class. We collect some systems which have the same symmetry characteristics as deuteron in this subsection. The binding energies, E_b, and corresponding RMS, $\mathcal{R}$, of these systems are tabulated in Table 2.

Table 2. Binding energy, E_b, and corresponding RMS, $\mathcal{R}$, for the systems with $\langle P_{36}^{sfc}\rangle \approx 0$. The units for E_b and RMS are in MeV and fm, respectively.

S	System		$\langle P_{36}^{sfc} \rangle$	Model I (Set I) E_b //$\mathcal{R}$	Model I (set II) E_b //$\mathcal{R}$
0	$NN(S=1,T=0)$ deuteron		$-1/81$	0.2 //1.63	-0.7 //1.68
-1	$N\Lambda$ $(S=0,T=1/2)$	$N\Lambda(S=0,T=1/2)$	0	-6.6 //1.63	-7.7 //1.69
		$N\Lambda - N\Sigma(S=0,T=1/2)$		-5.7 //1.59	-7.2 //1.66
	$N\Lambda$ $(S=1,T=1/2)$	$N\Lambda(S=1,T=1/2)$	0	-7.7 //1.68	-7.7 //1.68
		$N\Lambda - N\Sigma(S=1,T=1/2)$		-6.6 //1.63	-6.7 //1.64
	$N\Sigma(S=0,T=3/2)$		$-1/81$	-5.1 //1.58	-5.3 //1.59
-2	$\Lambda\Lambda$ $(S=0,T=0)$	$\Lambda\Lambda(S=0,T=0)$	0	-4.8 //1.54	-5.6 //1.58
		$\Lambda\Lambda - N\Xi - \Sigma\Sigma(S=0,T=0)$ H particle		-2.0 //1.15	8.2 //0.91
-3	$\Lambda\Xi(S=1,T=1/2)$		4/81	-8.1 //1.74	-7.7 //1.72
	$N\Omega(S=2,T=1/2)$		0	3.5 //1.18	12.7 //0.98
	$\Delta\Omega(S=3,T=3/2)$		0	4.4 //1.15	14.2 //0.96
-4	$\Xi\Xi(S=0,T=1)$		$-1/81$	4.1 //1.17	0.4 //1.30
-5	$\Xi\Omega$ $(S=1,T=1/2)$	$\Xi\Omega(S=1,T=1/2)$	1/81	9.5 //1.02	4.2 //1.14
		$\Xi\Omega - \Xi^*\Omega(S=1,T=1/2)$		32.9 //0.78	32.6 //0.77

The data in Table 2 shows that the deuteron is weakly bound in the Model I (Set I) case, which indicates that the chiral $SU(3)$ quark model, in principle, can reasonably describe the structure of deuteron[2]. It is also seen that in the single $N\Lambda$ channel and the coupled $N\Lambda - N\Sigma$ channel with $S = 0(or 1)$ and $T = 1/2$ cases and the single $N\Sigma$ channel with $S = 0$ and $T = 3/2$ case, no matter which set of model parameters is employed, the systems are not bound. These are in agreement with experiments. The H particle is also not bound in Set I but weakly bound in Set II. The resultant mass of H is close to the $\Lambda\Lambda$ threshold in both Set I and Set II, and this feature is consistent with the recent finding in experiments [13]. These results further convince ourselves that the chiral $SU(3)$ quark model is reasonable and reliable in the bound-state study.

It should be noted that $\langle P_{36}^{sfc} \rangle$ of these systems appoximately being zero means that the symmetry structure of this kind makes the quark-exchange effect less important, and consequently, the contribution from the kinetic energy term shows relatively repulsive nature to the kinetic energy of the relative motion between two well-separated interactive baryons (see Appendix), which makes interacting baryons apart. Therefore, very similar to deuteron, whether the two-baryon system is bound depends on the feature of the interaction between interacting baryons, especially that caused by chiral fields, namely the overall characteristics of the short- and medium-range $NPQCD$ effects, to a

[2]Of course, it is easy to fine-tune the mass of σ_0 so that the best agreement between the calculated and experimental binding energy of deuteron can be achieved. However, it is not necessary to give a very accurate mass of predicted dibaryon, we would relinquish this adjustment.

considerable extent. If the characteristics is attractive in nature, the system would be bound like deuteron, and we call it as a deuteron-like system. If it shows weak attraction or even repulsive feature, the system would not be bound anymore. It is also noticed that the OGE interaction provides repulsion in the deuteron, $N\Lambda$, $N\Sigma$, $\Xi\Xi(S=0,T=1)$ and $\Xi\Omega(S=1,T=1/2)$ systems. To form a bound state, a strong enough attractive interaction by the meson exchange must be requested. For instance, the π exchange, especially the tensor force, causes the weakly binding of deuteron and the relative strong attraction from the coupling between the chiral fields and quarks makes $\Xi\Xi(S=0,T=1)$ and $\Xi\Omega(S=1,T=1/2)$ bound. Then in the H particle case, although OGE interaction provides attraction, due to the repulsive effect from the kinetic energy term, the only attraction from OGE potential is not strong enough to cause binding. The attractive feature of the chiral field would be helpful to form a weakly bound H. But it is model parameter dependent. In the $N\Omega(S=2,T=1/2)$ and $\Delta\Omega(S=3,T=3/2)$ cases, OGE contributes nothing, the weakly bound behavior of these systems fully depends on the attractive features of the chiral fields. Moreover, it is noteworthy that very similar to the deuteron, the $\Lambda\Lambda - N\Xi - \Sigma\Sigma(S=0,T=0)$ and $\Xi\Omega - \Xi^*\Omega(S=1,T=1/2)$ systems are bounder than the $\Lambda\Lambda(S=0,T=0)$ and $\Xi\Omega(S=1,T=1/2)$ systems due to the channel coupling effect.

In summary, we predict that $N\Omega(S=2,T=1/2)$, $\Delta\Omega(S=3,T=3/2)$, $\Xi\Xi(S=0,T=1)$ and $\Xi\Omega(S=1,T=1/2)$ are weakly bound baryon-baryon states. The mass of the H particle is around the $\Lambda\Lambda$ threshold. $\Xi\Omega-\Xi^*\Omega(S=1,T=1/2)$ system is a bound state with a relative large binding energy due to the strong channel coupling.

3.2. The systems in which the expectation values of P_{36}^{sfc} operator are close to $-1/9$.

The systems in which $\langle P_{36}^{sfc}\rangle \approx -1/9$ are collected in this category. The binding energies, E_b, and corresponding root-mean-square radii, $\mathcal{R}$, of these systems are tabulated in Table 3.

Table 3. Binding energy, E_b, and corresponding RMS, $\mathcal{R}$, for the systems with $\langle P_{36}^{sfc}\rangle = -1/9$. The units for E_b and RMS are in MeV and fm, respectively.

S	System	$\langle P_{36}^{sfc}\rangle$	Model I (Set I) E_b //$\mathcal{R}$	Model I (set II) E_b //$\mathcal{R}$
0	$\Delta\Delta(S=3,T=0)$ (d^*)	$-1/9$	22.2 //1.01	18.5 //1.05
	$\Delta\Delta(S=0,T=3)$	$-1/9$	16.0 //1.10	13.5 //1.14
-1	$\Sigma^*\Delta(S=0,T=5/2)$	$-1/9$	24.6 //0.99	19.0 //1.04
	$\Sigma^*\Delta(S=3,T=1/2)$	$-1/9$	25.9 //0.95	29.3 //0.93
-5	$\Xi^*\Omega(S=0,T=1/2)$	$-1/9$	92.4 //0.71	76.5 //0.72
-6	$\Omega\Omega(S=0,T=0)$	$-1/9$	116.1 //0.66	98.5 //0.67

¿From this table, one sees that all the systems in this category have the feature of $\langle P_{36}^{sfc}\rangle = -1/9$. It indicates that the system has relatively higher anti-symmetry in the *spin-flavor-color* space. As a consequence, the contribution of the kinetic energy to the binding energy plays a relatively attractive role in comparision with the kinetic energy in two independ baryons [21] (see Appendix). This characteristics would bring six quarks closer. If the chiral fields can additionally provide attraction between interacting baryons, the deeply bound state may be established, such as $\Omega\Omega(S=0,T=0)$ and $\Xi^*\Omega(S=0,T=1/2)$. Even the contributions of chiral fields are mild, the system with the symmetry structure of this kind may still have the binding energy of several tens MeV. Therefore, in any case, the system in this category would be a bound state. However, it should be noticed that in most states here, such as $\Delta\Delta$ and $\Sigma^*\Delta$, both composed baryons have strong decay modes. Therefore, if the $\Delta\Delta$ and $\Sigma^*\Delta$ are not bound deeply enough, namely their masses are not smaller than the thresholds of $NN\pi\pi$ and $N\Lambda\pi\pi$, respectively, these four states should be bound states with broad widths. Only $\Omega\Omega(S=0,T=0)$ and $\Xi^*\Omega(S=0,T=1/2)$ are the most interesting systems. Both Ω's in $\Omega\Omega(S=0,T=0)$ can decay only through the weak mode, so that $\Omega\Omega(S=0,T=0)$ is a bound state with a narrow width. It is also possible that the mass of $\Xi^*\Omega(S=0,T=1/2)$ is smaller than the threshold of $\Xi\Omega\pi$ (with Set I), then this state could also be a narrow width bound state.

4. Effects of interactions induced by chiral-quark field couplings.

In this section, we would demonstrate another factor which dominates the binding behavior of the system concerned, namely the interactions caused by the chiral-quark field couplings.

The characters of chiral fiels are different case by case, and the importance and sensitivity of these fields in the bound-state problem of six-quark systems also dissimilar. In order to analyze the effect of the chiral field on the binding

energy of the baryon-baryon system, we build up other two models. In Model II, the π, K, η, η' and σ_0 are considered. This is so called extended chiral $SU(2)$ quark model. The Model III is called chiral $SU(2)$ quark model, in which only π and σ_0 fields are remained.

We arrange all concerned systems which are possibly bound into following types:

4.1. Deuteron-like systems.

To convince readers the the importance of the interaction for binding, we present the contributions of various terms, such as kinetic energy, OGE, pseudoscalar meson exchange and scalar mesons exchange terms to the total binding energy for the typical case $\Xi\Xi_{(0,1)}$ in table 4.

Table 4. Contributions of various terms to binding energy for $\Xi\Xi_{(0,1)}$, the unit for energy is in MeV.

	kine.	OGE	π	K	η	η'	σ	σ'	κ	ϵ
Model I Set 1	-17.3	-15.2	-1.2	-1.7	-1.4	-0.8	37.7	1.9	-1.2	6.2
Model II	-12.0	-5.5	-0.8	-1.1	-0.8	-0.5	26.0	–	–	–
Model III	-16.1	-15.8	-1.4	–	–	–	40.5	–	–	–

From the table, we sees that although the kinetic energy, OGE and pseudoscalar mesons provide the repulsive feature, the strong attractive effect from scalar mesons, especially σ meson, would compensate the repulsion and make the $\Xi\Xi_{(0,1)}$ system weakly bound.

We then demonstrate the binding energies and the corresponding root-mean-square-radii of the bound systems in Sect.3.1 with Models I (set I), II and III, respectively, in Table 5, except the H particle which was carefully studied in our previous paper [5].

Table 5. Binding energy, E_b, and corresponding RMS, $\mathcal{R}$, for deuteron-like systems in various chiral quark models. The units for E_b and RMS are in MeV and fm, respectively. The system is denoted by symbol $[B_1B_2]_{(S,T)}$ with B_1, B_2, S and T being baryons 1 and 2 and the total spin and isospin of the system, respectively.

Model	$\mathcal{S}=-5$	$\mathcal{S}=-4$	$\mathcal{S}=-3$		$\mathcal{S}=0$
	$[\Xi\Omega-\Xi^*\Omega]_{(1,1/2)}$	$[\Xi\Xi]_{(0,1)}$	$[N\Omega]_{(2,1/2)}$	$[\Delta\Omega]_{(3,3/2)}$	$d_{(S=1,T=0)}$
	E_b //$\mathcal{R}$	E_b //$\mathcal{R}$	E_b //$\mathcal{R}$	E_b //$\mathcal{R}$	E_b //$\mathcal{R}$
I (Set I)	32.9 //0.78	4.1 //1.17	3.5 //1.18	4.4 //1.15	0.2 //1.63
II	29.3 //0.79	-0.5 //1.33	31.8 //0.81	34.3 //0.80	2.1 //1.52
III	17.6 //0.86	3.1 //1.18	49.5 //0.74	49.6 //0.74	4.4 //1.41

As mentioned in the preceding section, the binding energies of the systems in this type are sensitive to the contributions offered by the chiral field. This

character is very similar to that of deuteron and can explicitly be seen in this table. In most cases in this type, say the systems with low strange number, when one switches the model from Model II to Model I (Set I) or even from Model III to model II, namely the strange clouds are taken into account step by step, additional strange-cloud-caused interactions would make the overall inter-baryon interaction less attractive in nature, and consequently the systems would become less bounder. In a word, these systems are bounder in the chiral $SU(2)$ quark model than in the chiral $SU(3)$ quark model. But, in high strangeness systems, additionally taking strange clouds into account would benefit the binding.

The channel sketches and the predicted mass ranges of these states with the different combinations of chiral fields, which are denoted by shaded areas, are plotted in Figs.2(a)-(d) for the $[\Xi\Omega - \Xi^*\Omega]_{(1,1/2)}$, $[\Xi\Xi]_{(0,1)}$, $[N\Omega]_{(2,1/2)}$ and $[\Delta\Omega]_{(3,3/2)}$ systems, respectively.

4.2. $\Delta\Delta$- and $\Omega\Omega$-like systems

Now, we analyze the role or impoatance of the interaction in the system in the third class or in subsection 3.2.. As is mentioned above, except the symmtry character $\langle P_{36}^{sfc}\rangle \approx -1/9$ of the system, the effect of the interaction is dominantly responsible for binding. A detailed study of the binding energies of the systems in this category show that, different with the contribution provided by the interaction in the second class, the contribution from exchange term of the interaction is substantially large and gernerally has two different character for various states in the class. Considering this difference together with the different decay mode, we further distinguish the states in this class into $\Delta\Delta$-like states and $\Omega\Omega$-like states. In $\Delta\Delta$-like states, where only weak decays exist, the direct and exchange terms of interactions play comparable roles in forming dibaryon and the binding energies of these states are only a few tens of MeV. As a specific example, the calculated result showes that in $\Delta\Delta_{(0,3)}$, the exchange term of the interaction induced by σ meson provides a binding energy of 17.0 MeV, which is comparable to the direct contribution of 16.0 MeV. While in $\Omega\Omega$-like states, where at most one strong decay mode exists, the exchange terms of interactions play much more important roles than the direct terms do and the binding energies of these states can reach nearly one

predicted some bound states in the $\mathcal{S} = -2, \ -3$ and -4 systems [27].

The $\Delta\Delta$-like state is the second type state. The system of this type is mostly symmetric in the *orbit* space. In these states, the interaction, especially the scalar meson induced interaction, dominates the binding behavior. Together with the symmetry behavior of the system, the relatively deeply-bound state can be formed. However, because both baryons in the system have strong decay modes, only when the predicted binding energy is lower than the threshold of the strong decay channel, say the $NN\pi\pi$ channel for the $\Delta\Delta$ system and the $\Lambda N\pi\pi$ channel for the $\Sigma^*\Delta$ system, the width of the bound state could be narrow. In our calculation, the predicted binding energies of $\Delta\Delta$ and $\Sigma^*\Delta$ are not large enough, so that the widths of these bound states should be rather broad. Although this kind of bound state might not easily be detected in experiments, it may worth to search in the future.

The third type state is the $\Omega\Omega$-like state, which is the most interesting state in our study. Same as those in the second type, the system in this type is mostly symmetric in the *orbit* space. Meanwhile, the strange chiral fields can offer rather strong attraction. As a result, these states are deeply bound states. If we believe that the chiral $SU(3)$ quark model is one of the most suitable models in describing the system with high strangeness, the predicted binding energy of $\Xi^*\Omega$ is possibly below the threshold of the strong decay channel $\Xi\Omega\pi$. Thus, both $\Omega\Omega$ and $\Xi^*\Omega$ can merely have weak decays, and consequently are deeply bound states with narrow widths.

It should be specially emphasized that the states of the second and third types possess the six-quark structure, and their inter-baryon distances are relatively short. These characteristics cannot be provided by the model on the baryon level. Thus, they are new dibaryon systems. The existences of this kind of dibaryons would be an important place to reveal QCD phenomenology.

Appendix.

In the framework of RGM [28], the upper bound is given by the expectation

value of the Hamiltonian

$$\langle H\rangle = \frac{\langle\Psi|H|\Psi\rangle}{\langle\Psi|\Psi\rangle}, \tag{24}$$

where $H = T + V$ is the Hamiltonian, with T and V being the kinetic energy operator and the potential operator, respectively, Ψ represents the trial wave function of the system and $\langle H\rangle$ denotes the upper bound of the system. The kinetic operator of a six-quark system can be written as:

$$T = \sum_{i=1}^{6} T_i - T_{CM}, \tag{25}$$

where T_i and T_{CM} denote the kinetic energy operators of the i-th quark and of the center of mass motion (CM), respectively. Substituting the trial wave function (Eq.(21)) and the antisymmetrizer $\mathcal{A}'$ (Eq.(22)) into projection equation

$$\langle[\hat{\phi}_A\hat{\phi}_B\chi_{CM}(\vec{R_{CM}})]_{ST}|H - E|\mathcal{A}'[\hat{\phi}_A\hat{\phi}_B\chi_{rel}(\vec{R})\chi_{CM}(\vec{R_{CM}})]_{ST}\rangle = 0, \tag{26}$$

one obtains RGM equation

$$\begin{aligned}\{ \; - \; & \frac{\hbar^2}{2\mu}\nabla^2_{\vec{R}} + V^{dir}_{rel}(\vec{R}) - E_{rel}\}\chi_{rel}(\vec{R}) \\ + \; & \int[K^T(\vec{R},\vec{R'}) + K^V(\vec{R},\vec{R'}) - E_{tot}N^{exch}(\vec{R},\vec{R'})]\chi_{rel}(\vec{R'})\, d\vec{R'} = 0,\end{aligned} \tag{27}$$

where $V^{dir}_{rel}(\vec{R})$ represents the relative potential between two clusters, E_{tot} and E_{rel} denote the total energy and the relative energy between two clusters, respectively, and $K^T(\vec{R},\vec{R'})$, $K^V(\vec{R},\vec{R'})$ and $N^{exch}(\vec{R},\vec{R'})$ describe the kinetic energy exchange kernel, the potential energy exchange kernel and the normalization exchange kernel, respectively. Expanding $\chi_{rel}(\vec{R})$ by well-defined basis functions

$$\chi_{rel}(\vec{R'}) = \sum_{i=1}^{n} c_i\phi_{rel}(\vec{R'},\vec{S_i}), \tag{28}$$

and left-multiplying $\phi_{rel}(\vec{R},\vec{S_i})$ to RGM equation and integrating over $\vec{R}$ and $\vec{R'}$, one obtains the secular equation of the bound state problem,

$$\begin{aligned}&\sum_{i=1}^{n}[H_{ij} - E_{tot}\; N_{ij}]\; c_j \\ = \; &\sum_{i=1}^{n}[H'_{ij} - E_{rel}\; N_{ij}]\; c_j = 0, \qquad (i = 1,\cdots,n)\end{aligned} \tag{29}$$

with H_{ij} and N_{ij} being the Hamiltonian and normalization kernels, respectively, and

$$E_{tot} = E_{in} + E_{rel}, \tag{30}$$

E_{tot}, E_{in} and E_{rel} being the total, inner cluster and relative energies, respectively. Apparently, H' can be written as:

$$\begin{aligned} H'_{ij} &= H_{ij} - E_{in}N_{ij} \\ &= [T_{ij} - E^T_{in}N_{ij}] + [V_{ij} - E^V_{in}N_{ij}]. \end{aligned} \tag{31}$$

In this equation, T_{ij} and V_{ij} is the kinetic energy and potential energy kernels, respectively, and the superscripts T and V denote the kinetic energy and potential energy parts, respectively. Then,

$$\begin{aligned} H^{T\prime}_{ij} &= T_{ij} - E^T_{in}N_{ij} \\ &= (T^{dir}_{rel})_{ij} + (T^{exch}_{rel})_{ij} \end{aligned} \tag{32}$$

with

$$(T^{dir}_{rel})_{ij} = \langle \phi_{rel}(\vec{R''}, \vec{S}_i)|(-\frac{\hbar^2}{2\mu}\nabla^2_{\vec{R'}})\delta(\vec{R''} - \vec{R'})|\phi_{rel}(\vec{R'}, \vec{S}_j)\rangle \tag{33}$$

and

$$(T^{exch}_{rel})_{ij} = \langle \phi_{rel}(\vec{R''}, \vec{S}_i)|K^T(\vec{R''}, \vec{R'})|\phi_{rel}(\vec{R'}, \vec{S}_j)\rangle. \tag{34}$$

To compute $H^{T\prime}_{ij}$ explicitly, we employ the Generating Coordinate Method (GCM) technique, which is equivalent to RGM. In GCM, we re-write

$$\Psi = \sum_{i=1}^{n} c_i\psi_i \tag{35}$$

with

$$\begin{aligned} \psi_i &= \mathcal{A}'[\hat{\phi}_A\hat{\phi}_B\phi_{rel}(\vec{R'}, \vec{S}_i)\chi_{CM}(\vec{R_{CM}})\chi_{ST}\chi_c] \\ &= \mathcal{A}'[\prod_{n=1}^{3}\phi_{0s}(\vec{r}_n - \frac{\vec{S}_i}{2})\prod_{k=4}^{6}\phi_{0s}(\vec{r}_k + \frac{\vec{S}_i}{2})\chi_{ST}\chi_c] \end{aligned} \tag{36}$$

and

$$\phi_{0s}(\vec{r}_n - \frac{\vec{S}_i}{2}) = N_n \exp -\frac{1}{2b_n^2}(\vec{r_n} - \frac{\vec{S}}{2})^2. \tag{37}$$

To ensure the total CM motion can explicitly be separated, we keep ω unchanged, namely

$$\omega = (m_u b_u^2)^{-1} = (m_s b_s^2)^{-1}. \tag{38}$$

If one temporarily ignores the flavor symmetry breaking, namely $b = b_u = b_s$ and $m = m_u = m_s$, for instance in the $(\Omega\Omega)$ or $\Delta\Delta$ or NN system, the following discussion would be flavor independent and it is easy to obtain the kinetic energy induced S-wave adiabatic *effective interaction*

$$\begin{aligned} E_{ii}^T &= \frac{H_{ii}^{T\prime}}{N_{ii}} - \frac{K_0}{3} \\ &= 2K_0 x[-1 + Ctgh(3x)\frac{1 - 9\langle P_{36}^{sfc}\rangle Cosh(x)/Cosh(3x)}{1 - 27\langle P_{36}^{sfc}\rangle Sinh(x)/Sinh(3x)}] \end{aligned} \tag{39}$$

with

$$x = \frac{S_i^2}{4b^2} \tag{40}$$

and

$$K_0 = \frac{3}{4}\hbar\omega. \tag{41}$$

According to the definition of the binding energy

$$E_b = -(M_{DB} - M_A - M_B), \tag{42}$$

where M_{DB}, M_A and M_B denote the masses of the dibaryon, baryon A and baryon B, respectively, the contribution of the kinetic energy to the binding energy of the dibaryon in the adiabatic approximation should be

$$E_b^T = -\sum_{i=1}^{n} c_i^2 E_b^T(S_i) \tag{43}$$

with

$$E_b^T(S_i) = E_{ii}^T + \frac{K_0}{3}, \tag{44}$$

where c_i is the wavefunction. We plot $E_b^T(S_i)$ versus S_i in Fig.4 (for convenience, we drop the subscript i in S_i in Fig.4). In this figure, the solid and

dashed curves denote the results with $\langle P_{36}^{sfc}\rangle = -1/9$ and $\langle P_{36}^{sfc}\rangle = -1/81$, respectively. Apparently, when $\langle P_{36}^{sfc}\rangle = -1/81$, $E_b^T(S_i)$ has less attractive character than that in the $\langle P_{36}^{sfc}\rangle = -1/9$ case. And when $\langle P_{36}^{sfc}\rangle \geq 0$, it would be even less attractive.

Apparently, E_b^T is always a negative number (or repulsive for binding). This indicates that, when off-diagonal matrix elements contribution can be neglected under adiabatic approximation, E_b^T always has a repulsive effect.

However, when calculating E_b^T, one should also take the off-diagonal matrix elements into account. Further calculation shows that the contribution of the off-diagonal matrix elements differs substantially in the system with $\langle P_{36}^{sfc}\rangle = -1/9$ to that in the system with $\langle P_{36}^{sfc}\rangle \approx 0$. In the former case, it is so large that E_b^T can be changed to a positive value (or attractive for binding). For instance, in the $\Omega\Omega_{(0,0)}$ dibaryon, the contribution of the diagonal matrix elements is -145.6 MeV while the contribution of the off-diagonal matrix elements is 154.2 MeV, and consequently $E_b^T = 8.6$ MeV. On the other hand, in the latter case, this contribution is not large enough to change the sign of E_b^T. For instance, in the deuteron case, the contribution of the diagonal matrix elements is -57.5 MeV while the contribution of the off-diagonal matrix elements is 43.0 MeV, and consequently $E_b^T = -14.5MeV$. The effect of the off-diagonal matrix elements can also simply be seen by diagonalizing the $-(E_{ij}^T + \frac{K_0}{3})$, called $\tilde{E}_{ij}^T$, matrix. In the $\langle P_{36}^{sfc}\rangle = -1/9$ case, some of diagonalized matrix elements $\tilde{E}_{ii}^T$ can be positive. Because

$$E_b^T = \sum_i^n \tilde{c}_I^2 \tilde{E}_{ii}^T, \tag{45}$$

where $\tilde{E}_{ii}^T$ is the diagonalized matrix element, and $\tilde{c}_i$ is the wave function after the unitary transformation that diagonalizes the $-(E_{ij}^T + \frac{K_0}{3})$ matrix, the resultant E_b^T becomes positive. While for the system with $\langle P_{36}^{sfc}\rangle \approx 0$, the diagonalized matrix elements are always negative, consequently, E_b^T always keeps a negative value.

The physics picture of the positive contribution (ot attractive contribution) of the kinetic energy operator to the total binding energy may be understood as the following. In the dibaryon with $\langle P_{36}^{sfc}\rangle = -1/9$, such as $\Omega\Omega_{(0,0)}$, six quarks interfere with each other very strongly due to the large quark exchange effect,

so that they cannot move as freely as they do in two independent baryons. So the expectation value of kinetic energy operator in such system (which is definitely positive) would be smaller than the kinetic energy in two independent baryons. While in system with $\langle P_{36}^{sfc} \rangle \approx 0$, the quark exchange effect is so weaker that the expectation value of kinetic energy operator is always larger than that the kinetic energy in two baryons.

References

[1] R.L.Jaffee, *Phys. Rev. Lett.* **38**, 195 (1977).

[2] A.Chodos, R.L.Jaffe, K.Johnson, et al., *Phys. Rev.* D **9**, 3471 (1974); T.DeGrand, R.L.Jaffe, K.Johnson, et al., *Phys. Rev.* D **12**, 2060 (1975).

[3] M.Oka and K.Yazaki, *Phys. Lett.* B **90**, 41 (1980); A.Faessler, F.Fernandez, G.Lübeck, et al., *Nucl. Phys.* A **402**, 555 (1983); M.Oka, K.Shimizu, K.Yazaki, *Nucl. Phys.* A **464**, 700 (1987); U.Straub, Z.Y.Zhang, K.B.Bräuer, A.Faessler, *Phys. Lett.* B **200**, 241 (1988); *Nucl. Phys.* A **483**, 686 (1988); A.Valcarce, B.Buchmann, A.Fernandez, A.Faessler, *Phys. Rev.* C **50**, 2246 (1994).

[4] K.Yazaki, *Prog.Theor.Phys.* Suppl. **91**, 146 (1987), and references therein.

[5] P.N.Shen, Z.Y.Zhang, Y.W.Yu, S.Q.Yuan, S.Yang, *J. Phys.* G **25**, 1807 (1999); *Chin. Phys. Lett.* , (1999).

[6] K.Shimizu, M.Koyama, *Nucl. Phys.* A **646**, 211 (1999).

[7] Z.Y.Zhang, Y.W.Yu, P.N.Shen, L.R.Dai, A.Faessler, U.Straub, *Nucl. Phys.* A **625**, 59 (1997).

[8] S.Yang, P.N.Shen, Z.Y.Zhang, Y.W.Yu, *Nucl. Phys.* A **635**, 146 (1998).

[9] G.S. Adkins et al., *Nucl. Phys.* B **228**, 552 (1983); E.M. Nyman, *Phys. Lett.* B **142**, 388 (1984).

[10] H.Georgi, Weak Interactions and Modern Particle Theory (Benjamin/Cummings)

[11] I.T.Obukhovsky and V.G.Kusainov, *Phys. Lett.* B **238**, 142 (1990); A.Buchmann, E.Fernandez and K.Yazaki, *Phys. Lett.* B **269**, 35 (1991); E.M.Henley and G.A.Miller, *Phys. Lett.* B **251**, 453 (1991).

[12] M.D.Scadron, *Phys. Rev.* D **26**, 239 (1982).

[13] K.Imai, **Hadrons and Nuclei with Strangeness**- *Proceedings of the First Sino-Japan Symposium on Strangeness Physics*, (to be published in 1999), and references therein.

[14] Y.W. Yu, Z.Y.Zhang and X.Q. Yuan, *High Energy Phys. and Nucl. Phys.* **23**, 859 (1999).

[15] M.Oka, K.Shimizu, K.Yazaki, *Phys. Lett.* B **130**, 365 (1983); K.Yazaki, **Hadrons and Nuclei with Strangeness**- *Proceedings of the First Sino-Japan Symposium on Strangeness Physics*, (to be published in 1999), and references therein..

[16] Y.W.Yu, Z.Y.Zhang and X.Q.Yuan, *Communi.Theor.Phys.* **31**, 1 (1999).

[17] D.Kamae and T.Fujita, *Phys. Rev. Lett.* **38**, 471 (1977).

[18] N.R.Walet, *Phys. Rev.* C **48**, 2222 (1993).

[19] F.Wang, J.L.Ping, G.H.Wu, et al., *Phys. Rev.* C **51**, 3411 (1995)

[20] X.Q.Yuan, Z.Y.Zhang, Y.W.Yu and P.N.Shen, *Phys. Rev.* C **60**, 045203 (1999); *Communi.Theor.Phys.* **32**, 169 (1999).

[21] Z.Y.Zhang, Y.W.Yu, C.R. Ching, et al., *Phys. Rev.* C **61**, 065204 (2000), and references therein. P.N.Shen, Q.B.Li, Z.Y.Zhang, et al., Proceedings of Hadron'99, Beijing, China, 1999, *Nucl. Phys.* A.

[22] R.Bilger and H.A.Clement, *Phys. Rev. Lett.* **71**, 42 (1993).

[23] G.Wagner, L.Ya.Glozman, A.J.Buchmann and A.Faessler, *Nucl. Phys.* A **594**, 263 (1995), and references therein.

[24] Q.B.Li and P.N.Shen, *Chin. Phys. Lett.* **17**, 182 (2000).

[25] Particle Data Group, *Euro.Phys.J.* C **3**, 353 (1998).

[26] P.J.G.Mulders, A.T.Aerts and J.J.Swarts, *Phys. Rev. Lett.* **40**, 1543 (1978); *Phys. Rev.* D **21**, 2653 (1980).

[27] T.A.Rijken, *Proceedings of Asia Pasific Conference on Few-Body Problems In Physics*, Noda/Kashiwa, Japan, 1999.

[28] K.Wildermuth and Y.C.Tang, *A Unified Theory of the Nucleus*, Academic Press Inc., 1977.

Figure captions

Fig.1. Λ-P scattering.

Fig.2. Energy level sketches for a.$[\Xi\Omega\text{-}\Xi^*\Omega]_{(1,1/2)}$, b. $[\Xi\Xi]_{(0,1)}$, c.$[N\Omega]_{(2,1/2)}$, d.$[\Delta\Omega]_{(3,3/2)}$, e.$[\Sigma^*\Delta]_{(0,5/2)}$ and $[\Sigma^*\Delta]_{(3,1/2)}$, f.$[\Delta\Delta]_{(0,3)}$ and $[\Delta\Delta]_{(3,0)}$, g.$[\Omega\Omega]_{(0,0)}$, h.$[\Xi^*\Omega]_{(0,1/2)}$.

Fig.3. Binding energy E_b with respect to b_u and m_s for systems with $\langle \mathcal{A}^{sfc} \rangle \approx 2$. The solid curves are for m_s=470 MeV, the dashed curves are for m_s=515 MeV.

Fig.4. In the S-wave case, the contribution to binding energy provided by the kinetic-energy related terms with different S in the adiabatic approximation.

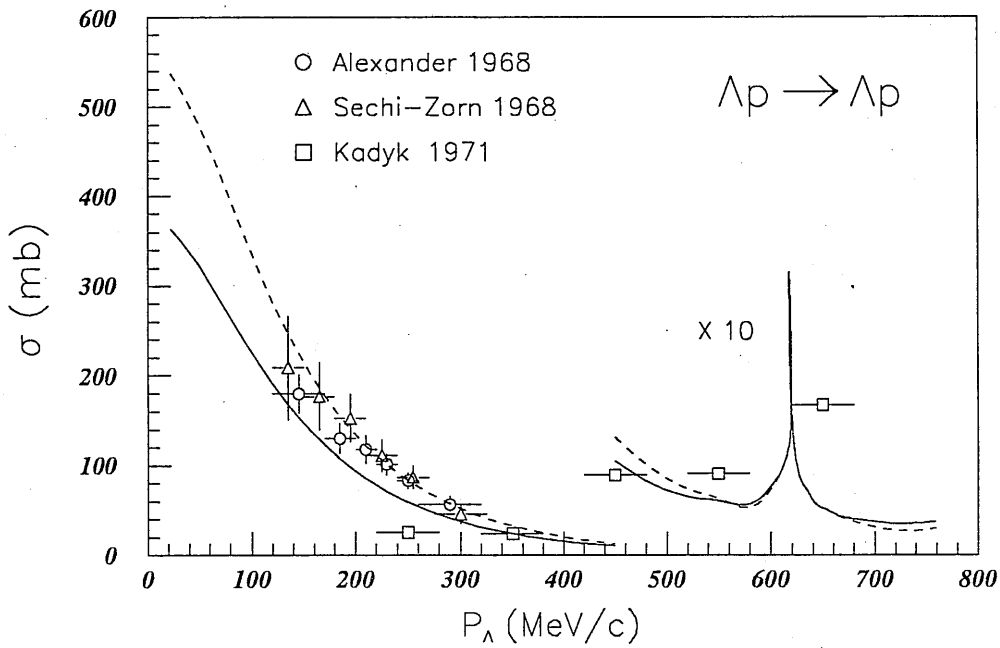
600
500
400
300
200
100
0
σ (mb)
0
100
200
300
400
500
600
700
800
P_Λ (MeV/c)
O Alexander 1968
Δ Sechi-Zorn 1968
□ Kadyk 1971
Λp → Λp
X 10

Fig. 1

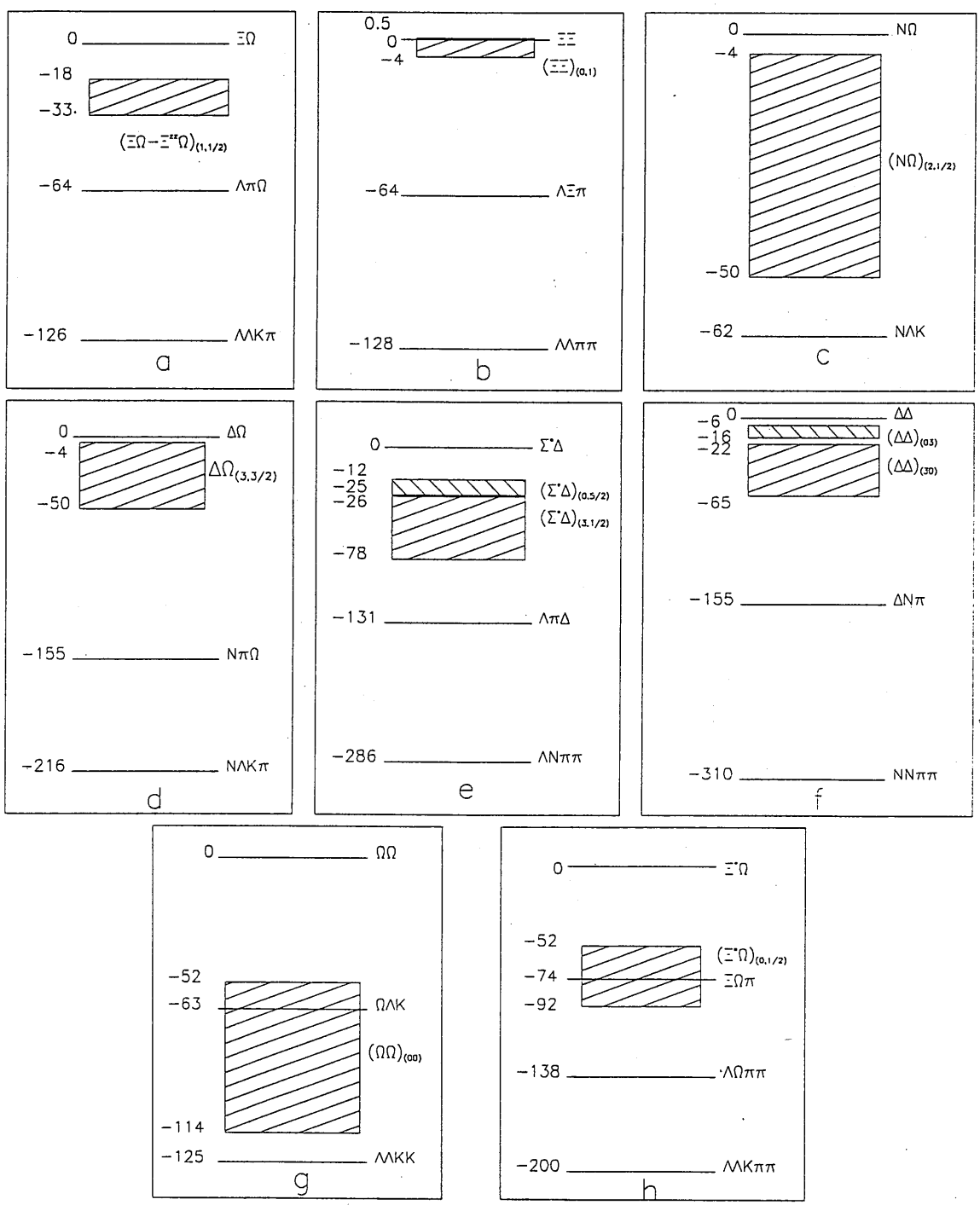
0
ΞΩ
−18
−33.
(ΞΩ−Ξ*Ω)(1,1/2)
−64
ΛπΩ
−126
ΛΛKπ
a
0.5
0
−4
ΞΞ
(ΞΞ)(0,1)
−64
ΛΞπ
−128
ΛΛππ
b
0
NΩ
−4
(NΩ)(2,1/2)
−50
−62
NΛK
c
0
ΔΩ
−4
ΔΩ(3,3/2)
−50
−155
NπΩ
−216
NΛKπ
d
0
Σ*Δ
−12
−25
−26
(Σ*Δ)(0.5/2)
(Σ*Δ)(3,1/2)
−78
−131
ΛπΔ
−286
ΛNππ
e
0
ΔΔ
−6
−16
−22
(ΔΔ)(03)
(ΔΔ)(30)
−65
−155
ΔNπ
−310
NNππ
f
0
ΩΩ
−52
−63
ΩΛK
(ΩΩ)(00)
−114
−125
ΛΛKK
g
0
Ξ*Ω
−52
−74
−92
(Ξ*Ω)(0,1/2)
ΞΩπ
−138
ΛΩππ
−200
ΛΛKππ
h

Fig. 2

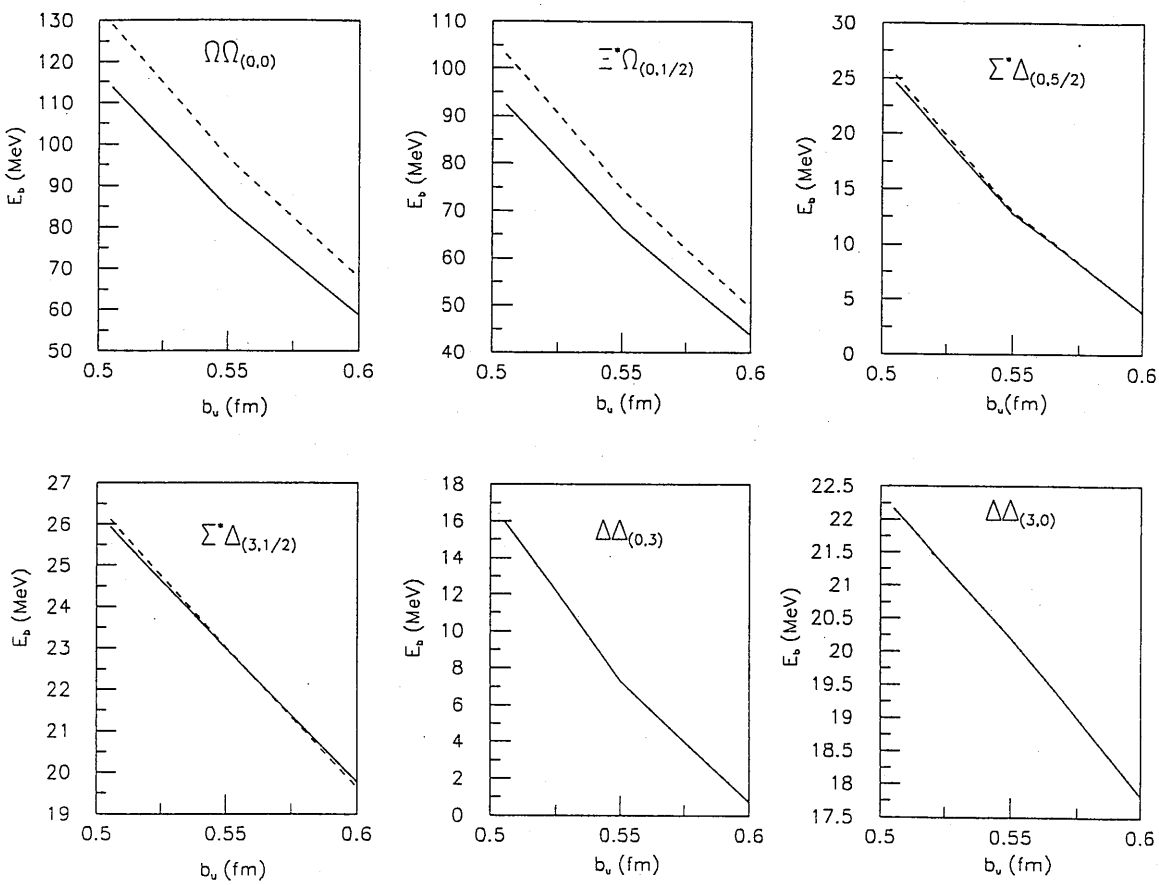
$\Omega\Omega_{(0,0)}$
$\Xi^*\Omega_{(0,1/2)}$
$\Sigma^*\Delta_{(0,5/2)}$
$\Sigma^*\Delta_{(3,1/2)}$
$\Delta\Delta_{(0,3)}$
$\Delta\Delta_{(3,0)}$
E_b (MeV)
b_u (fm)

Fig. 3

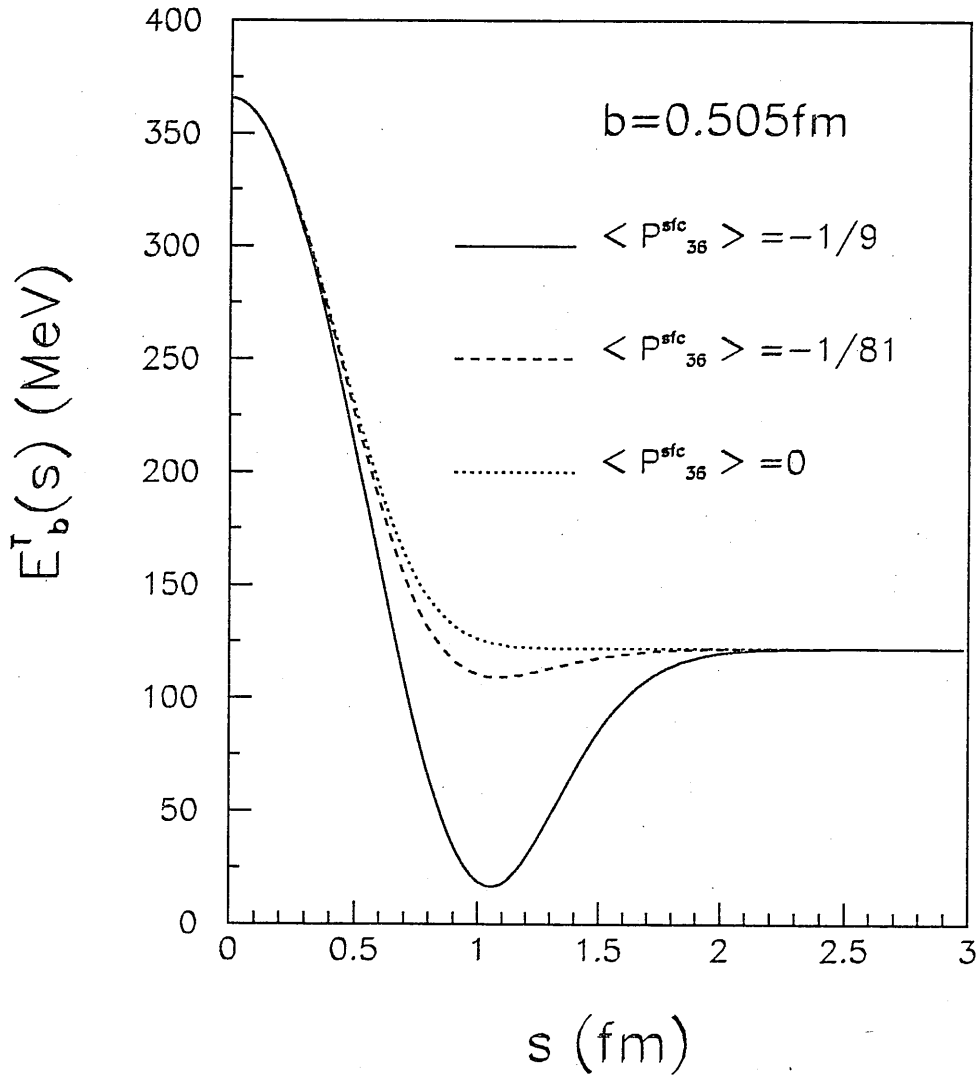
400
350
300
250
200
150
100
50
0
0
0.5
1
1.5
2
2.5
3
b=0.505fm
< P^sfc_36 > =−1/9
< P^sfc_36 > =−1/81
< P^sfc_36 > =0
E^T_b(s) (MeV)
s (fm)

Fig. 4

N^* and Meson Resonances in J/ψ decays*

BING-SONG ZOU,

Institute of High Energy Physics, Chinese Academy of Sciences,
P.O.Box 918 (4), Beijing 100039, P.R.China

(representing BES Collaboration)

Over sixty million J/ψ events have been collected by the BES Collaboration at the Beijing Electron-Positron Collider (BEPC). J/ψ decays provide an excellent place for studying excited nucleons and hyperons – N^*, Λ^*, Σ^* and Ξ^* resonances, as well as meson resonances, including possible glueballs and hybrids. Physics objectives, recent results and future prospects of light hadron spectroscopy at BEPC are presented.

PACS numbers: 13.25Gv, 14.40Cs, 14.20Gk, 13.65+i

1. Introduction

The Institute of High Energy Physics at Beijing runs an electron-positron collider (BEPC) with a general purpose solenoidal detector, the BEijing Spectrometer (BES)[1], which is designed to study exclusive final states in e^+e^- annihilations at the center of mass energy from 2000 to 5600 MeV. In this energy range, the largest cross sections are at the $J/\psi(3097)$ and $\psi'(3686)$ resonant peaks. Up to now, the BES has collected about 65 million J/ψ events and 18 million ψ' events. From J/ψ and ψ' decays, both meson spectroscopy and baryon spectroscopy can be studied.

Three main processes which play very important role for the light hadron spectroscopy are ψ hadronic decay into baryons and anti-baryons, ψ radiative decay, and ψ hadronic decay into mesons. In the following three sections, I will outline the physics objectives and summarize recent results for each of them. Future prospects are given in the final section.

* Presented at the Meson2002, 7th International Workshop on Production, Properties and Interaction of Mesons, Cracow, Poland, May 23-28, 2002

2. N^* and hyperons from J/ψ decays

Baryons are the basic building blocks of our world. If we cut any piece of object smaller and smaller, we will finally reach the nucleons, *i.e.*, the lightest baryons, and we cannot cut them smaller any further. So without mention any theory, we know that the study of baryon structure is at the forefront of exploring microscopic structure of matter. From theoretical point of view, since baryons represent the simplest system in which the three colors of QCD neutralize into colorless objects and the essential non-Abelian character of QCD is manifest, understanding the baryon structure is absolutely necessary before we claim that we really understand QCD.

Spectroscopy has long proved to be a powerful tool for exploring internal structures and basic interactions of microscopic world. Ninety years ago detailed studies of atomic spectroscopy resulted in the great discovery of Niels Bohr's atomic quantum theory[2]. Forty to sixty years later, still detailed studies of nuclear spectroscopy resulted in Nobel Prize winning discoveries of nuclear shell model[3] and collective motion model[4] by Aage Bohr *et al.* Comparing with the atomic and nuclear spectroscopy at those times, our present baryon spectroscopy is still in its infancy[5]. Many fundamental issues in baryon spectroscopy are still not well understood[6]. The possibility of new, as yet unappreciated, symmetries could be addressed with accumulation of more data. The new symmetries may not have obvious relation with QCD, just like nuclear shell model and collective motion model.

Joining the new effort on studying the excited nucleons, N^* baryons, at new facilities such as CEBAF at JLAB, ELSA at Bonn, GRAAL at Grenoble and SPRING8 at JASRI, we also started a baryon resonance program at BES[7], at Beijing Electron-Positron Collider (BEPC). The J/ψ and ψ' experiments at BES provide an excellent place for studying excited nucleons and hyperons – N^*, Λ^*, Σ^* and Ξ^* resonances[8]. The corresponding Feynman graph for the production of these excited nucleons and hyperons is shown in Fig. 1 where ψ represents either J/ψ or ψ'.

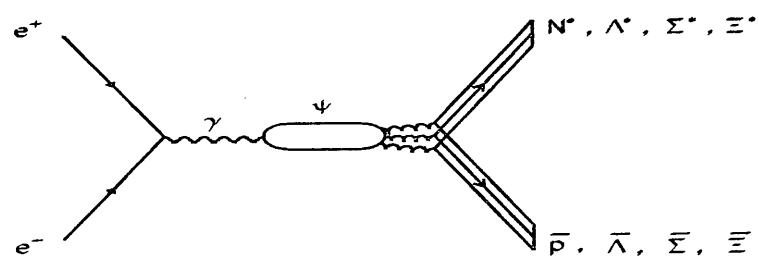

Fig. 1. $\bar{p}N^*$, $\bar{\Lambda}\Lambda^*$, $\bar{\Sigma}\Sigma^*$ and $\bar{\Xi}\Xi^*$ production from e^+e^- collision through ψ meson.

Comparing with other facilities, our baryon program has advantages in at least three obvious aspects:

(1) We have pure isospin 1/2 πN and $\pi\pi N$ systems from $J/\psi \to \bar{N}N\pi$ and $\bar{N}N\pi\pi$ processes due to isospin conservation, while πN and $\pi\pi N$ systems from πN and γN experiments are mixture of isospin 1/2 and 3/2, and suffer difficulty on the isospin decomposition;

(2) ψ mesons decay to baryon-antibaryon pairs through three or more gluons. It is a favorable place for producing hybrid (qqqg) baryons, and for looking for some "missing" N^* resonances which have weak coupling to both πN and γN, but stronger coupling to g^3N;

(3) Not only N^*, Λ^*, Σ^* baryons, but also Ξ^* baryons with two strange quarks can be studied. Many QCD-inspired models[9, 10] are expected to be more reliable for baryons with two strange quarks due to their heavier quark mass. More than thirty Ξ^* resonances are predicted where only two such states are well established by experiments. The theory is totally not challenged due to lack of data.

BES started data-taking in 1989 and was upgraded in 1998. The upgraded BES is named BESII while the previous one is called BESI. BESI collected 7.8 million J/ψ events and 3.7 million ψ' events. BESII has collected 58 million J/ψ events.

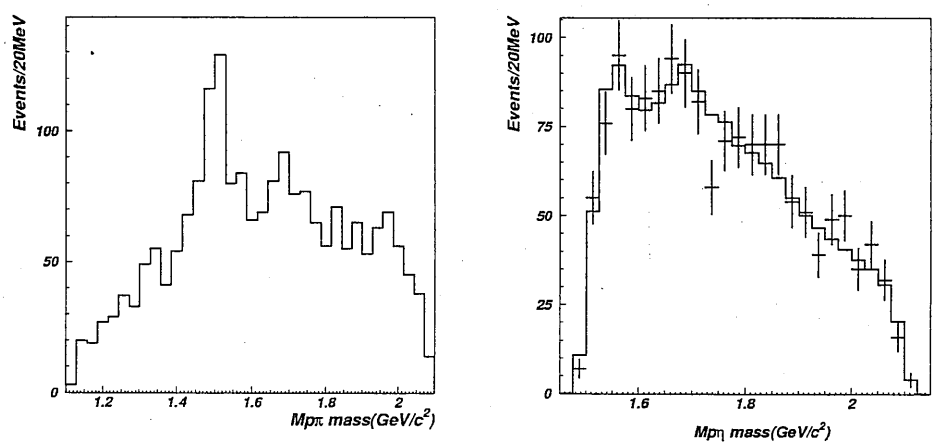

Fig. 2. left: $p\pi^0$ invariant mass spectrum for $J/\psi \to \bar{p}p\pi^0$; right: $p\eta$ invariant mass spectrum for $J/\psi \to \bar{p}p\eta$. BESI data

Based on 7.8 million J/ψ events collected at BESI before 1996, the events for $J/\psi \to \bar{p}p\pi^0$ and $\bar{p}p\eta$ have been selected and reconstructed with π^0 and η detected in their $\gamma\gamma$ decay mode[7]. The corresponding $p\pi^0$ and $p\eta$ invariant

mass spectra are shown in Fig. 2 with clear peaks around 1500 and 1670 MeV for $p\pi^0$ and clear enhancement around the $p\eta$ threshold, peaks at 1540 and 1650 MeV for $p\eta$. Partial wave analysis has been performed for the $J/\psi \to \bar{p}p\eta$ channel[7] using the effective Lagrangian approach[11, 12] with Rarita-Schwinger formalism[13, 14, 15, 16] and the extended automatic Feynman Diagram Calculation (FDC) package[17]. There is a definite requirement for a $J^P = \frac{1}{2}^-$ component at $M = 1530 \pm 10$ MeV with $\Gamma = 95 \pm 25$ MeV near the ηN threshold. In addition, there is an obvious resonance around 1650 MeV with $J^P = \frac{1}{2}^-$ preferred, $M = 1647 \pm 20$ MeV and $\Gamma = 145^{+80}_{-45}$ MeV. These two N^* resonances are believed to be the two well established states, $S_{11}(1535)$ and $S_{11}(1650)$, respectively. In the higher $p\eta(\bar{p}\eta)$ mass region, there is a evidence for a structure around 1800 MeV; with BESI statistics we cannot determine its quantum numbers.

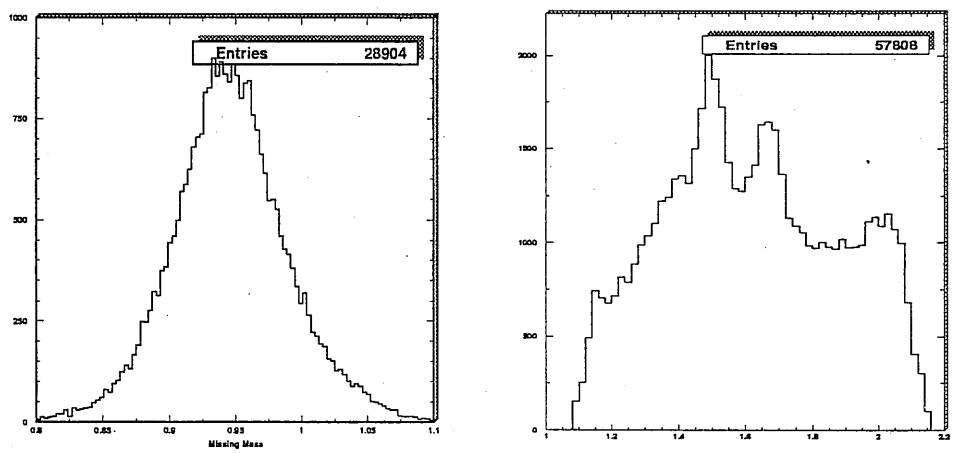

Fig. 3. left: missing mass spectrum against $p\pi^-$ for $J/\psi \to \bar{n}p\pi^-$; right: $p\pi^-$&$\bar{n}\pi^-$ invariant mass spectrum for $J/\psi \to \bar{n}p\pi^-$. Preliminary BESII data

With 58 million new J/ψ events collected by BESII of improved detecting efficiency, we have one order of magnitude more reconstructed events for each channel. We show in Figs.3 and 4 preliminary results for $J/\psi \to p\bar{n}\pi^-$ and $J/\psi \to pK^-\bar{\Lambda} + h.c.$ channels, respectively.

For $J/\psi \to p\bar{n}\pi^-$ channel, proton and π^- are detected. With some cuts of backgrounds, the missing mass spectrum shows a very clean peak for the missing antineutron with negligible backgrounds; The $N\pi$ invariant mass spectrum of 28,904 reconstructed events from half BESII data looks similar to the $p\pi$ invariant mass spectrum for $J/\psi \to p\bar{p}\pi^0$ as in Fig. 2, but with much higher statistics. Besides two very clear peaks around 1500 and 1670 MeV, the peak around 2020 MeV becomes clearer. This could be a "missing"

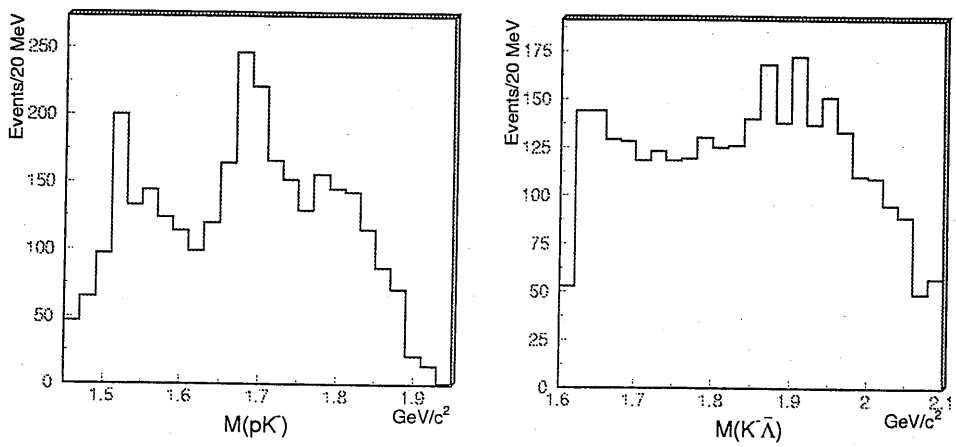

Fig. 4. left: pK invariant mass spectrum for $J/\psi \to pK\Lambda$; right: $K\Lambda$ invariant mass spectrum for $J/\psi \to pK\Lambda$. Preliminary BESII data

N^*. For the decay $J/\psi \to \bar{N}N^*(2020)$, the orbital angular momentum of $L = 0$ is much preferred due to the suppression of the centrifugal barrier factor for $L \leq 1$. For $L = 0$, the spin-parity of $N^*(2020)$ is limited to be $1/2+$ and $3/2+$. This may be the reason that the $N^*(2020)3/2+$ shows up as a peak in J/ψ decays while no peak shows up for πN invariant mass spectra in πN and γN production processes which allow all $1/2\pm$, $3/2\pm$, $5/2\pm$ and $7/2\pm$ N^* resonances around 2.02 GeV to overlap and interfere with each other there.

For $J/\psi \to pK^-\bar{\Lambda}$ and $\bar{p}K^+\Lambda$ channels, there are clear Λ^* peaks at 1.52 GeV, 1.69 GeV and 1.8 GeV in pK invariant mass spectrum, and N^* peaks near $K\Lambda$ threshold and 1.9 GeV for $K\Lambda$ invariant mass spectrum. The SAPHIR experiment at ELSA[18, 19] also observed a N^* peak around 1.9 GeV for $K\Lambda$ invariant mass spectrum from photo-production.

We are also reconstructing $J/\psi \to \bar{p}p\omega$, $pK\Sigma$, $\bar{p}p\pi^+\pi^-$ and other channels. Partial wave analyses of various channels are in progress.

3. J/ψ radiative decays

There are three main physics objectives for J/ψ radiative decays:

(1) Looking for glueballs and hybrids. As shown in Fig. 5, after emitting a photon, the $c\bar{c}$ pair is in a $C = +1$ state and decays to hadrons dominantly through two gluon intermediate states. Simply counting the power of α_s we know that glueballs should have the largest production rate, hybrids the second, then the ordinary $q\bar{q}$ mesons.

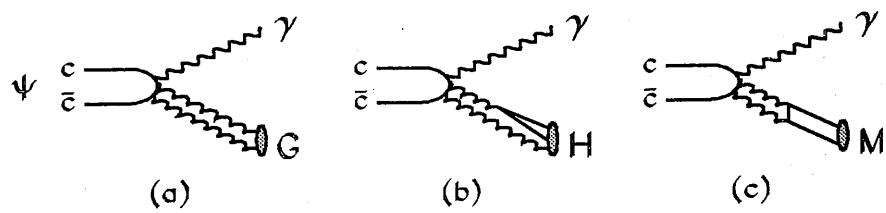

Fig. 5. ψ radiative decays to (a) glueball, (b) hybrid, and (c) $q\bar{q}$ meson.

(2) Completing $q\bar{q}$ meson spectroscopy and studying their production and decay rates, which is crucial for understanding their internal structure and confinement.

(3) Extracting $gg \leftrightarrow q\bar{q}$ coupling from perturbative energy region of above 3 GeV to nonperturbative region of 0.3 GeV. This may show us some phenomenological pattern for the smooth transition from perturbative QCD to strong nonperturbative QCD.

Up to now, we have mainly worked on glueball searches. One thing worth noting is that the J/ψ radiative decay has a similar decay pattern as 0^{-+}, 0^{++} and 2^{++} charmoniums, *i.e.*, η_c, χ_{c0} and χ_{c2}, as it should be, since all of them decay through two gluons. The 4π, $\bar{K}K\pi\pi$, $\eta\pi\pi$ and $\bar{K}K\pi$ seem to be the most favorable final states for the two gluon transition at $1 \sim 3$ GeV. The branching ratios for J/ψ radiative decay to these four channels are listed in Table 1. The sum of them is about half of all radiative decays. If glueballs exist, they should appear in these four channels. Therefore BES Collaboration has performed partial wave analyses (PWA) of these four channels[20, 21, 22, 23] based on BESI data. The main results have been summarized in Ref. [25]. Mesons with large branching ratios in the J/ψ radiative decays are a very broad $\eta(2190)$ for 0^{-+}, a broad $f_2(1950)$ for 2^{++}, $f_0(1500)$, $f_0(1710\text{-}1770)$ and $f_0(2100)$ for 0^{++}.

Table 1. Branching ratios for the four largest J/Ψ radiative decay channels (BR$\times 10^3$)

$\gamma 4\pi$	$\gamma\bar{K}K\pi\pi$	$\gamma\eta\pi\pi$	$\gamma\bar{K}K\pi$
14.4 ± 1.8 [24]	9.5 ± 2.7 [21]	6.1 ± 1.0 [5]	6.0 ± 2.1 [23]

With BESII data, all signals become clearer. For example, Fig. 6 shows the comparison of BESI and BESII data for $J/\psi \to \gamma\pi^+\pi^-\pi^+\pi^-$. For BESII data, we have performed partial wave analysis for the $\gamma\bar{K}K$ and $\gamma\pi^+\pi^-$ channels[26], where the main result is that $f_J(1710)$ peak in these

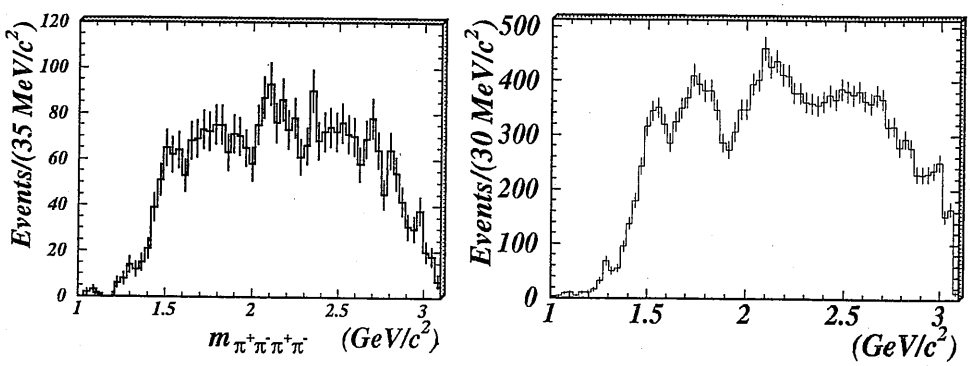

Fig. 6. Comparison of BESI (left) and BESII data (right) for $J/\psi \to \gamma\pi^+\pi^-\pi^+\pi^-$.

channels is definitely due to a 0^{++} particle.

4. J/ψ hadronic decays to mesons

There are mainly two physics objectives here:

(1) Looking for hybrids. Since ψ decays to hadrons through three gluons, final states involving a hybrid as shown in Fig. 7(a) are expected to have larger production rate than ordinary $q\bar{q}$ mesons as shown in Fig. 7(b,c).

(2) Extracting $u\bar{u}+d\bar{d}$ and $s\bar{s}$ components of associated mesons, M, via $\Psi \to M + \omega/\phi$ as shown in Fig. 7(b,c).

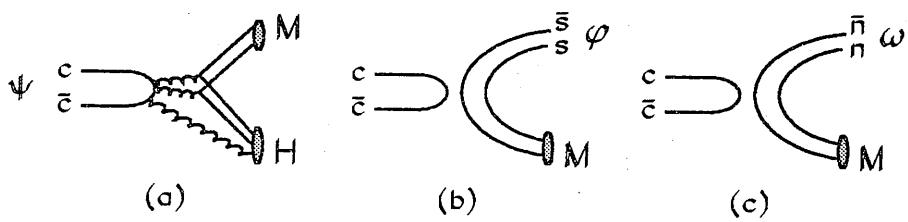

Fig. 7. ψ hadronic decays to (a) hybrids, (b) $s\bar{s}$, and (c) $n\bar{n} \equiv \frac{1}{\sqrt{2}}(u\bar{u}+d\bar{d})$ mesons.

In order to look for isoscalar 1^{-+} hybrid $\hat{\omega}$ decaying to 4π, we have studied $J/\psi \to \omega\pi^+\pi^-\pi^+\pi^-$ process[27]. A peak around 1.75 GeV in the 4π invariant mass spectrum is visible. But due to low statistics, no PWA is performed. No other structure is observed.

To investigate the $u\bar{u}+d\bar{d}$ and $s\bar{s}$ components of mesons, we have studied $J/\psi \to \omega\pi^+\pi^-$, ωK^+K^-, $\phi\pi^+\pi^-$ and ϕK^+K^- channels. The invariant mass spectra for these channels are shown in Fig. 8 and Fig. 9, which are similar to the previous ones by MARKIII and DM2 Collaborations, but with much higher statistics.

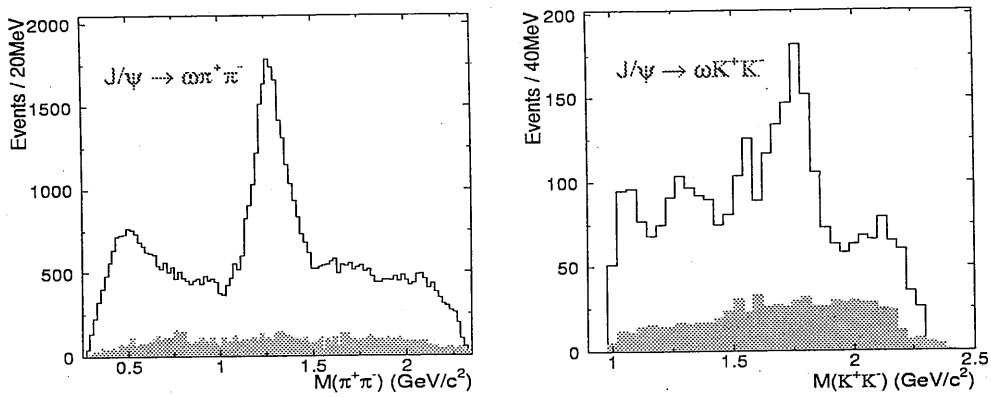

Fig. 8. left: $\pi\pi$ invariant mass spectrum for $J/\psi \to \omega\pi^+\pi^-$; right: K^+K^- invariant mass spectrum for $J/\psi \to \omega K^+K^-$. Preliminary BESII data

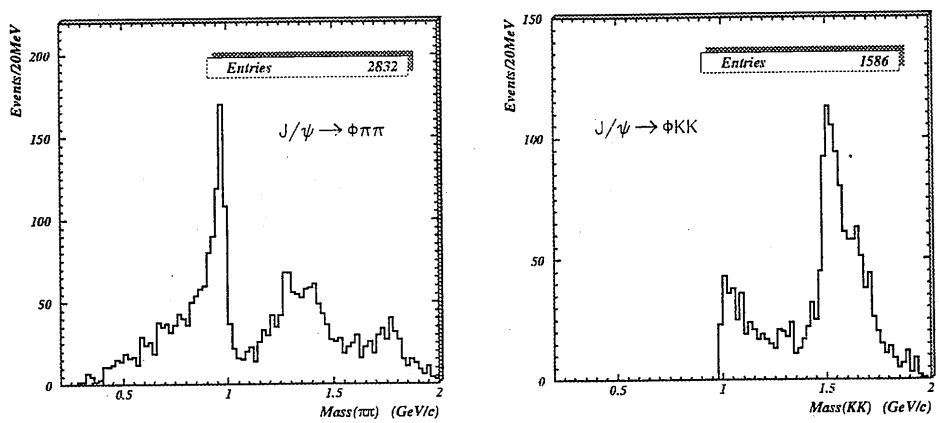

Fig. 9. left: $\pi\pi$ invariant mass spectrum for $J/\psi \to \phi\pi^+\pi^-$; right: K^+K^- invariant mass spectrum for $J/\psi \to \phi K^+K^-$. Preliminary half BESII data

For $J/\psi \to \omega\pi^+\pi^-$, there are two clear peaks at 500 MeV and 1275 MeV in the 2π mass spectrum corresponding to the σ and the $f_2(1275)$, respectively[28]. For $J/\psi \to \omega K^+K^-$, there is a threshold enhancement due to the $f_0(980)$ and a clear peak at 1710 MeV probably due to the $f_0(1710)$.

Preliminary results[28] of partial wave analyses indicate that (1) in the $\pi\pi$ mass spectrum of the $J/\psi \to \phi\pi^+\pi^-$ process all three peaks at 980 MeV, 1330 MeV and 1770 MeV are dominantly 0^{++}; (2) in the $K\bar{K}$ mass spectrum of the $J/\psi \to \phi K^+K^-$ the peak at 1525 MeV is due to $f_2'(1525)$ while the $K\bar{K}$ threshold enhancement and the shoulder around 1700 MeV are due to $f_0(980)$ and $f_0(1710)$, respectively.

In summary, the σ and $f_2(1275)$ appear clearly only in the $J/\Psi \to \omega + X$ process, the $f_2'(1525)$ appears clearly only in the $J/\Psi \to \phi + X$ process, and $f_0(980)$ and $f_0(1710\text{-}1770)$ appear clearly in both processes.

5. Future prospects

We are now working on the 58 million J/ψ events collected with BESII detector in the years from 1999 to 2001. Physics results on various channels of N^* and meson production are expected to be published in near future.

We have been taking $\psi'(3686)$ data since last year and hope to reach more than 20 million ψ' events in next year. The data of ψ' decays will extend our study on N^* and meson resonances to a broader energy range.

A major upgrade of the collider to BEPCII is planned to be finished in about 4 years. A further two order of magnitude more statistics is expected to be achieved. Such statistics will enable us to perform partial wave analyses of plenty important channels for both meson spectroscopy and baryon spectroscopy from the J/ψ and ψ' decays. We expect BEPCII to play a very important role in many aspects of light hadron spectroscopy, such as hunting for the glueballs and hybrids, extracting $u\bar{u}+d\bar{d}$ and $s\bar{s}$ components of mesons, and studying excited nucleons and hyperons, i.e., N^*, Λ^*, Σ^* and Ξ^* resonances.

Acknowledgments

We would like to thank the workshop organizers for their kind invitation and financial support for our participation of this very interesting and successful conference. This work is partly supported by the CAS Knowledge Innovation Project (KJCX2-N11) and National Science Foundation of China, and is written up during author's visit at ICTP, Trieste, Italy.

REFERENCES

[1] BES Collaboration, Nucl. Instr. Methods, **A344**, 319 (1994); *ibid.*, **A458**, 627 (2001).

[2] N.Bohr, Phil. Mag. **26**, 1-25, 471-502, 857-875 (1913).

[3] M.Mayer and J.Jensen, *Elementary Theory of Nuclear Shell Structure*, John Wiley and Sons, Inc., New York (1955).

[4] A.Bohr and B.Mottelson, *Nuclear Structure Vol.I, Single-Particle Motion* (1969) and *Vol.II, Nuclear Deformations* (1975), W.A.Benjamin, Inc., Reading, Massachusetts.

[5] Particle Data Group, Euro. Phys. J. **C15**, 1 (2000).

[6] S.Capstick and W.Robert, Prog. Part. Nucl. Phys. **45**, S241 (2000)..

[7] BES Collaboration, J.Z.Bai et al., Phys. Lett. **B510**, 75 (2001); BES Collaboration, H.B.Li et al., Nucl. Phys. **A675**, 189c (2000); BES Collaboration, B.S.Zou et al., *Excited Nucleons and Hadronic Structure, Proc. of NSTAR2000 Conf. at JLab, Feb 2000.* Eds. V.Burkert et al., World Scientific (2001) p.155.

[8] B.S.Zou, Nucl. Phys. **A684**, 330 (2001); Nucl. Phys. **A675**, 167 (2000).

[9] S.Capstick and N.Isgur, Phys. Rev. **D34**, 2809 (1986).

[10] L.Glozman, W.Plessas, K.Varga and R.Wagenbrunn, Phys. Rev. **D58**, 094030 (1998).

[11] M.Benmerrouche, N.C.Mukhopadhyay and J.F.Zhang, Phys. Rev. Lett. 77, 4716 (1996); Phys. Rev. D51, 3237 (1995).

[12] M.G.Olsson and E.T.Osypowski, Nucl. Phys. B87, 399 (1975); Phys. Rev. D17, 174 (1978); M.G.Olsson et al., *ibid.* 17, 2938 (1978).

[13] W.Rarita and J.Schwinger, Phys. Rev. **60**, 61 (1941).

[14] C.Fronsdal, Nuovo Cimento Suppl. **9**, 416 (1958); R.E.Behrends and C.Fronsdal, Phys. Rev. **106**, 345 (1957).

[15] S.U.Chung, *Spin Formalisms*, CERN Yellow Report 71-8 (1971); Phys. Rev. **D48**, 1225 (1993); J.J.Zhu and T.N.Ruan, Communi. Theor. Phys. **32**, 293, 435 (1999).

[16] W.H.Liang, P.N.Shen, J.X.Wang and B.S.Zou, J. Phys. **G28** (2002) 333.

[17] J.X.Wang, Comput. Phys. Commun. **77**, 263 (1993).

[18] M.Q.Tran *et al.*, Phys. Lett. **B445**, 20 (1998).

[19] C.Bennhold *et al.*, Phys. Rev. **C61**, 012201 (2000).

[20] BES Collaboration, J.Z.Bai et al., Phys. Lett. B472 (2000) 207.

[21] BES Collaboration, J.Z.Bai et al., Phys. Lett. B472 (2000) 200.

[22] BES Collaboration, J.Z.Bai et al., Phys. Lett. B446 (1999) 356.

[23] BES Collaboration, J.Z.Bai et al., Phys. Lett. B476 (2000) 25; Phys. Lett. B440 (1998) 217.

[24] L.Köpke and N.Wermes, Phys. Rep. 174 (1989) 67.

[25] B.S.Zou, Nucl. Phys. A 692 (2001) 362.

[26] Z.J.Guo, talk given at this conference.

[27] BES Collaboration, J.Z.Bai et al., High Ener. Phys. Nucl. Phys. 25 (2001) in Chinese.

[28] X.Shen, BES Collaboration, Nucl. Phys. B, Proc. Suppl. 93 (2001) 93.

中国高等科学技术中心

北京 8730 信箱，100080　　主任：李政道　　副主任：周光召、路甬祥

“重子、双重子和奇特夸克-胶子态”研讨会日程

4 月 22 日　　星期一　　上午　　主持人：　王凡

9:00 - 9:50	Prof.Lomon	R-matrix method for the quark/gluon to hadron transition - predicting a variety of structures.
9:50 - 10:10		休息
10:10 – 11:00	赵强	Baryon spectroscopy; Quark model and “missing resonances”
11:00 - 11:50	张宗烨	$(\Omega\Omega)_0$ Dibaryon

下午　　主持人：　赵维勤

1:30-2:20	赵强	Electromagnetic coupling of Baryons
2:20-3:00	沈彭年	Interactions of decuplet Dibaryons in quark cluster model
3:00-3:20		休息　　主持人：　宗红石
3:20-4:00	平加伦	NN interaction in extended QDCSM
4:00-4:30	庞侯荣	Dibaryons with strangeness

4 月 23 日　　星期二　　上午　　主持人：　邹冰松

9:00-9:50	赵强	Study baryon properties via meson photo- and electroproduction
9:50-10:10		休息
10:10-11:00	Prof.Lomon	The nucleon-nucleon interaction in the R-matrix model and predicted exotics.
11:00-11:50	王凡	Low energy QCD effective degrees of freedom

下午　　主持人：　宁平治

1:30-2:10	吕晓夫	Relation between realizations of chiral symmetry spontaneous breaking on quark and nucleon level
2:10-2:50	何汉新	NPQCD, quark confinement and hadron physics
2:50-3:10		休息　　主持人：　赵恩广
3:10-3:50	黄时中	Solution to Bargmann-Wigner equation
3:50-4:30	张永军	Parton distribution of Proton and flavor symmetry

4 月 24 日　　星期三　　上午　　主持人：张宗烨

9:00 - 9:50	Prof.Lomon	Hyperon-nucleon and hyperon-hyperon Interactions and exotics – the H-resonance
9:50 - 10:10		休息
10:10- 11:00	赵强	Present experimental projects on baryon physics
11:00-11:40	邹冰松	Light hadron physics from J/ψ decays
		下午　　主持人：　姜焕清
1:30- 2:00	沈肖雁	BESII experiments on J/ψ Physics
2:00-2:30	吴济民	Lattice QCD Study on hybrids
2:30-3:00	平荣刚	Study baryon structure from J/ψ decays
3:00- 3:20		休息
3:20- 8:00		Discussion and reception

4 月 25 日　　星期四　　上午　　主持人：祝玉灿

9:00-9:40	赵强	Perspectives of baryon physics in experiment and theory
9:40-10:10	梁伟红	Nucleon pole contribution in $J/\psi \to \pi N\overline{N}$
10:10-10:30		休息
10:30-11:00	季晓斌	Study on $J/\psi \to \pi N\overline{N}$
11:00-11:30	杨洪勋	Study on $J/\psi \to K\Lambda N$
11:30-12:00	陈 杰	Searching for 1^{-+} hybrid in $J/\psi \to \omega 2(\pi^+\pi^-)$

中国高等科学技术中心

北京 8730 信箱，100080　　主任：李政道　　副主任：周光召、路甬祥

“重子、双重子和奇特夸克-胶子”研讨会通讯录

序号	姓名	性别	单位及通讯地址	邮 编
1.	赵　强	男	Univ. of Surrey, UK	
2.	王　凡	男	江苏南京大学物理系	210093
3.	庞侯荣	女	江苏南京大学物理系	210093
4.	杨洪庭	男	江苏南京大学物理系	210093
5.	宗红石	男	江苏南京大学物理系	210093
6.	平加伦	男	江苏南京师范大学物理系 e-mail:jlping@pine.njnu.edu.cn	210097
7.	鲁希锋	男	江苏南京师范大学物理系	210097
8.	卢礼萍	女	江苏南京师范大学物理系	210097
9.	陈子乾	男	广西南宁市广西大学物理系	530004
10.	陆　晓	男	广西桂林市广西师范大学物电系 e-mail:luxiaof@263.net	541004
11.	宁平治	男	天津南开大学物理系 e-mail:ningpz@nankai.edu.cn	300071
12.	王秋玲	女	天津南开大学物理系 e-mail:nankai.edu.cn	300071
13.	谭玉红	女	天津南开大学物理系 e-mail:nankai.edu.cn	300071
14.	陈　杰	男	天津南开大学物理系	300071
15.	吕晓夫	男	四川成都四川大学物理系 e-mail:luxf@scu.edu.cn	610064
16.	陈为驹	男	安徽省安庆市安庆师范学院物理系 e-mail:chenwj@mail.hf.ah.cn	246011
17.	张　杰	男	安徽省安庆市安庆师范学院物理系 e-mail:zhjylh@aqtc.edu.cn	246011
18.	章礼华	男	安徽省安庆市安庆师范学院物理系 e-mail:zhanglh@aqtc.edu.cn	246011

19.	于秦生	男	安徽省安庆市安庆师范学院物理系 e-mail:zhanglh@aqtc.edu.cn	246011
20.	黄时中	男	安徽芜湖市安徽师范大学物理系	241000
21.	于　淼	男	合肥四号信箱 6#-303 中国科技大学 e-mail:second@mail.ustc.edu.cn	230027
22.	陈　童	男	合肥中国科技大学西区 2#621 室 e-mail:jiangshanjiao@163.com	230027
23.	龚建辉	男	合肥中国科技大学四号信箱 2#619 室 e-mail:jiangshanjiao@163.com	230027
24.	李志刚	男	石家庄河北师范大学物理系 e-mail:duancg@mail.hebtu.edu.cn	050016
25.	张印杰	男	石家庄河北师范大学物理系	050016
26.	何汉新	男	北京 275-18 信箱 中国原子能院	102413
27.	张肇西	男	中科院理论物理所 e-mail:zhangzx@itp.ac.cn	100080
28.	赵恩广	男	中科院理论物理所	100080
29.	陆景贤	女	中科院研究生院学报编辑部 e-mail:journal@gscas.ac.cn	100039
30.	张宗烨	女	中科院高能物理所	100039
31.	邹冰松	男	中科院高能物理所	100039
32.	季晓斌	男	中科院高能物理所 e-mail:jixb@mail.ihep.ac.cn	100039
33.	沙依甫加马力	女	中科院高能物理所四室 e-mail:sayipjamal@ihep.ac.cn	100039
34.	吴济民	男	中科院高能物理所理论室	100039
35.	姜焕清	男	中科院高能物理所核理论组	100039
36.	沈彭年	男	中科院高能物理所核理论组	100039
37.	沈肖雁	女	中科院高能物理所一室	100039
38.	祝玉灿	男	中科院高能物理所一室	100039
39.	杨洪勋	男	中科院高能物理所一室	100039
40.	平荣刚	男	中科院高能物理所	100039
41.	张　昭	男	中科院高能物理所四室	100039
42.	孙宝玺	男	中科院高能物理所四室	100039

43.	彭光雄	男	中科院高能物理所四室	100039
44.	梁伟红	女	中科院高能物理所四室	100039
45.	赵维勤	女	中科院高能物理所	100039
46.	张永军	男	北京大学物理系	100871
47.				
48.				
49.				
50.				